



DELFT UNIVERSITY OF TECHNOLOGY

ME-BMD MASTER THESIS

**The Design of The Endo-Tubular Friction Carrier**  
*A Bio-Inspired Alternative To Suction-Based Transport*

By:

Name	I.A. van de Steeg
Study Number	4108841

Date: February 4, 2018

# The Design of The Endo-Tubular Friction Carrier

by

**I. A. van de Steeg**

To obtain the degree of Master of Science in Mechanical Engineering at the Delft University of Technology, to be defended publicly on Wednesday February 14, 2018 at 13:30 AM.

An electronic version of this thesis is available at <http://repository.tudelft.nl/>.

Student number:	4108841
Project duration:	March 16, 2017 - February 14, 2018
Thesis supervisors:	Ir. A. Sakes, TU Delft Prof. Dr. Ir. P. Breedveld, TU Delft
Graduation committee:	Ir. A. Sakes, TU Delft Prof. Dr. Ir. P. Breedveld, TU Delft ir. J.W. Spronck TU Delft





## Preface

In this section of the report I would like to express my gratitude towards the people who have facilitated my life as a student and also towards those who contributed to the design process in any way. First of all I would like to dedicate a few sentences to my family. I am acutely aware of the fact that I would never have gone to the Delft University of Technology were it not for the encouragement and (financial) support of my family, for which I am grateful. The counsel and guidance that was ever present during my time as a student leaves me indebted to my family and I greatly acknowledge and appreciate the opportunities offered to me.

During numerous discussions and conversations about the design process, the manufacturing of the prototype, the structure of the report, the setup of the experiment or other affairs relating to this design project I have received countless remarks and recommendations from my daily supervisor ir. Aimée Sakes. Without her continued involvement with this project it would have been a very tedious and cumbersome enterprise. Moreover, my main thesis supervisor prof.dr.ir. Paul Breedveld was available on a regular basis to discuss design choices or provide assistance when I encountered obstacles during this process. I have enjoyed working together and am thankful for your counsel and commentary. In addition to my supervisors I have also appreciated the helpful remarks and biological background knowledge of M. Scali, MSc. Furthermore, I would like to thank ir. P. Posthoorn for his contribution to my project and for the continued interest in the production of the prototype and his willingness to provide answers regarding the design of the actuator.

Besides the theoretical design support I received during the design of this mechanism I would also like to convey my appreciation for the practical design support and manufacturing of this mechanism. The beautiful prototype which was skillfully manufactured by precision technician M. Lageweg was instrumental in determining the success of the designed mechanism. In addition, I am very grateful for the advice I received from my good friend J. van Engelenhoven who assisted me during the repairing of the prototype, which I received in a non-working condition. I also want to thank precision technicians D. Jager, R. van Starckenburg, H. van der Ster and A. Mol whose comments on my design have been very constructive and valuable. The small amount of parts is a testament to the amount of simplification that was a result of their helpful commentary. Finally, I would like to thank dr.ir. W.P. Breugem, prof.dr. J. Dankelman, dr.ir. S.A. Miedema and dr.ir. A.M. Talmon for their expertise and advice on the different types of sub-optimal behaviour which can occur in pipes and ducts. As one can imagine, it would be rather hard to design a purposeful solution to the problems that one encounters when designing a transport system within a tube without a clear definition of the types of problems which affect the efficacy with which transport within medical instruments takes place.

Biologically inspired devices provide a profound account of the unimaginable intricacy and subtlety that is found in nature. The Bio-Inspired Technology group at the Delft University of Technology proposes that engineers, scientists and others would be wise to look (back) at nature for providing solutions to existing problems. A famous conservationist once wrote: *“Not blind opposition to progress, but opposition to blind progress...”*. I regard the implementation and mimicking of the elaborate and simple solutions provided by nature as an earnest interpretation of the Delft University of Technology motto: Challenge the future. It is my sincere hope that the result of this design process, however minute, will be used thoughtfully and that this report and the findings within it contribute to the improvement of transport within medical instruments. Challenge the future!

Thank you all!



# Contents

<b>Glossary</b>	<b>1</b>
<b>1 Introduction</b>	<b>5</b>
1.1 Background: Transporting Material . . . . .	5
1.2 State of the Art in Laparoscopic Transport Mechanisms . . . . .	6
1.3 Problem Definition . . . . .	8
1.4 Goal of this Study . . . . .	8
1.5 Layout of this Report . . . . .	10
<b>2 Sub-optimal Behaviour in Laparoscopic Transport Mechanisms</b>	<b>13</b>
2.1 Introduction to Sub-optimal Behaviour Modes . . . . .	13
2.2 Categorization of Sub-optimal Behaviour Modes . . . . .	13
2.3 Sub-optimal Behaviour Modes . . . . .	14
2.3.1 Aspirated Tissue Diameter Expansion . . . . .	14
2.3.2 Accumulated Obstruction Friction . . . . .	14
2.3.3 Rotational Jamming . . . . .	15
2.3.4 Entry Obstruction . . . . .	15
2.3.5 Pressure Drop and Head-Loss . . . . .	17
2.3.6 Turbulence . . . . .	18
2.3.7 Non-Newtonian Liquid Obstruction . . . . .	18
2.3.8 Entrance Phenomena . . . . .	19
2.3.9 Coagulation . . . . .	19
2.4 Current Alternatives to Aspiration . . . . .	20
<b>3 Design Process of the Endo-Tubular Friction Carrier</b>	<b>23</b>
3.1 Design Goal . . . . .	23
3.2 Design Criteria . . . . .	23
3.2.1 Geometric Requirements . . . . .	23
3.2.2 Functional Requirements . . . . .	23
3.2.3 Medical Requirements . . . . .	23
3.3 Transport Mechanism Design Approach . . . . .	24
3.3.1 Initiation of Transport . . . . .	24
3.3.2 Stylized Version of Reality . . . . .	24
3.3.3 Creating Force . . . . .	25
3.3.4 Biological Inspiration . . . . .	25
3.4 Concept Categorization Theory . . . . .	25
3.5 Conceptual Solutions . . . . .	25
3.5.1 Solid Transport Methods . . . . .	25
3.5.2 Fluid Transport Methods . . . . .	28
3.6 Concept Selection Procedure . . . . .	30
3.6.1 Available versus Preferred Design Directions . . . . .	30
3.6.2 Relative Contact Complexity . . . . .	31
3.6.3 Miniaturization . . . . .	32
3.6.4 Primary Concept Selection . . . . .	32
3.6.5 Retracting Blade Transport . . . . .	33
3.6.6 Alternating Friction Pair Transport . . . . .	35
3.6.7 Selection Process Conclusion . . . . .	37
3.7 Final Conceptual Design . . . . .	38
3.7.1 Motion Sequence . . . . .	38
3.7.2 Blade Actuation . . . . .	39
<b>4 Prototype Development</b>	<b>45</b>
4.1 Prototype Manufacturing . . . . .	45
4.2 Prototype Assembly . . . . .	45

## CONTENTS

<b>5</b>	<b>Proof-of-Principle Experiment</b>	<b>49</b>
5.1	Goal of the Experiment . . . . .	49
5.2	Experiment Variables . . . . .	49
5.3	Experiment Facility . . . . .	49
5.3.1	Preparation of Artificial Tissue . . . . .	49
5.4	Experiment Protocol . . . . .	51
5.4.1	Sub-experiment I: Effect of Mixture Density and Particle Presence . . . . .	51
5.4.2	Sub-experiment II: Effect of Motion Sequence . . . . .	51
5.4.3	Sub-experiment III: Transport of Minced Meat . . . . .	51
5.5	Data Analysis . . . . .	51
<b>6</b>	<b>Experiment Results</b>	<b>55</b>
6.1	Sub-experiment I: Effect of Mixture Density and Particle Presence . . . . .	55
6.1.1	Mixture Density . . . . .	55
6.1.2	Particle Presence . . . . .	55
6.2	Sub-experiment II: Effect of Motion Sequence . . . . .	55
6.3	Sub-experiment III: Transport of Minced Meat . . . . .	55
<b>7</b>	<b>Discussion</b>	<b>61</b>
7.1	Summary of Main Findings . . . . .	61
7.2	Limitations, Implications and Recommendations for Future Research . . . . .	61
7.2.1	Procedural Limitations . . . . .	61
7.2.2	Prototype Limitations . . . . .	61
7.2.3	Improved Tissue Mimicking . . . . .	63
7.2.4	Medical Environment Imitation . . . . .	63
7.2.5	Addition of Microstructures and Alternative Motion Sequence . . . . .	63
7.2.6	Increase Motor Speed and Simplify Components . . . . .	64
7.2.7	Radial Locking . . . . .	64
7.2.8	Combination with Suction . . . . .	64
7.2.9	Generalization of Application . . . . .	65
7.3	Future Vision . . . . .	66
<b>8</b>	<b>Conclusion</b>	<b>67</b>
	<b>References</b>	<b>69</b>
	<b>Appendix A Database Search Queries</b>	<b>71</b>
A.1	Explanatory Note . . . . .	71
A.2	Espacenet Search Query . . . . .	71
A.3	FPO Search Query . . . . .	71
	<b>Appendix B Preliminary Knowledge of Fluid Mechanics</b>	<b>73</b>
B.1	Liquid Flow in Narrowing and Expanding Ducts . . . . .	73
B.2	Newtonian Versus Non-Newtonian Liquid Behaviour . . . . .	73
B.3	Flow Loss in Ducts and Boundary Layers . . . . .	74
	<b>Appendix C Biological Inspiration</b>	<b>77</b>
	<b>Appendix D Technical Drawings</b>	<b>79</b>
D.1	Assembly . . . . .	79
D.2	Blade Adapter . . . . .	80
D.3	Adapter Clamp . . . . .	81
D.4	Blade . . . . .	82
D.5	Suspending Frame - Stand 1 . . . . .	83
D.6	Suspending Frame - Stand 3 . . . . .	84
D.7	Suspending Frame - Stand 4 . . . . .	85
D.8	Outer Tube . . . . .	86

## CONTENTS

D.9 Suspending Frame - Base Plate . . . . .	87
D.10 Rotor . . . . .	88
<b>Appendix E Radial Locking Method</b>	<b>89</b>
<b>Appendix F Matlab Scripts for Data Analysis</b>	<b>91</b>
F.1 ANOVA Test Sub-experiment I - Pure Gelatin . . . . .	91
F.2 ANOVA Test Sub-experiment I - Grain Gelatin . . . . .	92
F.3 T-Test Sub-experiment I . . . . .	93
F.4 T-Test Sub-experiment II . . . . .	94
F.5 Script for Sub-experiment III . . . . .	95
<b>Appendix G Preparatory Experiment - Demonstration of Functionality</b>	<b>97</b>
<b>Appendix H Transport Rates of Sub-experiment I</b>	<b>99</b>



## Glossary

**Aspiration** Aspiration is commonly known to indicate the process of drawing breath. However, in medicine the term is also used to indicate the action of transporting fluid by means of suction from a transport site. 8

**Biocompatibility** Biocompatibility refers to the ability of a material or a device to exist within the body of a host without producing negative side effects. 24

**Failure mode** Failure modes are the modes of operation which can be considered to be less than the intended operating behaviour, i.e., sub-optimal operation modes. 7

**Laparoscopy** Laparoscopy refers to the surgery method in which instruments are inserted into the patients body by means of a small portal incision, also referred to as a portal. 5

**Morcellation** Morcellation refers to the division and subsequent transport of material from a host in order to extract harmful tissue or obtain knowledge on the type of tissue. 6

**Myoma** Myoma refers to a kind of malign tumor tissue which is made up out of a loose configuration of cells which are unable to provide specialized functions. 18

**Oviposition** Oviposition, from the Latin noun for egg '*ovi*' and the verb for laying '*ponere*', refers to the process in which a female of the insect order Hymenoptera deposits an egg in a suitable substratum. This deposition is done by means of an egg laying sheath, suitably called the *ovipositor*, attached to the rear of the female insect. 25, 77

**Retrograde** Retrograde movement is movement within the opposite direction, i.e., moving backwards. 38

**Shear thickening** A material is said to display shear thickening when the viscosity of the material is increased when the applied shear stress is increased. 73

**Shear thinning** A material is said to display shear thinning when the viscosity of the material is decreased when the applied shear stress is increased. 74

**Stenosis** Stenosis refers to the medical condition of a narrowing blood vessel or other type of duct which inhibits the passage of blood or other types of material. 73



## Abstract

**Background:** Minimally invasive surgery (MIS) is a surgical procedure which is characterized by inserting long and slender instruments through small porthole incisions. On many occasions tissue will have to be extracted from the operation site through one of these small portholes, therefore the sheaths of the instruments that are inserted into the body are limited in diameter. Less than optimal functioning of the transport of tissues which occurs within currently available transport mechanisms in laparoscopic instruments can be attributed to the selected method of transport, i.e.: aspiration (also commonly known as suction). The combination of modes of less-than-optimal functioning are referred to within this report as sub-optimal transport behaviour. The different modes of sub-optimal behavior limit the transport rate and the reliability with which the tissue can be extracted.

**Methods:** An analysis of the modes of sub-optimal behavior was used to formulate a list of qualitative and quantitative functional requirements which were used in order to produce several conceptual solutions. These conceptual solutions were subsequently divided into categories which are mutually exclusive and collectively exhaustive (the ACCREx method). The most promising conceptual solution was developed into a prototype and is based on the egg-laying needle in insects. The prototype was subsequently subjected to a test procedure in order to determine if it was able to transport tissue and to investigate several factors which may influence the transport rate. The effects of the gelatin mixture density, particle presence, motion sequence were assessed in several sub-experiments. In addition, minced meat was transported in order to accurately mimic morcellated tissue.

**Results:** From the results of Sub-experiment I it can be concluded that there was a statistically significant difference in inverted transport rate between the different batches of pure gelatin artificial tissue mimicking material ( $F(2,13) = 16.25$ ,  $p = 0.0003$ ). The average inverted transport rates for the batches D1, D2 and D3 are respectively  $ITR = 2.4984 \pm 0.5428 \frac{mg}{s}$ ,  $ITR = 4.2068 \pm 0.7379 \frac{mg}{s}$  and  $ITR = 2.5087 \pm 0.3360 \frac{mg}{s}$ . The highest ITR was attributed to mixture D2. From the results of Sub-experiment I it was also concluded that there was no statistically significant difference in inverted transport rate between the different batches of grainy gelatin artificial tissue mimicking material ( $F(2,10) = 0.25$ ,  $p = 0.7834$ ). The average inverted transport rates for the batches G1, G2 and G3 are respectively  $ITR = 4.3392 \pm 1.9478 \frac{mg}{s}$ ,  $ITR = 3.5579 \pm 1.7543 \frac{mg}{s}$  and  $ITR = 3.7950 \pm 1.2725 \frac{mg}{s}$ . The addition of particles was not statistically significant: the differences between D1 ( $ITR = 2.4984 \pm 0.5428 \frac{mg}{s}$ ) and G1 ( $ITR = 4.3392 \pm 1.9478 \frac{mg}{s}$ ) ( $h=0$ ,  $p = 0.0762$ ), D2 ( $ITR = 4.2068 \pm 0.7379 \frac{mg}{s}$ ), G2 ( $ITR = 3.5579 \pm 1.7543 \frac{mg}{s}$ ) ( $h=0$ ,  $p = 0.4347$ ) and D3 ( $ITR = 2.5087 \pm 0.3360 \frac{mg}{s}$ ) and G3 ( $ITR = 3.7950 \pm 1.2725 \frac{mg}{s}$ ) ( $h=0$ ,  $p = 0.0636$ ). Statistical analysis between the hexasected motion sequence (DH2) and trisected motion sequence (DT2) show that there was no significant difference in inverted transport rates DS2 ( $ITR = 2.5375 \pm 0.8870 \frac{mg}{s}$ ) and DT2 ( $ITR = 3.6754 \pm 2.1387 \frac{mg}{s}$ ) ( $h=0$ ,  $p = 0.3182$ ). Sub-experiment III shows that the prototype was able to transport compacted minced meat. The average inverted transport rate of the batch of minced meat is  $ITR = 2.1917 \pm 1.1367 \frac{mg}{s}$ .

**Conclusions:** The prototype has shown that the friction-based transport principle has the potential of becoming a viable and reliable alternative to suction as a transport method within laparoscopic instruments. Future work should be directed towards improving the speed with which transport occurs, to investigate what improvements can be made to increase the reliability and the development of the proof-of-principle prototype into a fully functional medical device.

## Index terms

Laparoscopic - Transport - Mechanism - Friction-based - Biological Inspiration



# 1 Introduction

## 1.1 Background: Transporting Material

The objective of transport is straightforward: to transfer an object (or multiple objects) from one location to another. Throughout the evolution of technology mankind has created a substantial amount of different transport methods of which interesting examples include the Archimedean screw and the Marly of which schematic representations are shown in Figure 1. The aim of both these examples of transport mechanisms is to transfer water from one location (i.e., a river or stream) to another (i.e., higher situated gardens). The Archimedean screw allows for the turning of the handle at (c) in a counterclockwise fashion to transport liquid. The Marly machine uses the current within a river (direction of flow indicated by the blue arrow) to rotate the wheel (d) along the path indicated by the curved blue arrow. This wheel is connected to a hammer-shaped object at (e) which activates the bar at (f) resulting in a seesaw-motion. This bar is connected by pistons to the tubes shown at (g), which consequently move up and down, creating a sub-ambient pressure in the pipes at (g). This decrease in pressure allows the mechanism to suck in water from the river (h) in order to pump water through the system of pipes onto a higher level. Liquids are known to adapt to the form of the container, which simplifies transport through a tube to a large extent when compared to objects with other material states, of which there are three: solid, gas, and plasma. Thus, when transporting liquids, the maximum volume of the container can be utilized. Though the transport of liquids also contains downsides, most notably the inability to discretely distinguish between segments of the total volume which would be the case for, e.g., a pair of marbles. In addition, leakage is a concern associated with transport of liquids. In the case of other examples of transport such as transport of solid matter through a tube (whereby the tube is sometimes also referred to by the terms: vessel, pipe, duct, channel or carrier in literature) which can be obstructed by a variety of reasons. However, the transport of matter through vessels is of great importance to a large amount of industries. The transport solution that is discussed in this document focuses on one field of application and use the circumstances related to this field

of application in order to provide a working environment and therefore, requirements for the design. However, it must be stressed that the continuous mode of transport discussed here can in theory be applied to a variety of other industries and fields of application.

In order to specify design requirements and identify relevant parameters for this project an area of application has been selected. In the case of this design process, the area of application is the medical environment. Tissue transport from the body of a host can be hindered by tissue which clogs the tube through which it passes, thus forming a blockade. The transport of tissue is of vital importance to medical conduct. Tissues that are harmful to the host, such as tumorous, infected, and dying tissue have to be extracted in order to prevent (further) harm to the host. In addition, tissues which require investigation through the taking of a biopsy, which can aid in identifying the malevolent nature of a tissue or to aid in the decision for a follow-up procedure, also have to be extracted from the host. The transport in both these examples can occur through a variety of methods.

The traditional method of surgery, commonly referred to as ‘open surgery’, consists of opening the patient by means of an incision through which the surgeon can view and extract the tissue directly. Another method of tissue transport is by means of laparoscopic surgery, which is a type of minimally invasive surgery. In laparoscopic surgery, a portal is created by means of a relatively small incision, approximately 5-15 [mm] in length, through which long and slender instruments, mostly endoscopes (narrow and long tubular examination instruments) and grasping equipment, can be inserted in order to extract material from the body of the host under indirect vision [1]. Proponents of laparoscopic surgery point to the benefit of a smaller incision for recovery purposes and cosmetic reasons, whereas the opponents of laparoscopic surgery criticize this method due to the reduced vision and the associated complications.

The instruments that are inserted into the body through the small entry incision are several millimeters in diameter (approximately 5 millimeters) which requires that tissues which need to be removed and exceed the diameter of the transport instrument have to be cut into

## 1. INTRODUCTION

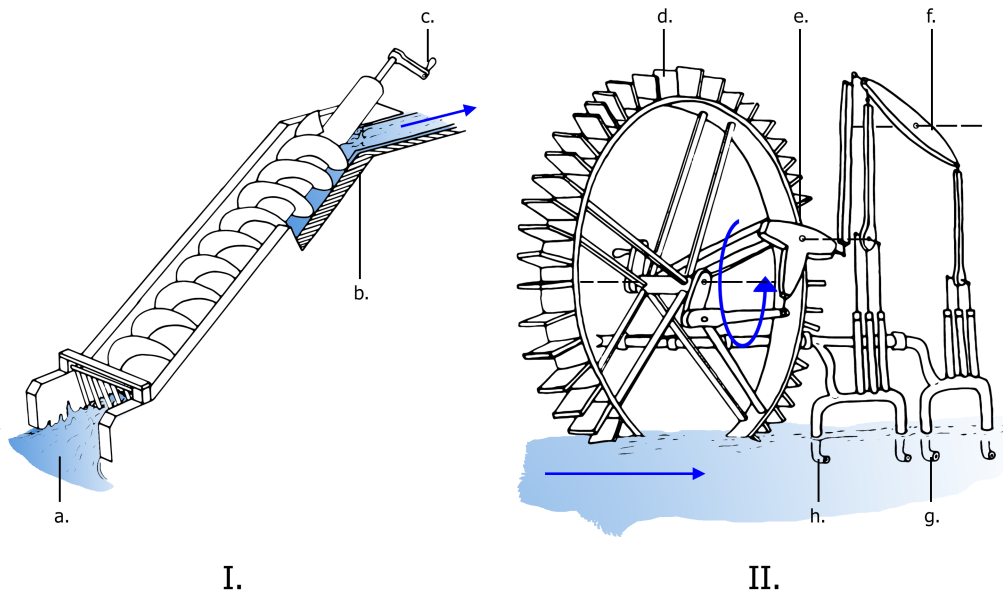


**Figure 1:** Schematic representation of two transport mechanisms. (I) Shows the Archimedean screw. The screw mechanism is aimed at relocating water (blue) from a lower level, at (a), to a higher level at (b). At the upper level one section of the mechanism was intentionally revealed in order to show the full screw. The direction of water flow on the higher level is indicated by the blue arrow. (II) Shows the mechanism known as the Marly machine. This mechanism uses the current within a river (direction of flow indicated by the blue arrow) to rotate the wheel (d) along the path indicated by the curved blue arrow.

smaller pieces. The fragmentation of tissue is known as morcellation and is achieved by using equipment referred to as morcellators. Morcellators are laparoscopic equipment which generally consist of a tube, which is provided with a means of transport such as suction, and a crushing or cutting element at the distal end.

### 1.2 State of the Art in Laparoscopic Transport Mechanisms

A patent search was conducted in order to investigate which methods of transport currently exist within laparoscopic equipment. Two patent databases, Espacenet and FPO, were consulted in order to provide a comprehensive view of extant instruments. The search queries for both patent databases are included within Appendix A. For the Espacenet database, the following search query was entered into the advanced search function:

```
(transport* OR evacuat* OR extract* OR retriev*) AND (instrument* OR device* OR tool*) AND tissue*
```

This patent search resulted in 190 documents. And in the FPO patent database, the following

search query was entered into the advanced search function:

```
ABST/((transport* OR retriev* OR extract* OR retract* OR evacuat*) AND (instrument* OR device* OR tool* OR morcellat*) AND tissue* AND laparos*) OR TTL/((transport* OR retriev* OR extract* OR retract* OR evacuat*) AND (instrument* OR device* OR tool* OR morcellat*) AND tissue* AND laparos*)
```

This patent search resulted in 48 documents. After exclusion and removal of duplicates 25 out of the 238 documents were included in this patent analysis. For additional information on the background of the advanced search queries, please see Appendix A. In the existing equipment, two fundamentally different modes of transport can be identified. The equipment that is contained within the branch of the first mode consists of instruments which extract parts of tissue in a piece-by-piece fashion. This mode shall be referred to as the *discrete* mode, please see Figure 2. (I) shows a medical grasper, US patent number 2004/0054377 A1 [2], consisting of an outer tube with handles and an inner tube with the grasping element,

## 1. INTRODUCTION

in which the inner tube is able to move freely throughout the outer tube. The three-pronged wire end on the right end of the instrument at (b) can be retracted by pulling the circular button on the left at (a) in the direction of the arrow. Through this motion, the three-pronged grasping element moves inwards on a piece of tissue (as indicated by the arrows) and can be pulled out by withdrawing the grasping element. According to the aforementioned definition, the transport system in instrument shown in drawing I qualifies as discrete. (II) shows a tissue retrieval system, US 2011/0184311 A1 [3], which functions in a similar fashion to the instrument shown in drawing I in the sense that its inner and outer tube can move relative to each other. However, instead of a grasping element this instrument is able to extract tissue through a foldable bag at (a), which can be pulled through the outer tube by moving the retracting handle at (b), in the direction of the arrow. (III) shows an electromechanical morcellation instrument, international publication number WO99/58066 [4]. The tissue is minced by the blades at (a), operated by the handle at (b), after which the resected tissue is sucked through the tube at (c) in the direction of the arrow. (IV) shows a morcellator head which can be attached to a laparoscopic tool in order to provide a means of morcellating and transport tissue. This morcellator head, international patent number WO 2014/066542 A1 [5], grinds up tissue through the rotation of the gear-shaped knives on the left of the morcellation head, at (a). The transport of the resected tissue will take place by means of aspiration at (b), in the direction of the arrow, and can therefore be considered a continuous transport system. In Figure 2, the instruments are boxed together by the nature of their transport system, i.e., discrete or continuous. Discrete modes of transport are characterized by the fact that the transport of tissue is intermittent and maximum amount of tissue transported is dependent on the amount of active transport attempts and the maximum volume of the container used for transport. *Continuous* modes of transport are characterized by their constant mode of operation. The maximum amount of tissue transported in this mode of operation is dependent on the transport rate and the length of operating time. By making the distinction between operating modes mutually exclusive, all analyzed equipment can be categorized in one of either categories, but never both. Furthermore,

the emphasis of this categorization procedure is on the *intended* mode of operation and not on accidental or sub-optimal behaviour modes. For example, if a continuous suction operated transport mechanism is blocked by a piece of tissue during transport, the mode of operation has been temporarily intermitted and it can be argued that the transport mode is discrete. However, such cases will be not included into this categorization procedure. A schematic representation of several patent drawings of existing laparoscopic devices and their intended modes of transport can be found in Figure 2. The drawings I and II both represent discrete modes of operation. In both these examples, the piece-wise transport of tissue is achieved by means of manual retraction, indicated by the direction of the arrows, of an inner tube, containing either a grasper or a foldable bag, within an outer tube. Instruments in which the transport takes place by means of aspiration are represented by examples III and VI. In both these instruments the transport of matter is achieved by means of suction. In addition, a selection of morcellator heads which are currently used is shown in Figure 3. These morcellator heads generally consist out of two tubes in which the outer tube is fixed and the inner tube is free to rotate or move linearly relative to the outer tube. The outer tube is provided with an opening (in A, B and D) and the inner tube is sharpened and fashioned into either a knife blade in order to resect tissue or a serrated knife blade for grasping and resecting tissue. After resection, the piece of tissue is sucked into the tube and extracted out of the body. Considering that the morcellation of the tissue (in A, B and D) is discrete in its function, the transport by means of suction, given constant pressure, is continuous. While the perpetual resection and transport of tissue by laparoscopic devices will inevitably lead to the filling of a container outside the body and considering that the holding capacity of the container is limited, one might argue the continuous transport category defined here is eventually also discrete. However, the defining element in this definition will be the amount of material which can be extracted in a single active transport attempt. An attempt, in the definition of this document, is characterized by a *single entry into the body* and a *single withdrawal from the body*. For example, if instrument II in Figure 2 is used in order to retrieve a piece of tissue from within a body, the holding capacity of the container shown at

## 1. INTRODUCTION

(a) limits the amount of tissue which can be extracted in one single attempt. However, the continuous mode of transport of instrument III in Figure 2, i.e., aspiration, does not require the instrument to be withdrawn in a single transport attempt and allows for continuous functioning.

### 1.3 Problem Definition

Currently existing transport mechanisms in tubes, primarily those applied in laparoscopic surgery, are subject to a large amount of functioning limitations which commonly result in sub-optimal behaviour. In this problem definition a distinction can be made between the two most widespread transport methods, i.e., continuous and discrete methods of transport. The current continuous transport systems that are coupled to morcellating devices are mainly based on aspiration, i.e., air suction. A schematic representation of the aspiration transport method is shown in Figure 4-A. Aspiration is achieved by lowering the pressure in the tube to a sub-ambient pressure. However, numerous problems arise from aspiration based transport. Firstly, due to several phenomena, tissue extracted by suction has a tendency to stick to the inner tube surface and clog the instrument. Furthermore, tissue lumps that are aspirated into a tube may get damaged, which can negatively influence investigation in the case of a biopsy.

There are also several inconveniences related to aspiration. First of all, instruments that rely on transport due to aspiration have to be connected, by cable, to a power source which produces a pressure difference. Secondly, the suction that is created in the tube of the instrument does not only affect the desired tissue but also the surrounding tissue. In the case of aspiration in an environment containing several types of liquid, discrimination between the suction of different types of liquid is nearly impossible.

Transport mechanisms that are coupled to discrete modes of transport are also prevalent among medical laparoscopic equipment. For example, consider a laparoscopic grasping instrument which is introduced into the body through a portal hole. The volume that can be extracted with one attempt is limited to lumps of tissue which can be (1) grasped by the instrument and (2) which diameter is smaller than that of the portal hole. In

addition, piece-wise tissue transport by means of a grasping instrument is not only relatively time consuming but also prone to failures regarding grasping contact with the tissue, e.g., slipping, returning to the exact previous location and damaging of tissue. Furthermore, the damaging of tissue fragments can inhibit subsequent microscopic investigation in the case of biopsies and can scatter tissue fragments that are potentially malign to the host. For biopsies and the removal and transport of small amounts of tissue a manual grasping instrument and a laparoscopic cutting tool can be utilized. A schematic representation of a grasping transport method is shown in Figure 4-B. This mechanism is characteristic for manual grasping laparoscopic equipment.

An example of an existing retrieval instrument which provides a continuous method of transport, by means of a grasper, is shown in Figure 5. This example shows a power morcellator from *Johnson & Johnson* which extracts material by grasping a piece of tissue and pulling it through a tube which has a sharpened edge. This sharpened edge is assumed<sup>1</sup> to be rotating at the moment of transport and the piece of tissue is subsequently resected and pulled through the tube. This mechanism is considered to be continuous since the resection of the total amount of tissue that has to be extracted can, in theory, be achieved by one entry attempt. However, it must be acknowledged that this method of transport can take multiple attempts in which case it would be considered discrete. This transport method is shown in Figure 4-C.

### 1.4 Goal of this Study

The goal of this study is the design, testing and presenting of a new method for continuous transport which is not subject to the problems associated with the current methods of transport in medical devices and which is embodied within a prototype. It must be stressed that the prototype will not be able to separate a piece of tissue from the surrounding biological tissue. The focus and goal of this study is

---

<sup>1</sup>Since the sale of several power morcellators, including the one shown here, has been prohibited in the United States after lawsuits against the use of such devices were successful, information regarding this power morcellator is scarce and mostly focuses on the side effects associated with its use rather than the way it functions. The functioning of this instrument is therefore based on knowledge of similar equipment.

# 1. INTRODUCTION

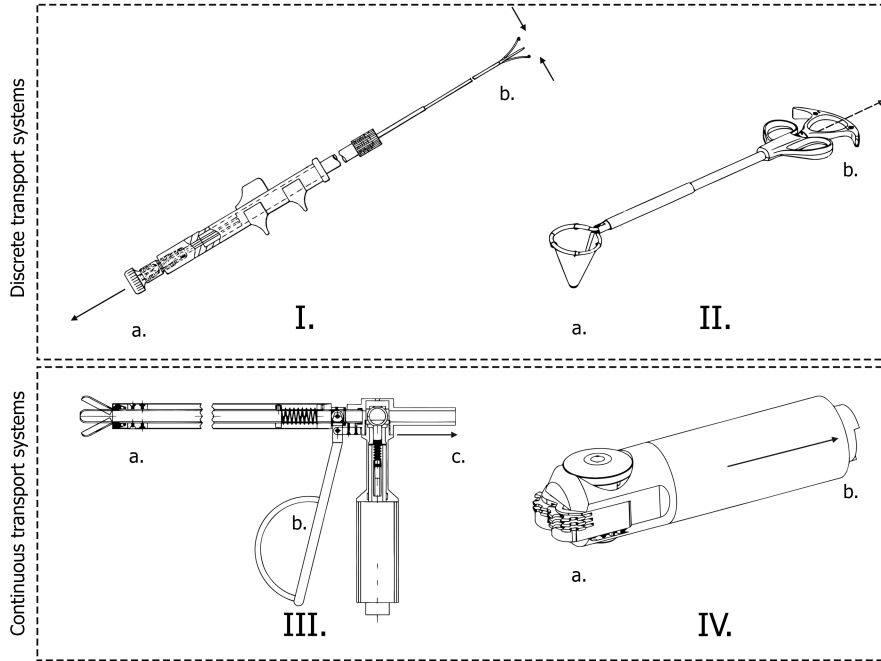


**Figure 2:** Examples of four patent drawings which broadly represent currently existing transport systems in laparoscopic medical equipment. (I) shows a medical grasper, US patent number 2004/0054377 A1 [2], consisting of an outer tube with handles and an inner tube with the grasping element, in which the inner tube is able to move freely throughout the outer tube. (II) shows a tissue retrieval system, US 2011/0184311 A1 [3], which functions in a similar fashion to the instrument shown in drawing I in the sense that its inner and outer tube can move relative to each other. (III) shows an electromechanical morcellation instrument, international publication number WO99/58066 [4]. (IV) shows a morcellator head which can be attached to a laparoscopic tool in order to provide a means of morcellating and transport tissue.

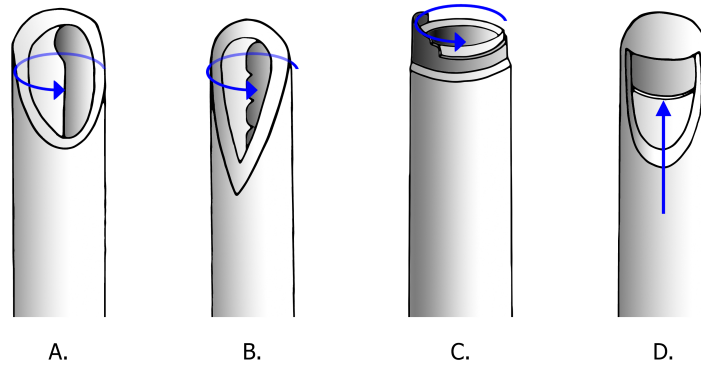


**Figure 3:** Schematic representation of four morcellator heads which are currently in use for the morcellation of tissue in laparoscopic equipment. In order to provide a cutting function, the inner tube is provided with a cutting edge (of which the cutting direction is indicated by the blue arrow) in each example and is able to rotate (A, B and C) or translate (D) relative to the outer tube. The piece of tissue which is consequently cut from its attachment surface is subsequently sucked into the tube. Variations on similar equipment are common and consist largely out of different inner tube slicing edges/contours. The volume in the tube is brought down to sub-ambient pressure in order to create a means of suction in order to extract tissue from its resection site to a volume or container outside of the body.

on the transport system and does not offer the function of disconnecting tissue from its location. This prototype will subsequently be subjected to a repeatable (close matching of the results of successive experiments under identical conditions) and reproducible (close matching

## 1. INTRODUCTION

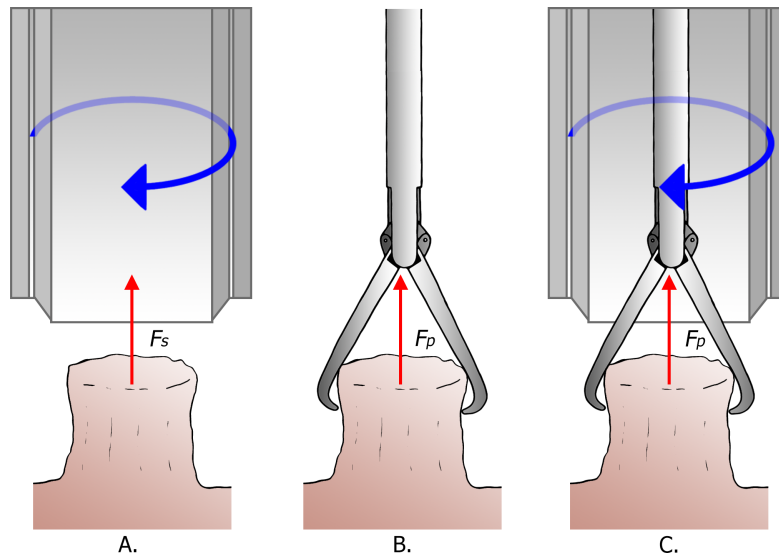


**Figure 4:** Schematic representation of three forms of transport used in extant equipment. (A) shows the method of transport based on aspiration. A suction force  $F_s$  (shown in red) is created by decreasing the pressure within the inner tube of the instrument which therefore sucks matter into the tube at the distal end. It should be noted that this example considers a rotating inner tube (direction of the blue arrow) and a fixed outer tube. The cutting is done by the rotating inner tube. (B) shows a grasping element at the distal end of a retrieval instrument which grasps a piece of tissue, represented by the pulling force  $F_p$  (shown in red), and is consequently withdrawn in order to retrieve this piece of tissue. Resection of this piece of tissue in (B) may occur by means of an additional cutting instrument, or by a rotating inner tube with a sharpened edge such as the one shown in (A). (C) shows a representation of the cutting and transport procedure for the *Johnson & Johnson electromechanical morcellator* (which can be found in Figure 5).

of the results under changed conditions) test procedure in order to validate its functionality and illustrate the working principle. The results of this experiment and the entirety of the design process will be collected and presented in this report.

### 1.5 Layout of this Report

In the ensuing sections the reader will encounter several distinct phases of the design process. At the outset an analysis of the existing problems relating to the transport of tissue in currently existing instruments is executed. After these problems have been identified the design requirements are listed and the subsequent conceptual solutions will be presented. These conceptual solutions (also referred to as concepts) will then be analyzed and compared and the most promising conceptual solution will be selected. This final conceptual solution will subsequently be developed into a functional prototype and this prototype will be subjected to a test procedure after which the results and the limitations of the design will be discussed.

Finally, these preceding phases will allow us to reach a conclusion on the functionality of this transport mechanism and give recommendations for future research/work.



**Figure 5:** *Johnson & Johnson* electromechanical morcellator. This example shows a power morcellator from *Johnson & Johnson* with a power source and two spare parts. The grasping element at the distal end of the instrument is used to extract tissue. As the tissue passes the sharpened orifice, also located at the distal end, the tissue is resected from the surrounding tissue. Instruments such as the one shown here have been the subject of several lawsuits in 2015 regarding the spread of postoperative malignant cancer as a result of the use of power morcellators. Picture acquired from [6].



**Figure 6:** *LiNA Medical* electromechanical morcellator. This example shows a power morcellator from *LiNA Medical*. The suction provided in this instrument at the distal end is used to extract tissue and while passing the sharpened orifice, also located at the distal end, the tissue is resected. Picture acquired from [7].



## 2 Sub-optimal Behaviour in Laparoscopic Transport Mechanisms

### 2.1 Introduction to Sub-optimal Behaviour Modes

*Failure modes* refer to several distinct modes of operation through which the intended operating manner of a device is not achieved. The intended operating manner of transport mechanisms which are under investigation in this study is considered to be the continuous transport of biological material, mostly solids and liquids, in medical applications. Solid biological material consists of tissues such as cancerous tissue and infected parts of organs. A distinction regarding liquids can be made on the basis of viscosity properties. Since liquid transport from the body is relatively simple to achieve for liquids which do not change in viscosity relative to the amount of applied pressure, the focus will be on liquids that do not conform to this behaviour. In other words, pumps and similar equipment apply shear stresses to a liquid in order to transport it through a tube. If the viscous properties of this liquid remain constant as a result of a change in applied pressure it is consequently referred to as being *Newtonian*, named after the discovery of a variation on the aforementioned relation by Sir Isaac Newton. While liquids which exhibit perfect Newtonian behaviour do not exist, a classic example of a liquid material state which approaches Newtonian behaviour quite accurately is water. Consequently, the transport method that is described within this report focuses on transporting materials which are either solids and/or non-Newtonian liquids. A good example of *non-Newtonian* behaviour is that of a cornflour and water mixture. The mixture responds like a fluid when stirred gently with a stick, but becomes more viscous as the stirring increases in speed. Even more surprising is that the surface of a volume of such a mixture can be struck with a fist or hammer and responds to such a strike with behaviour more akin to that of a flexible solid material like rubber. Biological examples of non-Newtonian liquids include blood and fat tissue. In the case of transport mechanisms intended for laparoscopic procedures, the sub-optimal behaviour modes that are of most importance to this study consist of modes which either (I) delay the transport of material through a tube by means of a constriction, or (II) inhibit

the continuous transport of material in a tube through a complete obstruction. In the ensuing section the modes of operation that lead to sub-optimal behaviour of the extant applied transport mechanisms, which are primarily based on aspiration, will be analyzed and the parameters that contribute to sub-optimal behaviour will be discussed. The different sub-optimal behaviour modes will be categorized based on what shall be described as different types of interaction friction. Information on several principles concerning fluid behaviour (i.e., liquid flow in narrowing and expanding ducts; Newtonian and non-Newtonian fluid behaviour; flow loss in ducts and boundary layers) is given in Appendix B.

### 2.2 Categorization of Sub-optimal Behaviour Modes

A subdivision strategy has been formulated in order to cover all identified transport modes of sub-optimal behaviour related to suction transport and help identify types of sub-optimal behaviour which might have been overlooked. All identified modes of sub-optimal behaviour are divided on the basis of the state of the matter which is transported. Three material states can be distinguished: ‘solid state modes’, ‘liquid state modes’ and ‘mixed state modes’. The subdivision has been graphically represented in Figure 7. The identification of the different modes of sub-optimal behaviour has been achieved by author and subsequently confirmed by experts on pipe flow, medical instrumentation and sub-optimal behaviour modes associated with suction. It should be noted that, while some of these modes described here may lead to complete transport failure, most of these modes will lead to sub-optimal behaviour to a lesser extent, i.e. the transport rate/function is lower than the intended transport rate that the instrument was designed for. However, the modes described here can, under more extreme circumstances, also eliminate the transport function entirely. In addition, the author acknowledges that the material state mode responsible for impaired functioning of the instrument can be difficult to identify. The author further acknowledges that some modes can also appear to occur in the ‘mixed state modes’ category. For example, rotational jamming can occur within a turbulent liquid flow. In such cases the author argues that both the turbulent liquid flow *and* the rotational jamming are separate causes for the impaired

functioning of the instrument. The situations in which specifically the combination of solid and liquid modes is responsible for the chain of events that leads to sub-optimal behaviour were placed in the ‘mixed state modes’ category.

### 2.3 Sub-optimal Behaviour Modes

#### 2.3.1 Aspirated Tissue Diameter Expansion

For a schematic representation of the distinct steps leading to this phenomenon, please see Figure 8. When a piece of flexible biological material, whilst still being attached to surrounding tissue, is sucked into the tube of a morcellation and/or retrieval instrument, the material is elongated from its attachment surface. While the volume remains equal, the diameter will consequently decrease slightly. After the resecting knife of the morcellator has severed the base of the piece of tissue from the attachment surface, the piece of tissue will be sucked into the tube. However, since the attachment surface has now been disconnected from the piece of tissue, there is no more counter force to the force created by the suction within the tube. The stretching of the tissue piece due to the forces acting in opposite directions will be undone and the length will decrease again. Due to the fixed volume, the result of this decreasing length will be an increase in diameter. This effect is called *Poisson’s effect* and a measure for the amount of this effect is the *Poisson’s ratio*. Poisson’s ratio is largely dependent on the type of material under strain. The increased diameter will now obstruct the tube of the instrument and prevent any further material from being sucked up into the tube or limit the transporting function of the instrument by negatively influencing the amount of suction exerted on the instrument’s distal end.

#### 2.3.2 Accumulated Obstruction Friction

In the case of relatively solid pieces of matter, the friction with the inner wall of the tube impedes the continuous rate of transport. The transport of the three pieces of tissue shown in Figure 9-A is characteristic of such sub-optimal behaviour. The pieces of tissue shown here experience mechanical friction due to the surface contact with the inner wall. Let us consider the following situation: a piece of biological tissue, Figure 9-B, which is roughly the same diameter as the inside of the tube

and is covered with blood and fatty tissue is sucked up into the tube. The segment quickly becomes stuck into the inner tube and the blood and fatty tissue fill the spaces through which suction is still applied, Figure 9-B. In addition, a multitude of smaller segments or several long strands of tissue (*coiling*) can also lead to such obstruction phenomena. Blood clotting can also be considered a type of accumulated obstruction friction. The interaction between the segment and the inner tube now consists of two modes, one of which is mechanical friction and the other being a viscous layer of liquid between the segment and the inner tube wall surface (B). The blood and fatty tissue are now subjected to shear forces which increase as a result of the relatively high velocity. This increased velocity is due to the fact that the applied suction within the tube is spread over a significantly smaller surface. This in turn, is caused by the accumulated tissue segments which now obstruct a large part of the inner tube. Because these liquids have a relatively high viscosity and are subject to high velocities and shear forces they resist the flow within the tube due to their non-Newtonian behaviour. As the amount of suction is increased in order to remove the blockade, resulting in higher shear forces and higher velocities, the effects of the obstructive behaviour are magnified. In addition, the fact that larger pieces of tissue undergo an increased amount of drag relative to smaller pieces of tissue increases this effect. Due to the increased drag and friction, the larger tissue pieces move at a lower speed. As the smaller particles overtake the larger particles, the cluttering of particles and the subsequent obstructing effect is increased.

Moreover, there is a phenomenon in dredging and offshore technique which may be also relevant to this sub-optimal behaviour. When pieces of matter which are relatively easy to deform adhere to each other, a situation can occur in which the ‘ball’ formed by the sticking objects can lead to a pipe obstruction. In the case of medical applications, the sticking tissues will most likely consists of non-Newtonian liquids such as fat or blood which adhere to each other. The solution for removing the forms of accumulated obstruction mentioned here may require the user to discontinue the build-up of suction in the tube in order to eliminate the increased viscosity effect of the non-Newtonian liquid and slowly regain suction in order to restore transport functionality and retrieve

## 2. SUB-OPTIMAL BEHAVIOUR IN LAPAROSCOPIC TRANSPORT MECHANISMS

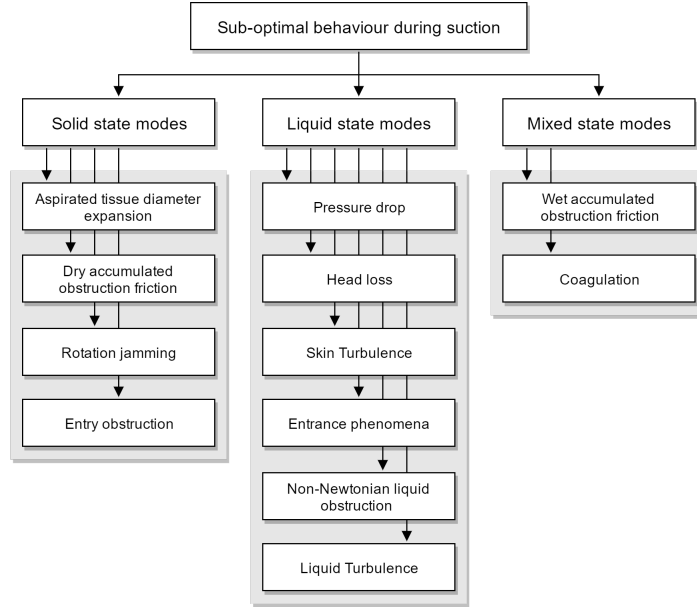


**Figure 7:** Schematic diagram of the categorization of the sup-optimal transport behaviour modes during suction conforming to the subdivision strategy. Categorization will be achieved on the basis of the material state of the matter that is transported. The total amount of modes can be subdivided into the three major categories: ‘solid state modes’, ‘liquid state modes’ and ‘mixed state modes’.

the elements currently within the tube of the instrument. Nonetheless, the aforementioned solution cannot be considered an intended mode of operation and is consequently a form of sub-optimal behaviour in itself.

### 2.3.3 Rotational Jamming

The sub-optimal behaviour mode known as rotational jamming can be described as the rotary motion of a piece of relatively solid tissue which blocks the tube’s diameter and even though it may not entirely block the passage at once, it does serve as a barrier for other pieces of tissue which can adhere and clog to one another and eventually will lead to failure regarding the transport of tissue. A schematic representation of such a scenario is shown in Figure 10. In drawing (A) the relatively solid pieces of tissue are visualized within the tube. The direction of the force  $F_s$  created by the suction is indicated by the arrow. This mode will be triggered when the relatively long and stiff piece of tissue is rotated such that it spans across the inner diameter of the tube. Since this piece will probably not obstruct the entirety of the passage there will still exist small pockets through which the suction force is exercised. These passages will be more prone to obstruction since smaller pieces will move into these smaller channels

with relatively less velocity and consequently these channels will also get obstructed. The pieces of tissue still to be extracted will clutter against this large piece of debris and form an increasingly solid barrier (B). The friction forces will eventually counteract the suction force and the transport functionality of the instrument will be eliminated entirely.

### 2.3.4 Entry Obstruction

If a piece of tissue of significant size is sucked up into the tube by means of suction, the entry to the tube can get (partially) obstructed, see Figure 11. This obstruction will limit the functioning of the transport due to the constriction of the flow diameter. The blockage will limit the amount of possible liquid flow and will also limit the transport of (semi-) solid pieces of tissue. In addition, the obstruction of smaller solid pieces of tissue will lead to multiple situations which are similar to dry accumulated obstruction friction.

## 2. SUB-OPTIMAL BEHAVIOUR IN LAPAROSCOPIC TRANSPORT MECHANISMS

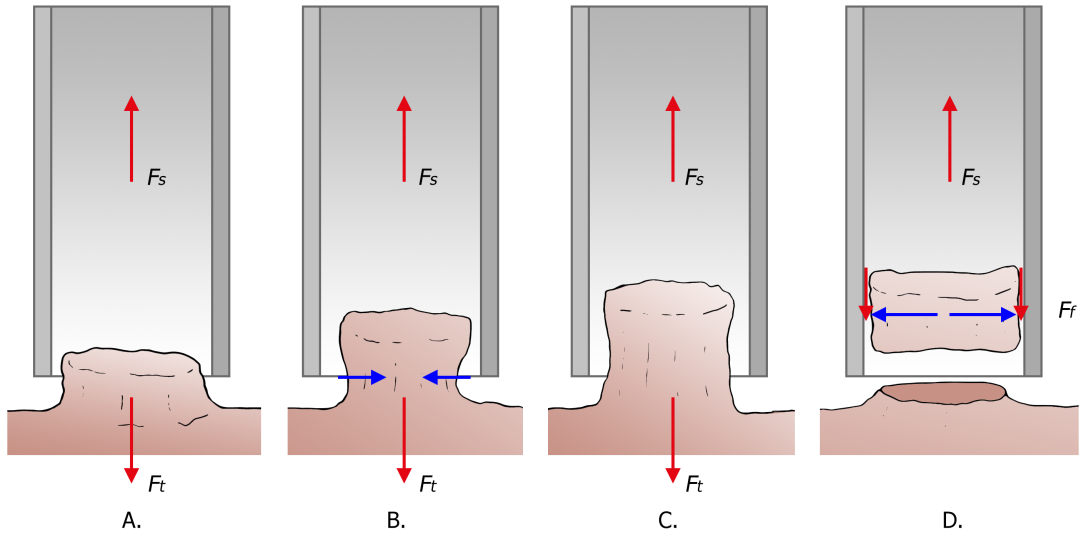


**Figure 8:** Schematic representation of the sub-optimal behaviour known as *aspirated tissue diameter expansion*. This schematic representation displays the steps by which this mode can occur. In grey, a cross section of the tube of a transport instrument is displayed, the pink areas represent tissue. The arrows representing forces are shown in red, while the arrows showing the deformation directions are shown in blue. In drawing (A), the tissue that is meant to be resected is enveloped by the distal end of the transport instrument. The upward pointing arrows within the tubes indicate the force  $F_s$  [N] created by the suction, while the downward pointing arrows indicate the force  $F_t$  [N] exerted by the tissue in reaction to  $F_s$  [N]. (B) shows the tissue being sucked into the tube of the distal end of the transport instrument and stretches slightly. In (C), the tissue is stretched even further. Between steps (C) and (D), independent of the method, the base of the tissue sample being enveloped by the tube is severed from its attachment surface. (D) further shows the tissue segment being sucked into the tube of the instrument. However, the diameter increases and causes friction  $F_f$  [N] with the inner surface of the tube as a result of the fact that  $F_t$  [N] is no longer able to exert force after the severing of the connection.

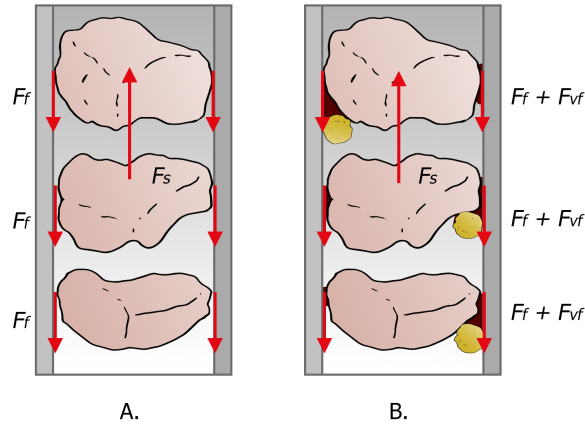


**Figure 9:** Schematic representation of the sub-optimal behaviour known as *accumulated obstruction friction*. In grey, a cross section of the tube of an transport instrument is displayed, the pink areas represent tissue. This representation displays the forces (shown in red) active in the situation without fatty tissue (yellow) and blood (brown) within the crevasses of the tube (A) and a representation of a situation with fatty tissue and blood (B), likewise noted with the term wet accumulated obstruction friction. The forces within the tube in situation (A) are solely represented by the forces due to mechanical friction ( $F_f$ ). The situation in (B) however, shows that now the openings in the tube are filled with fatty tissue and blood, which in turn create their own resistance to the suction force due to the high viscosity in combination with the non-Newtonian behaviour ( $F_f + F_{vf}$ ).

## 2. SUB-OPTIMAL BEHAVIOUR IN LAPAROSCOPIC TRANSPORT MECHANISMS

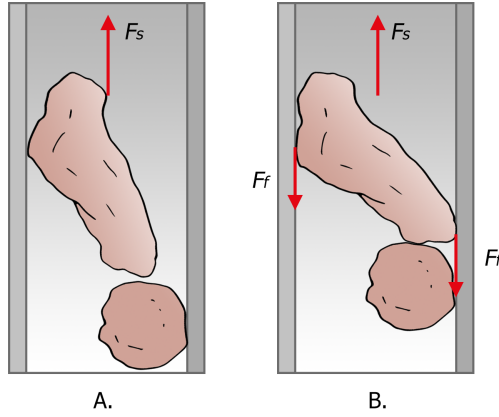


**Figure 10:** Schematic representation of the sub-optimal behaviour known as rotational jamming. The arrows representing forces are shown in red. In grey, a cross section of the tube of an transport instrument is displayed, the pink areas represent tissue. This representation shows two situations in which functionality is about to be impeded but still allows for transport, the first is shown in (A). The second situation, shown in (B), shows that the largest of the two pieces of relatively solid tissue is caught between opposite sides of the internal tube wall and hence creating a barrier for other debris and tissue objects which further limit passage along the tube. The friction forces  $F_f$  [N] which subsequently limit the passage of the piece of tissue are indicated by the arrows alongside the inner diameter of the tube. The direction of the force created by the suction, i.e.,  $F_s$  [N], is also indicated by the red arrow.

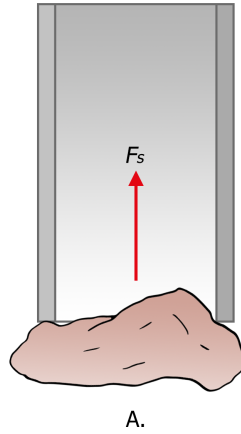


**Figure 11:** Schematic representation of the sub-optimal behaviour known as entry obstruction. In grey, a cross section of the tube of an transport instrument is displayed, the pink area represents a segment of tissue. This representation shows a situation in which the transport functionality is impeded (A) by blocking the entrance to the tube. The direction of the force created by the suction, i.e.,  $F_s$  [N], is also indicated by the red arrow.

### 2.3.5 Pressure Drop and Head-Loss

One of the friction loss phenomena, i.e., the boundary layer, is explained within Appendix B. However, in order to estimate an amount of pressure loss due to friction phenomena the Darcy-Weisbach equation (Equation 1) can be applied. The Darcy-Weisbach equation relates the pressure difference  $\Delta P$  in [Pa] to the length of the pipe  $L$  and the diameter of the pipe  $D$ , both expressed in meters [m]. In addition, the

velocity of the flow  $v$  in [ $\frac{m}{s}$ ] and the density of the liquid  $\rho$  in [ $\frac{Kg}{m^3}$ ] are related to the pressure difference. In order to represent the characteristics for different types of flow within different types of ducts, the dimensionless Darcy friction factor  $f_D$  (with typical values between 0 and 0.1) has been introduced. The expression of this experimentally verified quantity differs for laminar- and turbulent flow and for rough- and

smooth wall surfaces.

$$\Delta P = f_D \cdot \frac{L}{D} \cdot \frac{\rho \cdot v^2}{2} \quad [\text{Pa}] \quad (1)$$

Equation 1 can also be rewritten in order to obtain an expression which represents the loss of pressure due to a height difference known as the head-loss  $\Delta h$  in [m], please see Equation 2. In this situation, the suction applied should also counteract the forces of gravity. In Equation 2 and 3 the contribution of gravity to the pressure loss can be represented by the term  $\Delta P = \rho \cdot g \cdot \Delta h$  in [Pa]. If this equation is expressed per height unit  $L$  in meters [m] the dimensionless parameter  $S$  is obtained.

$$S = \frac{\Delta h}{L} = \frac{\Delta P}{L \cdot \rho \cdot g} \quad [-] \quad (2)$$

$$S = \frac{\Delta h}{L} = f_D \cdot \frac{1}{2 \cdot g} \cdot \frac{\langle v \rangle^2}{D} \quad [-] \quad (3)$$

Pressure loss due to a relatively limited height difference for a typical laparoscopic suction instrument is not necessarily of pivotal importance to the functioning of a transport instrument by itself. Nevertheless, this behaviour is still classified as sub-optimal since it inhibits the intended mode of operation and is applicable to every situation in which the instrument is not held absolutely horizontal.

### 2.3.6 Turbulence

Turbulence is a phenomenon which occurs during certain types of liquid flow and can be determined by calculating the Reynolds number. Turbulence is characterized by increased friction between the liquid layers and the irregular motion of the particles within the liquid flow. The turbulence that can occur due to the circumstances under which the transport mechanisms operate are related to the transport by means of suction. The turbulence between the layers of the liquid is denoted with the term *liquid turbulence*. The friction that occurs here is due to the fact that the particles are not contained by the viscous forces of the flow. Since these particles are no longer contained by the viscous forces, regional vortexes occur. This behaviour leads to a loss of energy since these interactions cause friction and consequently produce heat. The interaction with particles of rigid surfaces also increases the amount of friction. This friction mode will be referred to by the term *skin turbulence*. This is a different mode of sub-optimal behaviour, since the interaction includes two different entities.

### 2.3.7 Non-Newtonian Liquid Obstruction

The transport of non-Newtonian liquids, such as fat (or more specifically: white adipose tissue), takes place under aspiration. As mentioned before, the behaviour of non-Newtonian liquids is not the same as Newtonian liquids and can therefore pose difficulties in transport when compared to a Newtonian liquid such as water. The white adipose tissue discussed here is considered to be in a semi-liquid state. The boundary layer representation, which is a prediction of the velocity profile of the flow and its shape, can be used to estimate the behaviour of non-Newtonian liquids within laparoscopic suction equipment. In Figure 12, a small pipe representative of the sheath of a laparoscopic instrument is shown to have aspirated some fatty tissue into the tube (A). The velocity profile of this tissue and its behaviour is shown in (B). The parameters associated with the pressure difference  $P$  [Pa] in the tube of the white adipose tissue flow within the pipe can be represented by the Hagen-Poiseuille equation shown in Equation 4. This equation is an expression of the pressure difference within a tube and this in turn is a measure for the amount of material flow. It has to be noted that this equation does not reflect the situation at the entrance of the pipe, since pipe entrance flow phenomena are different from fully developed flow.

$$\Delta P = \frac{8 \cdot \mu \cdot L \cdot Q}{\pi \cdot r^4} \quad [\text{Pa}] \quad (4)$$

The parameters length  $L$  [m] and radius  $r$  [m] can be decided upon when designing the instrument. The volumetric flow rate  $Q$  [ $\frac{\text{m}^3}{\text{s}}$ ] is the property which is of most influence to current instrument design as it represents the amount of matter in volume which can be transported per time unit. Typical tissue removal rates for morcellation and transport devices range between several grams, approximately  $1.15 \cdot 10^{-4}$  [ $\frac{\text{Kg}}{\text{s}}$ ] for the *Steiner morcellator* by Karl Storz, to approximately  $6.73 \cdot 10^{-4}$  [ $\frac{\text{Kg}}{\text{s}}$ ] for the *VarioCarve morcellator* by Olympus [8]. While these removal rates may not be necessarily representative for volumetric flow rates for non-Newtonian liquids, they do provide an indication for the removal rate for similar procedures with tissue in comparable material states, since according to Driessen *et al.*: “the consistency of myomas (tumorous tissue) can be variable (e.g., soft, cystic, calcified, or very hard)”.

## 2. SUB-OPTIMAL BEHAVIOUR IN LAPAROSCOPIC TRANSPORT MECHANISMS

As explained within Appendix B, Equation 25, the radius is of great importance to the necessary pressure and velocity difference within the tube. In essence, the viscosity properties of fat increase when the shear force is increased. From the expression it can be gathered that such a decrease in pressure can be achieved by increasing the radius  $r$  [m], though the radius is always bound to the maximum diameter of the portal hole. The portal hole diameter consequently limits the ability to increase the diameter and therefore lower the pressure. Additionally, the viscosity will be greatest in the centre of the pipe as is shown in (B), since the velocity profile shows that the maximum occurs in the centre, see Figure 12. For small diameters this may completely diminish transport functionality due to the build-up of pressure within the tube which results in an increase in shear forces in the tissue segment and hence increases the viscosity of the segment. It must be noted that the velocity of the fatty tissue is limited at the interface with the pipe. It can be argued that the slower moving fatty tissue at the outside of the fatty tissue segment, represented by the sections between the pipe and the dashed lines in Figure 12 (A), may act as a kind of lubricant as the viscosity of these sections is lower.

The observation of the maximum velocity occurring in the centre of the non-Newtonian laminar velocity profile is also true for the velocity profile of laminar Newtonian flow shown in Figure 12-C. Nevertheless only the centre of the laminar Newtonian velocity profile is subjected to the largest velocity. This profile further shows that at either side of the maximum the velocity decreases until it reaches the inner tube diameter. Observed from the center line of the tube, each outward reaching velocity layer is provided by a slower moving adjacent velocity layer which acts as a lubricant. Lubrication in this sense is achieved by a less viscous material layer.

### 2.3.8 Entrance Phenomena

When a liquid is sucked into a partially submerged pipe, assuming that the flow in this example is turbulent, the suction within the pipe leads to the creation of small vortices, as indicated by the circular blue arrows in Figure 13. The creation of such vortices will lead to an increase in friction and will contribute

to sub-optimal functioning of the transport mechanism. However, it must be noted that the contribution of turbulence phenomena in this mode are minor compared to other sub-optimal behaviour modes.

### 2.3.9 Coagulation

Coagulation, also known as blood clotting, is a process in which blood is transformed from its liquid state to (semi-) solid state. When it transforms, it also passes the viscoelastic state. Coagulation is initiated when blood comes into contact with a foreign body, such as the steel tube through which it passes during transport, and can also be initiated by enzyme activation. Blood can only be extracted by means of a puncture or wound to the patient, introduced during the operation. The platelets within the blood flow adhere to a blood vessel under the influence of thrombin, or the metal tube, leading to an accumulation of blood platelets [9]. The speed with which this coagulation takes place increases when air is introduced into the reaction. This process can occur relatively quickly and the fact that blood coagulates in such a short period of time is a well established problem that inhibits, for example, the successful transport of blood during blood sampling procedures. Blood itself is subject to a liquid behaviour known as shear thinning. This entails that as the shear on blood is increased, its viscosity decreases. This would make it the opposite of an ideal lubricant. Therefore, the idea that moving blood can act as a type of lubricant is unlikely. However, for speeds which are significantly larger the viscosity between the layers is increased to such an extent that the liquid layer relative to each other will resist motion. This behaviour, known as the 'Stribeck effect', may lead to increased blood friction between layers at higher speeds and can therefore be considered to be a kind of lubricant. Concluding, blood can coagulate during the process of transport. If the blood clot is not adhered to an inner wall surface it can contribute to the accumulated obstructed friction modes described above. On the other hand, if the blood clot does come into contact with the wall, the result will be a constriction of the flow diameter within the tube.

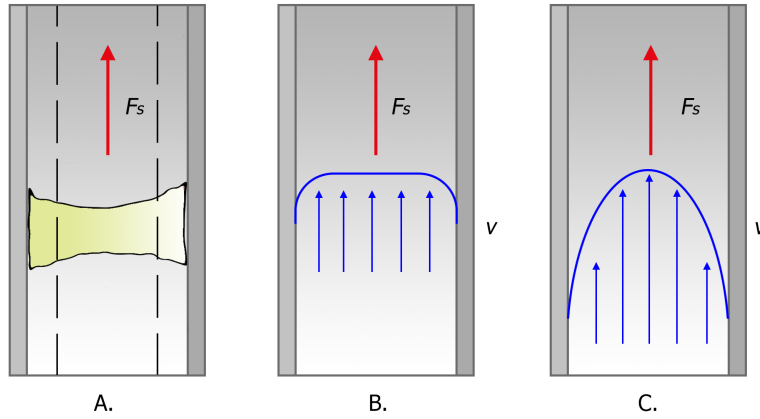


**Figure 12:** Schematic representation of the sub-optimal behaviour associated with the transport of non-Newtonian liquids such as white adipose tissue which exists in a semi-liquid state. This schematic representation displays the steps by which the sub-optimal behaviour can occur. In grey, a cross section of the tube of an transport instrument is displayed. The arrows representing forces are shown in red, while the arrows showing velocities are shown in blue. In (A) the transport of a piece of fatty tissue is visualized. The dashed lines represent the edges of what is considered to be a distinction between slow moving and fast moving fatty tissue. The velocity profile associated with laminar non-Newtonian liquid pipe flow which leads to this distinction is shown in (B). The velocity profile associated with laminar Newtonian liquid pipe flow is shown in (C).

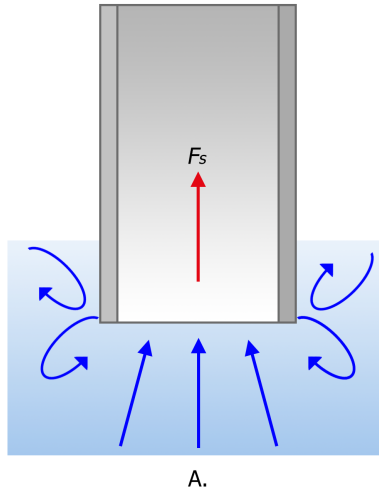


**Figure 13:** Schematic representation of the sub-optimal behaviour known as entrance phenomena. In grey, a cross section of the tube of an transport instrument is displayed, the blue area represents liquid. The blue arrows indicate flow directions. This representation further shows a situation in which the transport functionality is impeded (A) by flow losses due to entrance flow phenomena. The direction of the force created by the suction, i.e.,  $F_s$  [N], is indicated by the red arrow.

## 2.4 Current Alternatives to Aspiration

The modes of sub-optimal behaviour defined in the prior subsections describe the different situations through which such behaviour may occur. The different modes have been

categorized according to the interaction between the different material states. From this analysis it can be concluded that there are a multitude of situations which result in sub-optimal behaviour associated with transport by means of suction. One of the most crucial observations that can be made from the outset, is that the type of

## 2. SUB-OPTIMAL BEHAVIOUR IN LAPAROSCOPIC TRANSPORT MECHANISMS

obstruction can be caused by a large amount of factors, including the shape and size of the obstructing element(s), the consistency of the material, the amount of elements forming the obstruction, the conditions under which transport occurs, and the surface roughness of the interacting elements.

In order to evade the modes related to suction transport one might argue that mechanical transport by means of a grasper might be preferable. And for certain types of transport the use of a grasping instrument can indeed prove to be superior to suction. For example, the transport of relatively solid pieces of matter can be achieved by means of a grasping tool. If a piece of relatively hard tissue gets stuck during transport by means of graspers, the use of a relatively small amount of force and twisting manoeuvres can easily undo the obstruction of the pipe. In addition, the grasping instrument is not susceptible to sub-optimal behaviour due to pipe flow phenomena. Nonetheless, the use of a grasping instrument is also susceptible to several types of sub-optimal behaviour. The most obvious behavioural flaw of the grasping element relative to the suction instrument is that it is unable to transport or extract matter which is not relatively solid. Adipose tissue, for example, is relatively deformable and may be covered with some kind of (body) liquid which further impedes the transport. Moreover, grasping equipment is unable to transport liquid out of the body. Some difficulties can also arise from the discrete method of transport which is most common in grasping equipment. The piece-by-piece transport method which is most characteristic for the majority of currently existing grasping equipment is not only relatively more time consuming than continuous modes of transport but is also prone to introducing bacteria and other types of contamination into the body cavity. In addition, some design aspects which may negatively influence the functionality are associated with the use of grasping equipment. For example, the diameter of the outer tube through which the instrument is retracted should always be adjusted for the fact that the grasper at the distal end of the instrument should be able to be pulled inwards with a piece of tissue enclosed within the blades/shears, please see Figure 14-A. Another disadvantage of transport by means of a grasping element is that the beak of the transport instrument has to envelop a piece of tissue in order to grasp it

entirely, a representation of this disadvantage is given in Figure 14-B. In short, there must be space around the tissue in order to extract it. Thirdly, there should be a surface to make contact with, please see Figure 14-C. Finally, attempts to make the outer tube flexible or steerable are hindered by the fact that the tube contains an instrument within it, which should be able to bend and curve to the same extent as the tube and does not constrict the transport, please see Figure 14-D. A biopsy forceps, which is commonly enveloped within a flexible tube, should be able to bend in order to retrieve tissue. However, it is subject to buckling. In short, the identified modes discussed in this section all lead to sub-optimal behaviour since the intended mode of operation, i.e., optimal or intended behaviour, is diminished. These identified modes are mostly related to the transport mechanism which was chosen and not necessarily a result of occurrences that are not linked to the design of the instrument. As a concluding statement, the preferred method of transport is the continuous mode of transport, since this method does not require a constant re-introduction into the operation area and is therefore less time consuming and the working environment is less prone to contamination than discrete modes of transport.

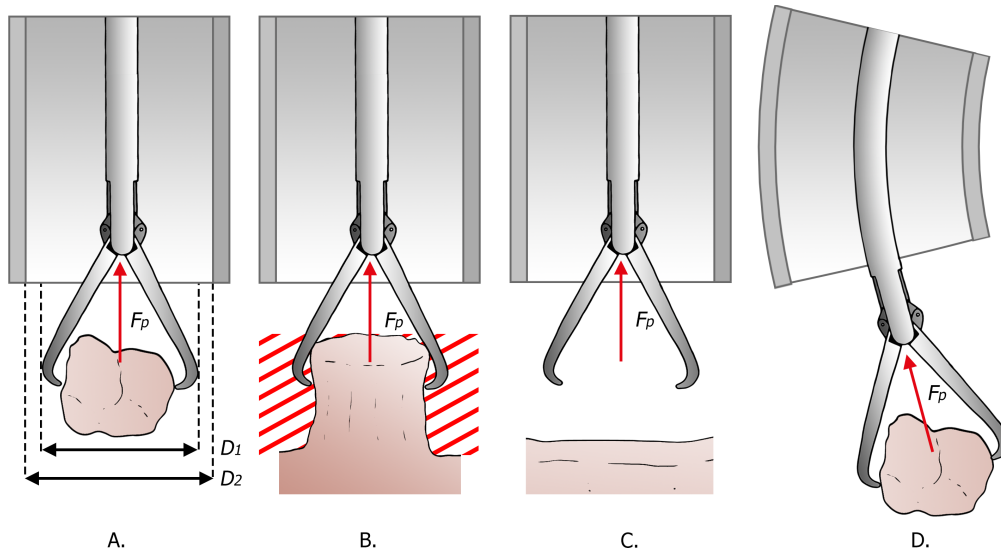


**Figure 14:** Schematic representation of the complications associated with the transport of tissue by means of mechanical transport. Forces are shown in red. In (A), the expanded diameter  $D_2$  necessary for transporting the grasping element combined with a piece of tissue, with a combined diameter of  $D_1$ , is shown. In drawing (B), the red hatched area indicates the amount of space necessary for the grasping beak to envelop and access the piece of tissue. In drawing (C) the situation in which there is no tissue to make contact with is shown. Drawing (D) shows the complications associated with the combination of the grasping element and the outer tube when bent. If this combination were to follow a curved path as shown here, transport by means of grasping a piece of tissue would be complicated by the beak's width.

### 3 Design Process of the Endo-Tubular Friction Carrier

#### 3.1 Design Goal

The goal of this design process, as stated in Section 1.4, is a new method of transport which is not subject to the sub-optimal behaviour associated with aspiration during transport as described in Section 2.3. Therefore, the focus will not be on adding to or improving upon current transport mechanisms to make them less prone to sub-optimal behaviour (e.g., by increasing the diameter) or by decreasing the effect of the sub-optimal behaviour on them (e.g., by increasing the pressure difference).

#### 3.2 Design Criteria

In order to provide boundary conditions and define several quantitative goals for the design process, the criteria in the sections stated below were established. Most of these criteria can be obtained from observing the conditions that currently existing transport mechanisms in laparoscopic equipment are subject to. If these criteria (or requirements) are met, it can be ensured that the novel transport mechanism will be able to surpass the transport function found in currently existing extraction devices.

##### 3.2.1 Geometric Requirements

**Transport Mechanism Length :** The transport mechanism should be able to be implemented and used in medical instruments which require a transport function. These instruments are currently approximately 250 mm long. It is the intention of the author to design and construct a transport method that is length independent or which can operate over a length of 250 mm. The desired transport mechanism length is denoted with  $L_d$  (see Figure 15).

**Transported Tissue Length :** The mechanism should be able to transport tissue segments regardless of the length of the tissue segment. However, the tissue segment has to be severed from the extraction site by a morcellator head in order to be transported. A tissue segment with a length of 5 mm as well as 200 mm long strips of tissue should be able to be transported: i.e., the transport mechanism is tissue length independent. The maximum tissue

length which can be transported is therefore only limited by the length of the transport mechanism.

**Transport Mechanism Diameter :** Internal catheters for suction and grasping equipment such as those reported by Driessen *et al.* [8] range from approximately 10 to 15 mm. The author of this document believes that the size of a transport mechanism can be further minimized if novel transport methods are applied. The desired outer diameter  $r_d$  of the transport mechanism is 5 millimeters, see Figure 15.

##### 3.2.2 Functional Requirements

**Only Transport :** The mechanism is intended for the transport of tissues, not the detachment of the tissue from the surrounding tissue or the morcellation of tissue. Processes which occur before transport were not the focus of this design process. However, it should be noted that this transport system should be able to manage all tissues which pass the currently existing morcellation heads.

**Continuous Transport :** The intended mode of operation for the transport mechanism is the *continuous* operating mode. The desired function of the transport mechanism should not be interrupted during service in order to clean or empty the transport mechanism to maintain in operation.

**Semi-solid Matter Transport :** The transport mechanism will be designed to transport solid matter and non-Newtonian liquids. In addition, it should be noted that the substance and solidity of the tissue on which the author will be focusing will be the tissue which can be morcellated by existing morcellator heads. Since the author is not developing a morcellator head, the final design will rely upon existing morcellation heads to decrease the size of the tissue to such an extent that the device discussed in this document will be able to transport it.

##### 3.2.3 Medical Requirements

**Laparoscopic Instrument Cleaning :** The new transport mechanism, discussed in this document, will be used in laparoscopic procedures. A functional prototype based on this new transport mechanism should

### 3. DESIGN PROCESS OF THE ENDO-TUBULAR FRICTION CARRIER

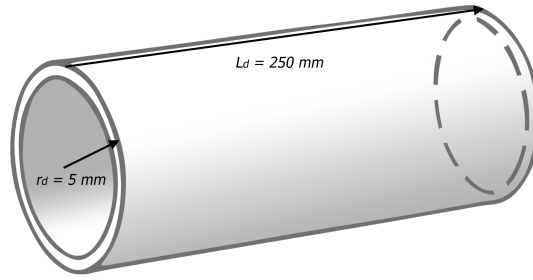


**Figure 15:** Schematic representation of the desired radius and the length of the transport mechanism. In grey, a cross section of a tube of a transport instrument is displayed. The desired radius and length of the transport mechanism are denoted with  $r_d$  and  $L_d$  respectively. Both of these parameters are measured in millimeters.

therefore be able to endure currently existing preparatory measures concerned with the decontamination and sterilization of surfaces of laparoscopic equipment. In addition, the transport mechanism should be able to be implemented into a hand-held device to conform to currently available methods of operating.

**Bio-compatible Materials** : In order for the mechanism to function safely, the materials that are used in the construction of the transport mechanism should all be biocompatible. In short, biocompatibility refers to the use of the mechanism within the body of a host without producing negative side effects.

**Isolated Transport** : The transported tissue should be transported in such a way that no transportable matter can escape the transport mechanism during transport.

### 3.3 Transport Mechanism Design Approach

#### 3.3.1 Initiation of Transport

In classical mechanics, the basic understanding of transport is the relocation of an object at location A to a location B. This requires that movement of the object takes place between A and B. This movement allows for the relocation of masses and the phenomena concerning the relocation of objects are therefore sometimes also referred to as mass transfer phenomena. Since the topic of this document concerns the design of a transporting mechanism which move tissue out of the body, the author is interested in the phenomena that cause movement. From mechanics it can be understood that Newton's second law of motion [10], shown in Equation 5, illustrates the relation between an object with

mass  $m$ , in [Kg], and the force  $f$ , in [N], required to accelerate  $a$ , in  $[\frac{m}{s^2}]$ , the object.

$$F = m \cdot a \quad [N] \quad (5)$$

To bring about movement in an immobile object, for example: a football lying on the ground, the football has to be accelerated into the desired direction. If the same football, rolling in one direction over a football field at a (constant) certain speed receives a force which is not in line with its rolling direction it will force the football to divert from its otherwise straight path or it can be decelerated. Therefore, it can be stated that in order to enable the transport of an object in a desired direction the application of a force onto this object in the desired transport direction is necessary. This same statement also holds for other types of matter, such as volumes of liquid. From this observation it can be concluded that the transport of matter within a conduit can be achieved by means of applying a force in the desired transport direction, i.e. out of the body cavity.

#### 3.3.2 Stylized Version of Reality

In order to categorize the conceptual designs which are created during this design process, a categorization procedure has to be established. This categorization will be based on the applied forces which lead to motion and on the different types of medium which can create these forces. The phenomena responsible for motion are applied forces on objects which, as a result of this applied force, will be subject to an acceleration in the direction of the force. This force has to be applied to a surface of the object. However, reality is random and therefore the real tissue is stylized in order to more accurately define the tissue geometry. If a piece of tissue is considered, one can imagine that it can take the

### 3. DESIGN PROCESS OF THE ENDO-TUBULAR FRICTION CARRIER

form of an almost endless variety of shapes and sizes. The arbitrary and loosely defined shapes commonly used in physics in order to describe an object with an arbitrary shape, which are also referred to as potato shapes, do not allow for a clear definition of the back, side or front plane(s) of the object. In order to theoretically distinguish between the different surfaces of the object the random potato shape will be stylized into a cylinder, see Figure 16. For a cylinder, the surfaces are rather easy to determine. In addition, the cylinder shape also conforms to the type of rigid outer shaft which will most likely be used. Please remember that in order to transport this stylized object it should be severed from the surrounding tissue. However, the detachment from the surrounding tissue is not the focus or aim of this study. The back plane will be defined as the plane which is closest to the extraction site, the blue coloured plane shown in Figure 17-A. Now that the back plane has been defined, the front plane will be determined as the plane which is directly opposite and parallel to the back plane, see Figure 17-B. The surfaces which connect the frontal and the back plane will subsequently be referred to as the side plane, see Figure 17-C. Now that the surfaces of the stylized object have been defined, it is important to define which kind of forces can be applied to such surfaces and what type of contact is required in order to apply them. A depiction of the different surfaces and the type of force needed to act upon these surfaces in order to initiate movement is shown in Figure 18. From this schematic representation it can be observed that in order to uniquely initiate movement there has to be either a push force on the back plane, a shear force on the side plane or a pull force on the front plane.

#### 3.3.3 Creating Force

Force can be created by a solid object, such as a pair of medical pliers, but can also be the result of a pressure difference in a certain volume of water. This means there are different material states which can exert forces upon an object and this distinction can be used to separate different force application methods. For this process only gases, liquids and solids will be considered. Gases and liquids will be combined, as is common, under the term *fluids* as shown in Figure 20 since they perform similarly for the purpose of creating forces.

#### 3.3.4 Biological Inspiration

In addition to brainstorming about possible methods of transport, transport solutions as they are found in nature also served as an inspiration for the concepts discussed here. An example of a biologically inspired transport method is the ovipositor. The ovipositor is a with which female wasps lay eggs, this process is called oviposition. The ovipositor, indicated in Figure 19 by the black arrow, is used by the female of the wasp to lay eggs in a host creature or site. More information about this biological inspiration can be found in Appendix C.

### 3.4 Concept Categorization Theory

The concepts that were created can now be placed into the (sub)categories which have been established in Section 3.3. For the purpose of this study the investigation of all possible methods of creating a force able to initiate movement within the desired direction are of interest. So, the first division step will discern between the two possible material state categories which can initiate movement: solid transport methods and the methods of transport which are the result of fluid flow phenomena. The concepts can be further subdivided by discerning between the location at which the force will be applied. As described in Section 3.3 the three surfaces of a stylized version of a piece of tissue at which contact can be achieved is the back plane, the side plane or the front plane, see Figure 17. Methods of adhesion which require an intermediate layer, such as adhesion by means of a type of glue, were placed within the solid transport category since these methods do not require fluid behaviour phenomena in order to function.

### 3.5 Conceptual Solutions

#### 3.5.1 Solid Transport Methods

*Force applied at: Back*

**Peristaltic Transport** : In Figure 21 a schematic drawing of the peristaltic transport mechanism is displayed. The peristaltic transport mechanism can be used to transport tissue, shown in pink, by pushing at the back of the tissue cylinder. This pushing force is achieved by radially pulling the outer wall inwards, as is shown in Figure 21, which can be achieved by means of tightening a (or several)

### 3. DESIGN PROCESS OF THE ENDO-TUBULAR FRICTION CARRIER

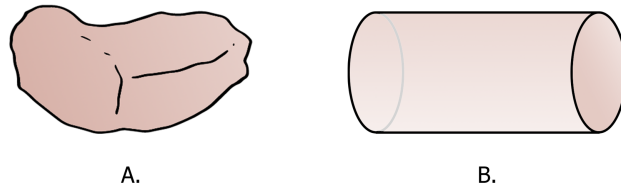


**Figure 16:** Schematic representation of a randomly shaped piece of biological tissue (A) and its stylized depiction (B).

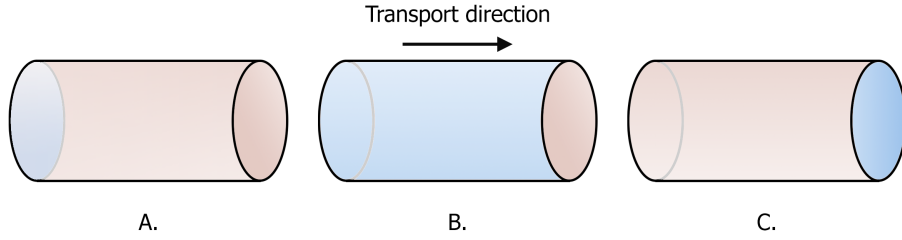


**Figure 17:** Schematic representation of a stylized depiction of a randomly shaped piece of biological tissue and the location of its back plane (A), its side plane (B) and its front plane (C) shown in blue. The transport direction is indicated by the black arrow.

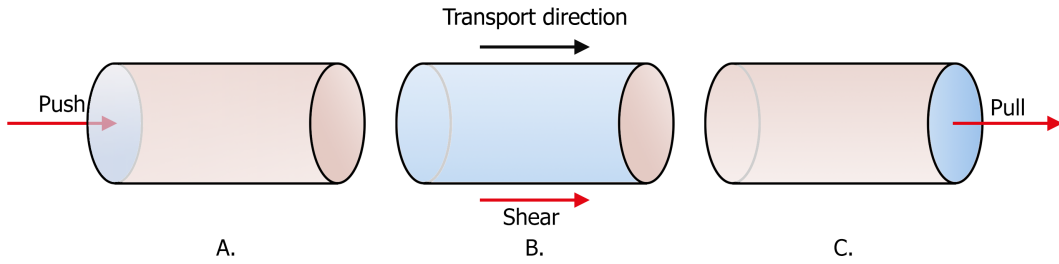


**Figure 18:** Schematic representation of a stylized depiction of a randomly shaped piece of biological tissue and the location of its back plane (A), its side plane (B) and its front plane (C) shown in blue and the types of forces which have to be applied to those surfaces in order to initiate movement shown in red. The transport direction is indicated by the black arrow.



**Figure 19:** Photograph of a female variant of *Gasteruption jaculator*. The ovipositor (A) is indicated by the black arrow. Figure acquired from [11] and adapted by author.

noose (s), shown in orange, which will create a funnel shaped surface which acts as a wedge. If these nooses are placed at repetitive intervals along the tube and tightened in a consecutive sequence, tissue material can be transported along the desired transport direction.

### 3. DESIGN PROCESS OF THE ENDO-TUBULAR FRICTION CARRIER

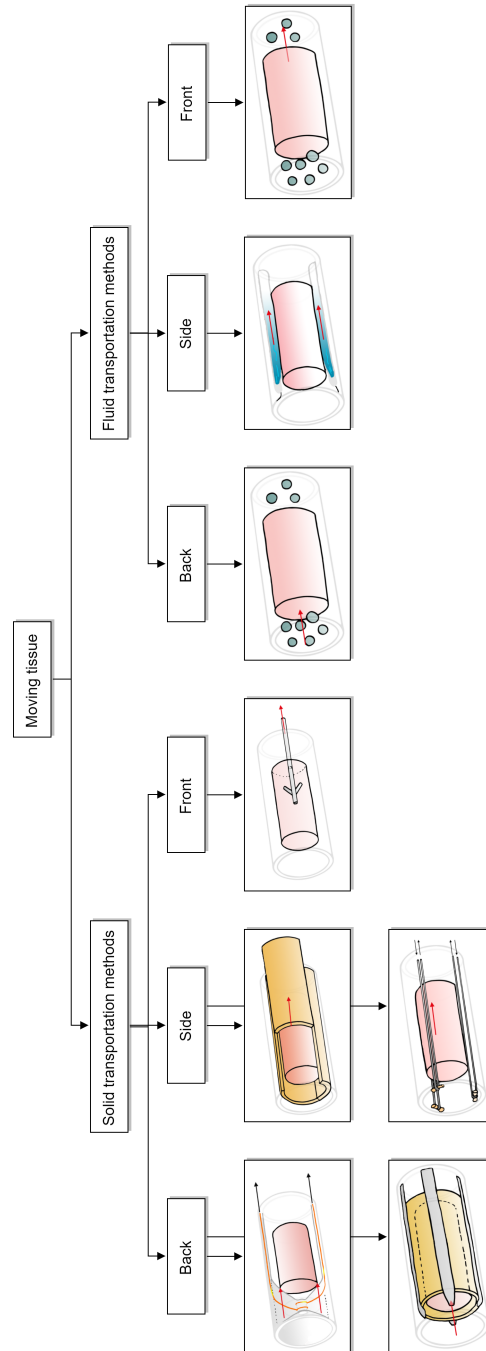


**Figure 20:** Schematic overview of the conceptual solutions within the categorization as described in Section 3.4. Since only fluid and solid transport methods will be included, all conceivable mechanisms and methods which can be used for the purpose of *moving tissue* can be divided into either *solid transport methods* or by *fluid transport methods*. As described in Section 3.4, the material state in both division categories refers to the method by which movement is achieved and does not refer to the material state of the matter which will be transported. This movement will be achieved by generating a force. The conceptual solutions can be further subdivided by discerning between the location at which this force will be exerted. The author will discriminate between the back plane, the side plane and the front plane as described in Section 3.3. The concepts that will not be discussed (not shown here) are deemed to be similar, or the transport system relies on a similar principle, to the shown concepts.

### 3. DESIGN PROCESS OF THE ENDO-TUBULAR FRICTION CARRIER

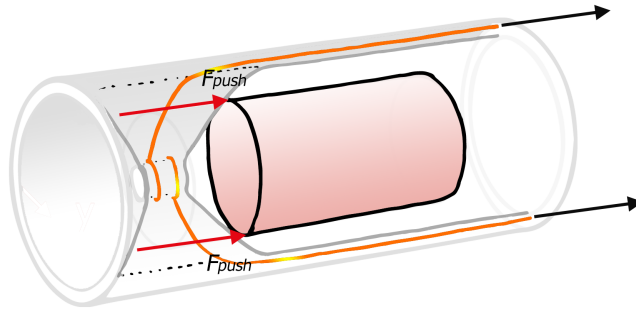


**Figure 21:** Schematic drawing of the peristaltic transport mechanism. Movement is achieved by means of a pushing force at the back of the tissue cylinder, shown in pink, which is the result of a consecutive sequence of inward pulling nooses, shown in orange, which operate in a manner similar to that of peristaltic bowel movements.

**Retracting Blade Transport** : In Figure 22 a schematic drawing of the retracting blade transport mechanism is displayed. Transport is achieved by means of several curved strips of material, shown in grey, which are pointed towards the center of the outer tube. These strips are held back by an inner tube, shown in yellow, which keeps the strips from regaining their curved shape. This inner tube can be retracted in the desired transport direction, so that the strips will bend inwards and will form a shape grip at the back of the tissue cylinder, shown in pink. These strips can consequently be retracted together with the inner tube in order to transport the tissue in the desired transport direction. When the inner tube is pushed in the opposite direction, the strips are again flattened against the outer tube.

*Force applied at: Side*

**Alternating Friction Pair Transport** : In Figure 23 a schematic drawing of the alternating friction transport method is displayed. In this concept the three curved surfaces, shown in yellow, are all in contact with the cylindrical piece of tissue, shown in pink. In a stylized representation of reality each curved surface exerts an equal amount of friction force upon the tissue cylinder when moved. If two of these curved surfaces are moved simultaneously, the amount of friction force of the surfaces combined will always be greater than that of the remaining curved surface. Therefore, the piece of tissue will be moved with these two retracting curved surfaces. This method can be used to transport the piece of tissue in the desired transport direction by alternating which pair of the curved surfaces are moved simultaneously. As mentioned in Section 3.3.4, this method

of transport was biologically inspired by the ovipositor of a wasp.

**Cable Conveyor Transport** : In Figure 24 a schematic drawing of the cable conveyor concept is displayed. This concept relies on a friction contact between the three cables, shown in grey, and the cylindrical piece of tissue, shown in pink. The three cables are looped around six pulleys, shown in orange: three at the extraction side of the conveyor transport system (shown) and three in the handle (not shown), so that an endless conveying motion can be achieved. This requires at least three of the six pulleys to be powered but this can be done within the handle without taking up room in the transport tube.

*Force applied at: Front*

**Harpoon Transport** : In Figure 25 a schematic drawing of the harpoon transport is displayed. The transport method in this concept is based on anchoring a harpoon within the tissue. By retracting the harpoon the piece of tissue can be transported in the desired transport direction. Examples of other methods of making contact with the front of the tissue cylinder are wet- and dry adhesion or suction.

#### 3.5.2 Fluid Transport Methods

*Force applied at: Back*

**Transport by Pressure Difference** : In Figure 26 a schematic drawing of the pressure difference transport mechanism is displayed. In this concept the transport method relies on an increased pressure, displayed as a larger amount of blue particles, at the back of the tissue,

### 3. DESIGN PROCESS OF THE ENDO-TUBULAR FRICTION CARRIER

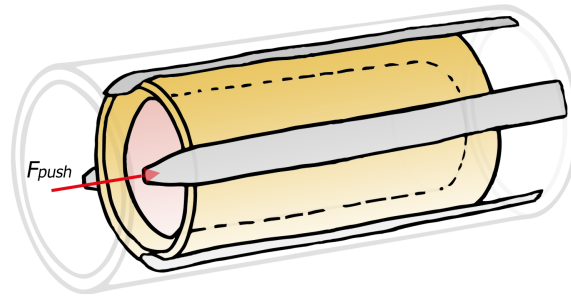


**Figure 22:** Schematic drawing of the retracting blade transport method. Within this transport mechanism several bent strips of material, shown in grey, are pointed towards the center of the outer tube. These strips are held back by an inner tube, shown in yellow, which keeps the strips from regaining their curved shape. As the inner tube is pulled in the desired transport direction, the strips will tend to bend inwards. When these strips are retracted they exert a force on the back of the tissue cylinder, shown in pink, by forming a shape grip. When these strips are retracted in the desired transport direction, the piece of tissue is transported as well. When the inner tube is again pushed in the opposite direction of the desired transport direction, the blades are again flattened against the sides of the outer tube. By making several versions of this mechanism in the longitudinal direction the tissue can be transported.

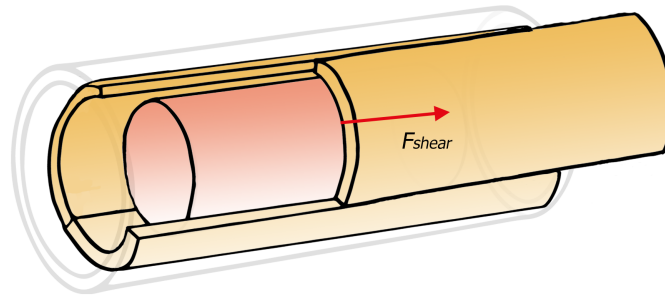


**Figure 23:** Schematic drawing of the alternating friction transport method. The transport method in this concept is based on the theory that two of the three contacting surfaces, of which it is assumed that each is subject to an equal amount of friction with the stylized tissue cylinder, will exert twice the amount of friction on the piece of tissue than the remaining surface. This principle can be used to move the piece of tissue by developing a sequence in which two surfaces retract and due to the larger amount of friction will move the piece of tissue with them. By alternating which two surfaces retract, the tissue can be transported.

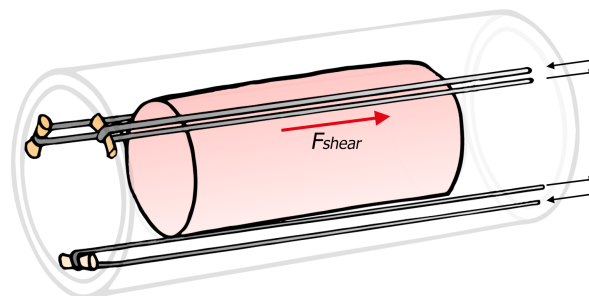


**Figure 24:** Schematic drawing of the cable conveyor concept. The transport method is achieved by wrapping cables, shown in grey, around pulleys, shown in orange, of which the pulleys in the handle are powered. The friction between the cables and the cylindrical piece of tissue, shown in pink, ensures that the piece of tissue moves in the desired transport direction.

shown in pink, as is displayed in Figure 26. The lower pressure occurs at the front of the tissue,

### 3. DESIGN PROCESS OF THE ENDO-TUBULAR FRICTION CARRIER

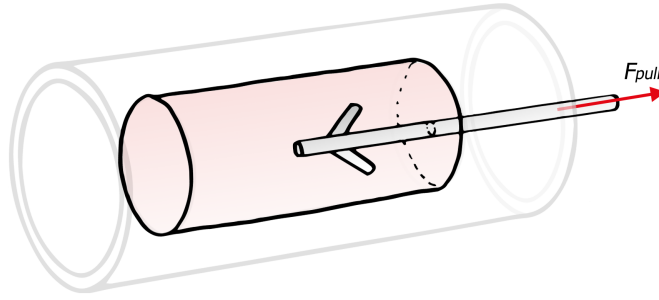


**Figure 25:** Schematic drawing of the harpoon transport concept. This transport method relies on anchoring a ‘harpoon’ within the piece of tissue, shown in pink, and transporting the tissue by retracting the harpoon in the desired transport direction.

which is symbolized by a smaller amount of blue particles. The relative pressure difference between the volumes at the back and the front of the tissue cylinder will result in a ‘pushing’ effect which acts in the direction of the desired transport direction. A concept based on the opposite principle can also be placed within the ‘front’ category. Even though lowering the pressure at the front can be considered to be the same movement principle, it does not occur at the back and can therefore be placed in a different category in the solution tree. It can therefore be stated that this lowering of the pressure at the front can result in a ‘sucking’ action.

*Force applied at: Side*

**Fluid Film Friction Transport** : In Figure 27 a schematic drawing of the fluid film friction transport method is displayed. The wet adhesion, or fluid friction, between the fluid film, shown in blue, and the piece of tissue, shown in pink, ensures that the tissue will not be subject to friction with the wall and is transported along the desired transport direction by the fluid film. The fluid film is injected from the distal end of the tube and flows along the outer tube’s inner surface in the desired transport direction. For this concept to work a fluid has to be selected with high cohesive and adhesive properties and which can sustain sufficient surface tension.

### 3.6 Concept Selection Procedure

A primary selection is necessary in order to dedicate the time and the resources towards the concepts which are believed to be most likely to work according to the functional requirements. In order to make a rough primary selection, a few preferred properties or characteristics

have been formulated so that the concepts can be prioritized. These preferred characteristics are a way of indicating the concepts which are perceived to be more feasible or promising than others. Since they are not formulated as demands or requirements they are not meant to determine in advance which specific concept is the most feasible or will be selected for the final design.

#### 3.6.1 Available versus Preferred Design Directions

The volume of an object in three-dimensional space can be defined according to three directions which are perpendicular to each other. In thin-walled structures, for example the transverse tube section shown in Figure 28, it makes sense to anchor such a coordinate axis within the wall of the tube. If the coordinate axis in Figure 28 is placed within the thin wall, three main directions can be identified. The first, the x-axis, is the radial direction. It points towards the center of the circular tube. The second direction, the y-direction, is the tangential direction which is perpendicular to the x- and z-direction. Then there is a third direction, which points in the direction of the transport. From the directions shown here, combined with the understanding that transport should take place within the diameter of such a tube, it can be observed that design freedom in the x-direction will lead to a restriction of the inner diameter. In addition, it can be observed that there is a large amount of usable space in the z-direction when compared to the x-direction. If moving components are necessary for the functioning of the transport mechanism it would benefit the slenderness of the design if these were situated in such a fashion that they utilize the space in the z-direction.

### 3. DESIGN PROCESS OF THE ENDO-TUBULAR FRICTION CARRIER

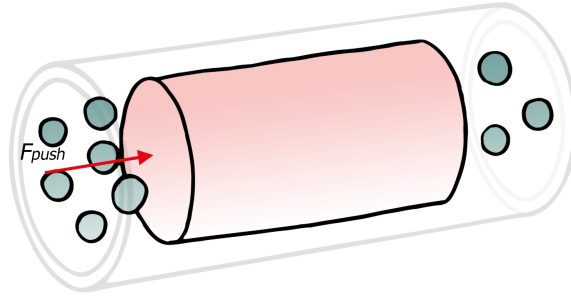


**Figure 26:** Schematic drawing of the pressure difference transport method. The transport method in this concept relies on a relative pressure difference between the back and at the front of the stylized version of the tissue, shown in pink. Since the pressure at the back of the tissue cylinder is relatively larger, displayed as a larger amount of blue particles, than the pressure at the front of the tissue it will be 'pushed' in the desired transport direction.

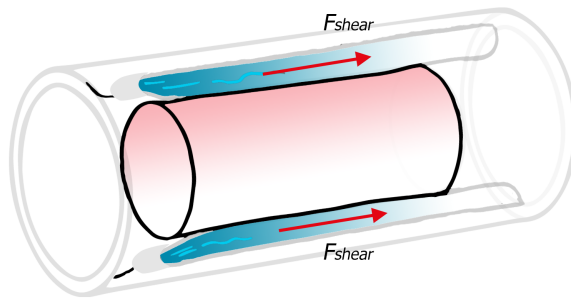


**Figure 27:** Schematic drawing of the fluid film friction transport method. The wet adhesion between the fluid film, shown in blue, and the tissue cylinder, shown in pink, ensures that the tissue cylinder is carried along the desired transport direction.

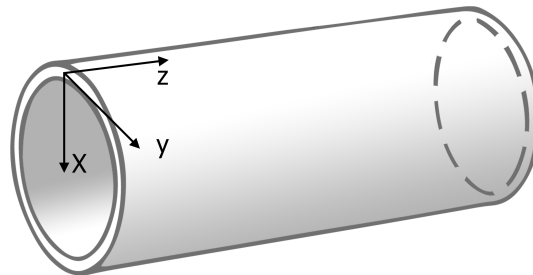


**Figure 28:** Schematic representation of a transverse section of a circular transport tube. The x, y and z design directions are shown in the wall of the cylinder. From this representation, it can also be observed that there is inverse relation between design freedom in the x-direction and the maximum transport volume within the tube.

#### 3.6.2 Relative Contact Complexity

The forces on the surfaces as identified in Section 3.3 can be arranged by order of their relative contact complexity, see Figure 29. This figure shows the stylized piece of biological tissue with all possible forces (push, shear and pull) acting upon the tissue on the aforementioned application areas. In addition, the figure indicates the relative minimum complexity of the contact required in order to apply the

force. This theoretical approach can aid in identifying the least complex contact type by which force can be applied to a surface. The least complex contact type is of interest to the design process since the freedom in the design directions is limited with respect to the x-direction as explained in Section 3.6.1 and graphically represented in Figure 28. In order to apply a push force to an object, a simple point contact will suffice. The shear

### 3. DESIGN PROCESS OF THE ENDO-TUBULAR FRICTION CARRIER

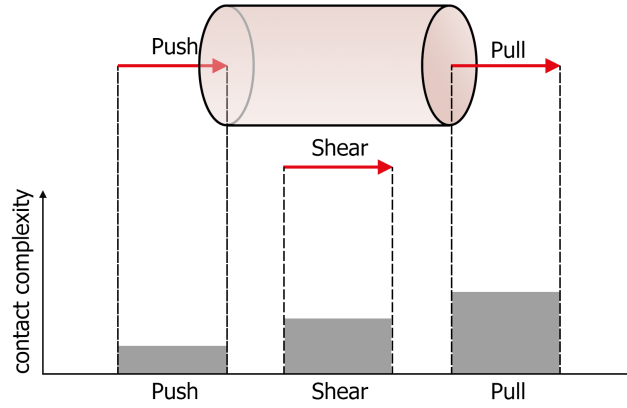


**Figure 29:** Schematic representation of a stylized depiction of biological tissue and the types of forces which have to be applied to those surfaces in order to initiate movement. A graphical depiction of the theoretical contact complexity is shown below the biological tissue. On the vertical axis the amount of contact complexity is shown while the location is shown on the horizontal axis.

forces, on the other hand, can only be applied by means of friction contact or a type of lateral adhesion (chemical, interlocking etc.). If a force is transmitted by means of a point contact to the side plane of the cylinder it will not accelerate in the desired transport direction. The forces which pull on the front plane of the cylinder require gripping contact or perpendicular adhesion. Perpendicular adhesion is relatively hard to achieve since the direction of the pulling force is directly opposite to the bond between the adhering surfaces. In addition, the gripping contact requires interlocking of the surface topologies which occurs on a much smaller scale. From these observations it can consequently be stated that the relative contact complexity necessary to provide motion to the piece of tissue increases in magnitude as the location moves from the back to the front of the object, see Table 1.

#### 3.6.3 Miniaturization

As the scale of a mechanical construction decreases, the issues concerning miniaturization become more relevant. Since the desired diameter of the transport system is limited when compared to existing instrumentation the ability to effectively miniaturize the different transport systems is important. As a rule of thumb, the minimum dimension of key elements which can be manufactured is tenths of millimeters. For instance, the minimum wall thickness, wire diameter and axis diameter are 0.2 mm, 0.2 mm and 0.5 mm, respectively. This means

that the concepts which incorporate mechanical components such as gears, levers, pistons and other such elements are hard to manufacture and function correctly in a 5 mm diameter tube. While it is possible to produce smaller sizes of the aforementioned examples, it is more expensive and less practical for a mechanical construction which will be used in a medical environment. In addition, methods of transport which do not require effective sealing methods, such as tightly fitting gaskets, in order to prevent the loss of transportable matter are preferred.

#### 3.6.4 Primary Concept Selection

As mentioned, the three aspects described in Subsections 3.6.1, 3.6.2 and 3.6.3 are used to indicate which concepts, as described in Section 3.5, appear to be the most successful at meeting the design criteria. In Table 2 a list of all concepts, shown in the left column, and the three criteria which are used to prioritize the concepts, shown in the top row, are displayed. In short, the concepts which are mainly designed in the z-direction, require the most simple method(s) of contact and are the least complex to produce. When these three criteria are taken into consideration it is believed that the concepts *retracting blade transport* and *alternating friction pair transport* are the most likely to succeed and these will therefore be subjected to further conceptual development.

### 3. DESIGN PROCESS OF THE ENDO-TUBULAR FRICTION CARRIER

**Table 1:** Overview of the types of forces which can be applied to the stylized depiction of the randomly shaped piece of tissue and the type of contact necessary to apply each force. The last row indicates the relative complexity of the aforementioned type of contact.

	<b>Push</b>	<b>Shear</b>	<b>Pull</b>
<b>Types of contact</b>	Point contact	Friction contact Adhesion (parallel)	Gripping contact Adhesion (perpendicular)
<b>Relative complexity of contact</b>	Low	Medium	High

**Table 2:** Overview and comparison of the concepts. The three main criteria with which all concepts will be examined are shown in the top row. The concepts are shown in the left column. In the second column the main design direction is indicated, in the third column, the relative contact complexity is indicated and finally some keywords on the manufacturability of each concept is displayed in the fourth column.

Concept name	Main design direction	Relative complexity of contact	Manufacturability and miniaturization
Peristaltic transport	x-direction (temporary)	Low	Relies on intricate cable system, flexible wires/inner tube or compliant inner tube
Retracting blade transport	x-direction (temporary)	Low	Compliant springs and tubes, existing examples of similar systems
Alternating friction pair transport	z-direction	Medium	Flat design, simple components: mainly tube sections
Cable conveyor transport	x-direction	Medium	Delicate pulley system but simple components
Harpoon transport	x-direction	High	Simple design, requires launch/anchoring mechanism
Transport by pressure difference	x-direction	Low	Only requires a pump mechanism
Fluid film friction transport	z-direction	Medium	Requires small channels and sustained pressure

#### 3.6.5 Retracting Blade Transport

The sequence that is necessary in order to successfully transport the tissue in this method is shown in Figure 30. The first drawing shows the initial situation, see Figure 30-1. In Figure 30-2, the inner tube, shown in grey, is retracted in the direction of the arrow. Simultaneously with retracting the inner tube, the strips of the mechanism, shown in orange, bend inward to recover their initial bent shape, this is shown in Figure 30-3. Now that a shape grip is achieved the strips together with the inner tube can be retracted, this is shown in Figure 30-4. Figure 30-5 shows the inner tube together with

the bent strips being returned to their initial positions. Such a mechanism, when placed in a linear pattern along the tube, will enable transport of the tissue. The minimum thickness of the bending strips should be determined in order to achieve tissue transport successfully while still maintaining a construction that is as slender within the x-direction as possible. The maximum force which will be exerted on those blades can be simulated by determining the situation in which the amount of friction between the tissue cylinder and the inner wall of the transport tube is at its peak. This friction can be approximated by using the

### 3. DESIGN PROCESS OF THE ENDO-TUBULAR FRICTION CARRIER

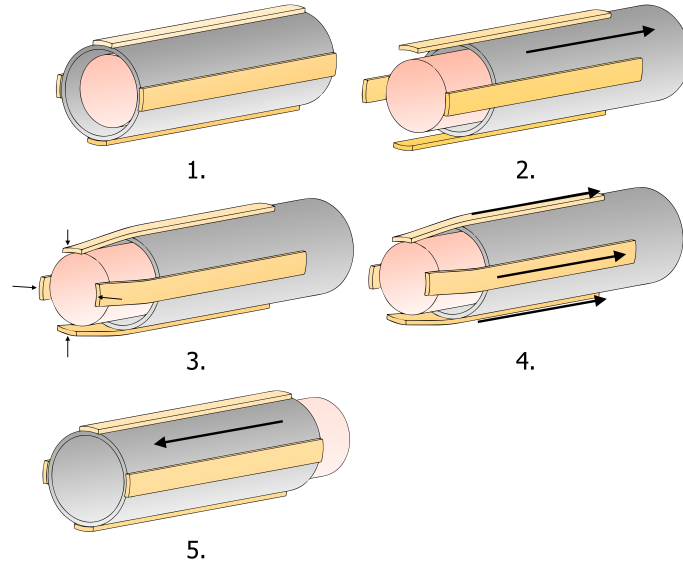


**Figure 30:** Schematic representation of the *retracting blades transport mechanism*. The stylized depiction of biological tissue is shown in pink, the strips of the transport mechanism are shown in orange and the inner tube is shown in grey. (1) shows the initial situation. In (2) the inner tube is retracted in the direction of the arrow, which allows the strips of the mechanism to bend inward to recover their initial bent shape, shown in (3). Now that a shape grip is achieved the strips and the inner tube can be retracted so that the tissue is also moved, see (4). The inner tube can be returned to its initial position after moving the tissue, see (5).

friction formula, shown in Equation 6. Known parameters are the gravity constant  $g = 9.81 \frac{m}{s^2}$ , the friction coefficient  $\mu \approx 1$ , the density of bone  $\rho = 1920 \frac{kg}{m^3}$  and the dimensions  $r = 2.5 \cdot 10^{-3} [m]$  and  $L = 250 \cdot 10^{-3}$ . The dimensions are those of the instrument itself it is assumed that these values are representative since this approximation is only to determine the order of magnitude. In addition, the bone density is higher than the density of soft tissues such as organs ( $\rho \approx 1040 \frac{kg}{m^3}$ ) and therefore the density of bone was selected for this calculation.

$$F_f = \mu \cdot F_N = \mu \cdot m \cdot g \quad [N] \quad (6)$$

$$F_f = \mu \cdot V \cdot \rho \cdot g \quad [N] \quad (7)$$

$$F_f = \mu \cdot \pi \cdot r^2 \cdot L \cdot \rho \cdot g \quad [N] \quad (8)$$

As a numerical value the friction force that has to be surpassed in order to initiate movement is shown in Equation 9.

$$F_f \approx 9.25 \cdot 10^{-2} \quad [N] \quad (9)$$

Now that the friction force has been determined parametrically it can be identified that the friction force is at a maximum when the tube is in a horizontal position. Now that the maximum friction is identified the focus will shift to minimizing the thickness of the bending

strips while still maintaining the ability to transport tissue. The minimum thickness of the strips is 0.2 mm and if maximum friction on one strip (with a minimum blade thickness) is assumed, instead of four, the most extreme loading situation can be simulated. Such strips can be made from materials such as stainless steel or Nitinol, which is an alloy of nickel and titanium which exhibits superelasticity. The flexibility of the material should be taken into account since the strips will be deformed. In order to determine if the strips can cope with this loading situation, a Finite Element Method analysis was performed on a model of a Nitinol strip, Figure 31. This is seen in Figures 32 and 33. If circumstances such as those described above on one strip are simulated a minimal deflection of just several tenths of millimeters results from a force equal to  $F_f$ , see Figure 32. In addition, the material stress remains well below the yield strength of Nitinol as a result of the same force application, see Figure 33. However, if the circumstances of Figure 30.5 are simulated, i.e.: the inner tube is pushed back so that the strip of Nitinol is again pushed flat against the wall of the outer tube, the material starts to deform in the plastic region, see Figure 34. Regardless of peak-stress reducing measures, such as filleting the sharp

### 3. DESIGN PROCESS OF THE ENDO-TUBULAR FRICTION CARRIER

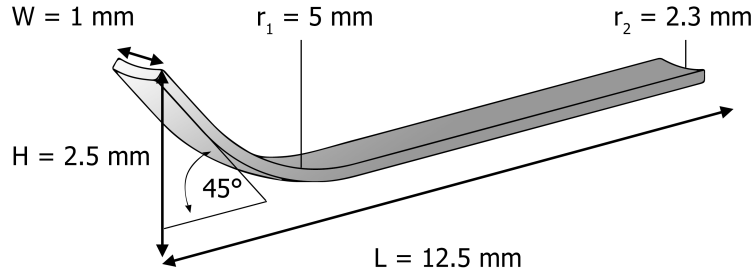


**Figure 31:** Three-dimensional model of one strip of the retracting blades transport mechanism. The length, height and with are denoted with the symbols  $L$ ,  $H$  and  $W$  respectively. Radii are indicated by the symbol  $r$ . The dimensions of this model are selected so that a order of magnitude force estimate can be established. All measurements are expressed in millimeters.

edges, the deformation seems to remain within the plastic region when a sufficient displacement is achieved. To minimize friction between the sliding components materials should be selected which possess low coefficients of friction with regards to each other, e.g., polymers on stainless steel. In addition it is important to select a material for the retraction blades with high flexibility characteristics so that plastic deformation can be avoided.

#### 3.6.6 Alternating Friction Pair Transport

In order to transport tissue, this transport method relies on friction between the surfaces of three internal blades, called A, B, and C, and a stylized piece of tissue. In a stylized situation, the tissue cylinder undergoes a combined friction which is comprised of three equal components of this total friction, one for each blade, please see Equations 10 and 11. If each blade contributes a third of the total friction it can be stated that two of the blades will always provide twice the amount of friction of the remaining one, please see Equation 13. Maintaining friction between the tissue and the blades can be achieved by increasing the surface roughness. Adding barbs or ridges to the surfaces of the blades may be necessary for increasing the friction with the tissue. Furthermore, when the tube that houses this mechanism is placed vertically the friction will be minimal. The barbs and ridges provide increased friction in situations in which the mechanism is held at an angle.

$$F_{fA} = F_{fB} = F_{fC} \quad [\text{N}] \quad (10)$$

$$F_f = F_{fA} + F_{fB} + F_{fC} \quad [\text{N}] \quad (11)$$

$$F_f = 3 \cdot F_{fA} \quad [\text{N}] \quad (12)$$

$$2 \cdot F_{fA} > 1 \cdot F_{fA} \quad [\text{N}] \quad (13)$$

This principle, that the friction of two blades always exceeds the friction of one blade, can be used in order to move tissue in the desired transport direction. Several steps are required in order to transport this tissue. For a schematic representation of these steps, please see Figure 35. In Figure 35-1 the blades and the letters that are assigned to them for this explanation are shown. Figure 35-2 shows a stylized piece of tissue, (shown in pink) being enveloped by the blades. In Figure 35-3 blades B and C are moved in the direction of the arrow, thus transporting the tissue. In order to move blades B and C backwards without simultaneously transporting the tissue, they are moved separate from each other. Figure 35-4 shows blade C being retracted, while Figure 35-5 subsequently shows blade B being retracted. It should be noted that the length of the segment shown here was chosen arbitrarily in order to illustrate the transport mechanism. Linear movements such as those shown here can be achieved by using a cam and follower system in the handle of the instrument where the criterion of a limited diameter as stated in Section 3 no longer applies. The sequence that is shown in Figure 35 is summarized in Table 3. The speed at which the extraction will have to take place is determined by the transport rate. In order to approximate the transport rate, an estimate for the weight of a 10 mm tissue segment will first be established, see Equation 14.

$$W_{1cm} = \pi \cdot r^2 \cdot L \cdot \rho_{tissue} \quad [\text{Kg}] \quad (14)$$

$$W_{1cm} = \frac{\pi \cdot (0.0025)^2 \cdot 1040}{100} [\text{Kg}] \quad (15)$$

$$W_{1cm} \approx 0.2 \cdot 10^{-3} \quad [\text{Kg}] \quad (16)$$

In order to comply with, for example the maximum rate as reported by Driessen *et al.* [8],

### 3. DESIGN PROCESS OF THE ENDO-TUBULAR FRICTION CARRIER

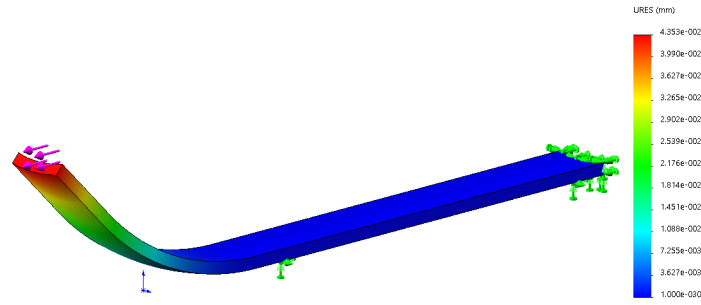


**Figure 32:** Finite element analysis results of the deflection of one strip of Nitinol under the circumstances described. The range of occurring stress magnitudes are shown on the scale on the right side of the picture. The deflection is limited to only tenths of millimeters while the stress is well below the plastic deformation limit.

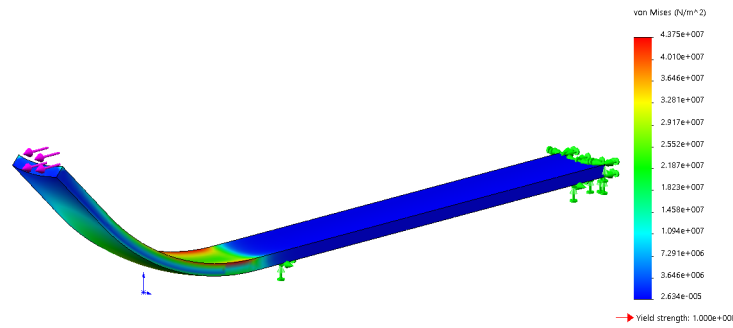


**Figure 33:** Finite element analysis results of the stress distribution in one strip of Nitinol under the circumstances described. The range of occurring stress magnitudes are shown on the scale on the right side of the picture. The peak stress, indicated by at the red arrow, is well below the value at which plastic deformation starts to occur.

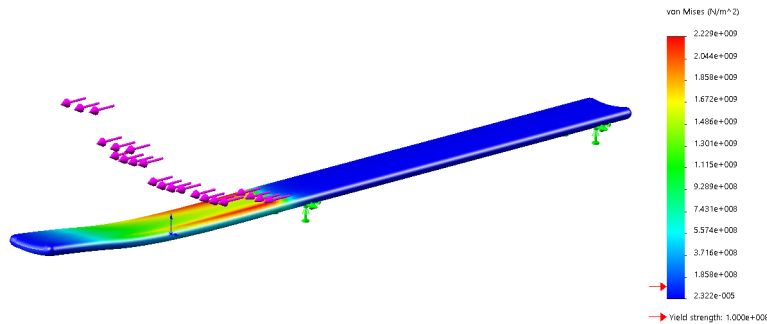


**Figure 34:** Finite element analysis results of the stress distribution in one filleted strip of Nitinol as it is pushed back in a straight position (also shown in Figure 30-5). The range of occurring stress magnitudes are shown on the scale on the right side of the picture. The peak stress at which plastic deformation starts to occur is indicated by at the red arrow.

a transport rate of  $7 \cdot 10^{-4} \left[ \frac{Kg}{s} \right]$ , and assuming that the blades operate back and forward with a stroke of 5 mm, the sequence shown in Table 3 should take place with a frequency of approximately 7 Hz. However, if the stroke length increases, the frequency of the movement

can subsequently be lower. Such a sequence can be driven by using a cam and follower system. If it proves to be more efficient to move some blades separate from other blades multiple cam and follower systems can be combined. For example, by combining a three-dimensional

### 3. DESIGN PROCESS OF THE ENDO-TUBULAR FRICTION CARRIER

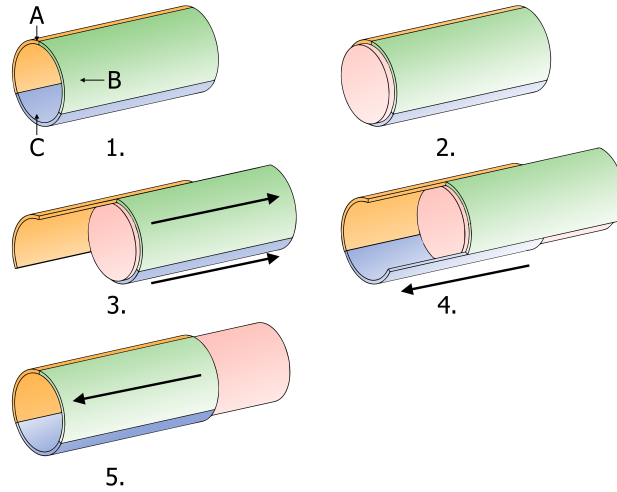


**Figure 35:** Schematic representation of the *alternating friction pair transport mechanism*. The stylized depiction of biological tissue is shown in pink. The three blades, indicated by A (orange), B (green) and C (blue) are shown in (1). A stylized tissue cylinder is introduced in (2). Steps (3) to (5) show the actual movements which lead to the transport of tissue. In (3), blades B and C are moved in the z-direction subsequently transporting the cylinder of tissue with them. Blade C is again moved to its initial position, shown in (4). Consequently, blade B is moved back to its initial as well. Repeating steps 3-5 will result in transporting the piece of tissue further.

**Table 3:** Overview of the sequence with which the blades are moved back- and forward in order to transport the tissue cylinder.

Step No.	Blade A (orange)	Blade B (green)	Blade C (blue)	Transport result on tissue
Step 3	Stay in place	Forward	Forward	Forward
Step 4	Stay in place	Stay in place	Backward	Stay in place
Step 5	Stay in place	Backward	Stay in place	Stay in place

cam and follower system as shown in Figure 36-1 and a barrel type cam system as shown in Figure 36-2 two separate motions can be achieved while only using one cam, see Figure 36-3. It should also be considered that the tissue, as a result of gravity, will be subject to increased friction with the blade directly under it, depicted by blade C in Figure 35. The influence of gravity can be reduced by always including the blade directly under the tissue in the motion sequence or by increasing the amount of blades so that several blades will always be positioned directly under the tissue. To ensure that the blades are only able to move forward and backward in the z-direction they have to be 'locked' in the x- and y-direction. To achieve locking in these directions slots can be created in the outer tube, which envelops the whole system. Another option is locking the blades relative to each other by providing the edge

of one blade with a groove while the adjoining blade is provided with a tongue. A minimum amount of friction between the blades and other parts within the construction can be achieved by choosing materials which possess low coefficients of friction with regards to each other. Examples of material combinations which result in low friction are sintered bronze on stainless steel, or polymers on stainless steel.

#### 3.6.7 Selection Process Conclusion

While the intrusion into the x-direction is non-permanent in the retracting blades transport mechanism, the author still prefers a mechanism mainly designed within the z-direction. In addition, in order for the retracting blades transport mechanism to work, several of these mechanisms have to be placed along the tube. Furthermore, the blades of

### 3. DESIGN PROCESS OF THE ENDO-TUBULAR FRICTION CARRIER

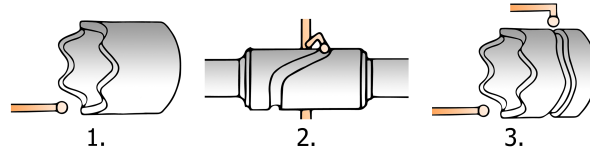


**Figure 36:** Schematic representation of possible cam and follower systems which can be used to drive the motion sequence of this concept. In (1), a three-dimensional cam and follower system is shown. A barrel type cam and follower system is shown in (2). By combining these cam and follower systems, shown in (3), two separate motion sequences can be achieved while driving only one cam.

the retracting blades mechanism work most efficiently when used in a pulling motion. This means that there is a restriction on the length of the tissue which can be transported within the current design. Since the alternating friction pair transport method is mainly designed in the z-direction, contains relatively simple parts and can function continuously the author has decided to develop the alternating friction pair transport mechanism into a prototype.

## 3.7 Final Conceptual Design

### 3.7.1 Motion Sequence

The motion sequence of the oviposition process can be characterized by a number of steps, shown in Figure 37. In order to transport tissue, this transport method relies on friction between the surfaces of six internal blades, referred to with the letters A to F (Figure 37), and a stylized piece of tissue. In a stylized situation, the tissue cylinder undergoes a combined friction which is comprised of six equal components of this total friction, one for each blade, please see Equations 17 and 18. If each blade contributes one sixth of the total friction it can be stated that four of the blades will always provide twice the amount of friction of the remaining two blades, please see Equation 20. Maintaining friction between the tissue and the blades can be achieved by increasing the surface roughness. Adding barbs, spines or ridges to the surfaces of the blades may be necessary for increasing the friction with the tissue and also to prevent retrograde movement. The ovipositor which serves as a biological inspiration to this mechanism is itself provided with a surface microstructure in order to prevent retrograde movement [12]. Further information about the biological inspiration for this project is provided in Appendix C.

$$F_{fA} = F_{fB} = \dots = F_{fF} \quad [\text{N}] \quad (17)$$

$$F_{total} = \sum_{i=A}^F F_i = F_{fA} + F_{fB} + \dots + F_{fF} = 6 \cdot F_{fA} \quad [\text{N}] \quad (18)$$

$$5 \cdot F_{fA} > 1 \cdot F_{fA} \quad [\text{N}] \quad (19)$$

And also;

$$4 \cdot F_{fA} > 2 \cdot F_{fA} \quad [\text{N}] \quad (20)$$

This theoretical principle, that the friction of the majority of blades always exceeds the friction of the minority of blades (assuming that all blades experience equal amounts of friction) can be used in order to move tissue in the desired transport direction. A multitude of consecutive steps are required in order to transport tissue in the desired transport direction. In order to investigate the result of different types of motion on the reliability of the transport, two different motion sequences were developed. In Figure 37-1 and 37-2 the different blade configurations and the letters that are assigned to them for this explanation are shown. The blades are assigned letters A to F in a clockwise fashion, starting from the top right blade. The blades of the first motion sequence are arranged into two triples which will move back and forth in an alternating motion. Figure 37-1 shows the configuration blade: A (black) and blades B, C, D, E and F (cyan). The blades are spread in an interchanging pattern so that the (small) forces of gravity and the amount of surface contact between the triples with irregularly shaped pieces of transportable tissue affects all blades as equal as possible. In Figure 37-2 the blades are divided into three pairs: the yellow pair, consisting out of blades A and D, the orange pair, consisting out of blades B and E, and the blue pair, consisting out of blades C and F. In this configuration, two pairs move backward while one pair moves forward. In such a situation, the friction exerted upon the tissue by the retreating pairs is twice as large as the advancing pair. In this configuration, the blades of each pair oppose each other so that the (small) forces of gravity and the

### 3. DESIGN PROCESS OF THE ENDO-TUBULAR FRICTION CARRIER

amount of surface contact between the pairs with irregularly shaped pieces of transportable tissue affects each pair equally. Figure 37-3 shows an isometric view of a length section of the six blades. It should be noted that the length of the segment shown in Figure 37-3 was chosen arbitrarily in order to illustrate the configuration. The motion sequences for both the hexasected- and the trisected reciprocating motions as described have been graphically represented in an isometric representation in Figures 38 and 39. In Figure 38 the colour coding corresponds to the code shown in Figure 37-1. In Figure 38-1 it can be seen that the single black blade (A) is at the minimum stroke location while the other blades move backward in a stepped manner. In Figure 38-2 it can be seen that the single black blade (A) is at the maximum stroke location while the other blades are gradually moving backwards in a stepped manner. This retreat backwards in a stepped manner continues as each time, another blade is pushed forward while the other 5 blades in the configuration are moving backwards. In order to save time and resources the decision was made to utilize an existing functioning method of actuation. The design by P. Posthoorn [13], shown in Figure 40, which converts rotary motion into linear reciprocating motion by means of an interchangeable barrel cam was used as a basis for this design. Similar to the proposed design in this document this robot is equipped with a barrel cam in order to linearly move the sliding components, which are attached to its surface, back- and forward. In order to understand what is on the inside of this mechanism see Figure 41. The barrel cam (3) and rotary motor (5) within the frame of the endoluminal robot (1) and the six sliders (4) connected to the barrel cam drive. The slides on top of the mechanism are connected by means of small axles onto which ball bearings have been attached. These ball bearings follow the trajectory on the surface of the barrel cam. The rotary motor is fixed to the frame by means of an adjustment screw (6). Similarly, the motor is attached to the barrel cam by an adjustment screw (7). The prototype is protected from debris and dirt by a semi-spherical cap (2). The blue frame ends in a collar through which electric cables can be inserted to provide the motor with power.

#### 3.7.2 Blade Actuation

A barrel cam drive consists of a cylindrical cam with (several) followers which follow the path which is placed on the surface of the barrel cam. This drive is therefore capable of converting a rotary motion to a linear motion. Since the blades in our design will only move in a linear fashion with a maximum stroke as shown in Figure 38 and Figure 39, a barrel cam drive is a very suitable method of enabling the desired motion sequences. In order to provide two different motion sequences, as shown in Figure 38 and Figure 39, two separate barrel cams are required. The speed with which the blades will move up and down can be calculated by determining the speed with which the hexasected motion sequence is completed once. As there is only one wave in the hexasected sequence, one full stroke of a blade is completed for every rotation. Concerning this motor, the time required for one rotation is approximately 1.3 seconds. The stroke for this barrel cam is 5.2 mm. Therefore the blades will move with speed of  $SSH = 4 \frac{mm}{s}$  for the hexasected motion sequence, see Equation 21.

$$SSH \approx 4 \quad \left[ \frac{mm}{s} \right] \quad (21)$$

The speed with which the blades will move up and down can be calculated by determining the speed with which the trisected motion sequence is completed once. As there are two waves in the trisected sequence, two full strokes of a blade are completed for every rotation. Concerning this motor, the time required for one rotation is approximately 1.3 seconds. The stroke for this barrel cam is 5.7 mm. Therefore the blades will move with a speed, called the stroke speed (SST),  $SST = 8.77 \frac{mm}{s}$  for the trisected motion sequence, see Equation 22.

$$SST \approx 8.77 \quad \left[ \frac{mm}{s} \right] \quad (22)$$

The parts of the final prototype design which have been made transparent in Figure 42 are additions to the mechanism in order to convert it to a prototype capable of transporting tissue. A rendered illustration of the prototype is shown in Figure 43. The structures, shown in Figure 44 in (red), are added to the sliding components of the existing prototype. These structures allow for a slightly curved and slender diameter blade adapter (blue) to be clamped by means of two screws. This blade adapter is attached to blade (purple) at the frontal end of the prototype. Six of these blade adapters are added to the endoluminal robot in order to convert

### 3. DESIGN PROCESS OF THE ENDO-TUBULAR FRICTION CARRIER

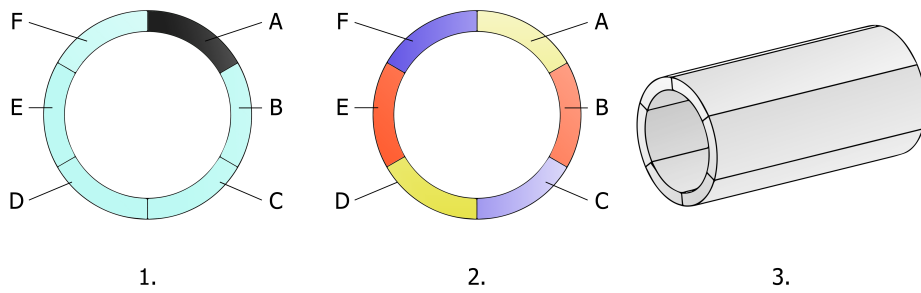


**Figure 37:** Schematic representation of the hexasected- (1) and the trisected (2) reciprocating blade configurations. The blades of both blade configurations are assigned letters A to F in a clockwise fashion, starting from the top right blade. Figure (3) shows an isometric view of a length section of the six blades.

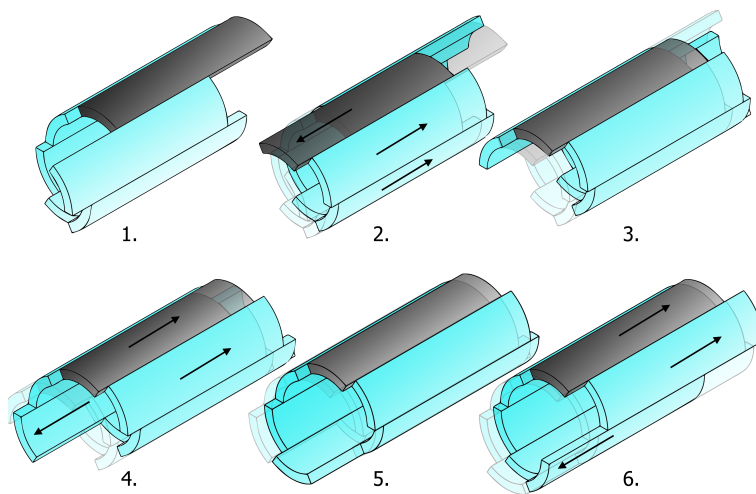


**Figure 38:** Graphic representation of the hexasected reciprocating motion sequence. The colour coding corresponds to the code shown in Figure 37-1. In (1) to (6) it can be seen that every time one single blade is at the maximum stroke location while the other blades are gradually moving backwards in a stepped manner. This retreat backwards in a stepped manner continues as each time, another blade is pushed forward while the other 5 move backwards.

its functionality. The six blades move within a tube in order to ensure that the motion remains linear. In addition this tube is made of brass to decrease the amount of friction between the steel blades and the tube, see Figure 45. In order to slide the brass tube and the prototype out of the frame the screws which are indicated by the green arrows should be removed. The fixing screws, indicated with the blue arrows, should subsequently be loosened in order to allow the prototype and the tube to slide out through the slots within parts of the frame in the direction of the black arrows. The six blades move within a tube in order to ensure that the motion remains linear. In addition this tube is made of brass to decrease the amount of friction between the steel blades and the tube, see Figure 45. In order

to slide the brass tube and the prototype out of the frame the screws which are indicated by the green arrows should be removed. The fixing screws, indicated with the blue arrows, should subsequently be loosened in order to allow the prototype and the tube to slide out through the slots within parts of the frame in the direction of the black arrows. The six blades move within a tube in order to ensure that the motion remains linear. In addition this tube is made of brass to decrease the amount of friction between the steel blades and the tube, see Figure 45. In order to slide the brass tube and the prototype out of the frame the screws which are indicated by the green arrows should be removed. The fixing screws, indicated with the blue arrows, should subsequently be loosened in order to allow the

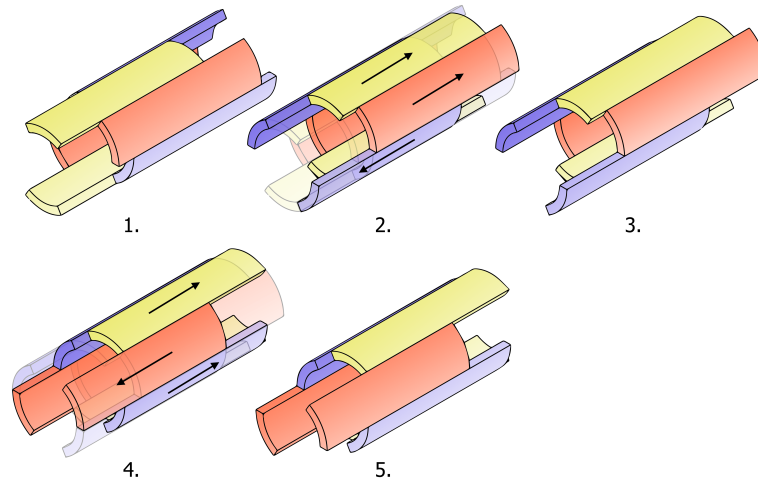


**Figure 39:** Graphic representation of the trisected reciprocating motion sequence. The colour coding corresponds to the code shown in Figure 37-2. Step 1 shows the yellow blade pair at the maximum stroke location, the orange blade pair at  $-\frac{1}{4}$  stroke location and the blue blade pair at the minimum stroke location. Step 2 shows how the yellow blade pair retreated to the  $-\frac{1}{4}$  stroke location, the orange blade pair retreated to the minimum stroke location and the blue blade pair advanced to the maximum stroke location. Step 3 shows how the blue pair is at the maximum location, the yellow blade pair is at the  $-\frac{1}{4}$  stroke location and the orange blade pair is at the minimum stroke location. Step 4 shows how the yellow blade pair retreated further back to the minimum stroke location, the orange blade pair advanced to the maximum stroke location and the blue blade pair retreated to the  $-\frac{1}{4}$  stroke location. Step 5 shows the yellow blade pair at the minimum stroke location, the orange blade pair is at the maximum stroke location and the blue blade pair is at the  $-\frac{1}{4}$  stroke location.

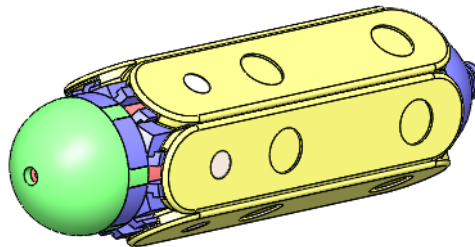


**Figure 40:** Schematic representation of the endoluminal robot by P. Posthoorn [13] which is used to actuate our mechanism.

prototype and the tube to slide out through the slots within parts of the frame in the direction of the black arrows.

### 3. DESIGN PROCESS OF THE ENDO-TUBULAR FRICTION CARRIER

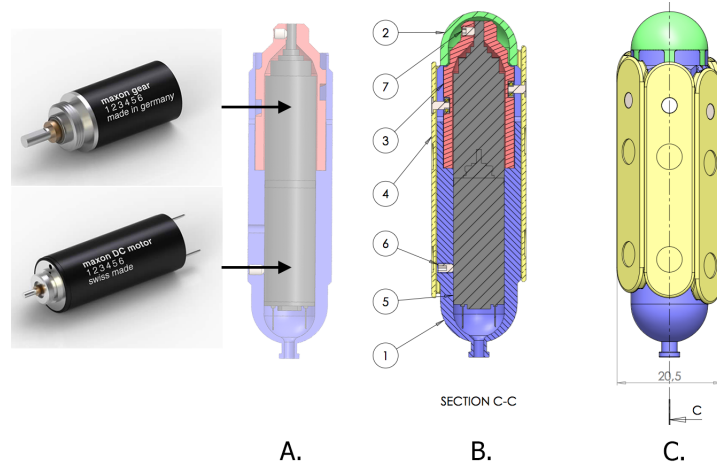


**Figure 41:** Schematic representation of the actuation prototype (A) within the endoluminal robot. The motor consists of a 256:1 gearbox [14] and a rotary DC motor [15]. (B) shows cross-section c-c of the endoluminal robot. (C) Assembled endoluminal robot. Figure adapted by the author from [13].

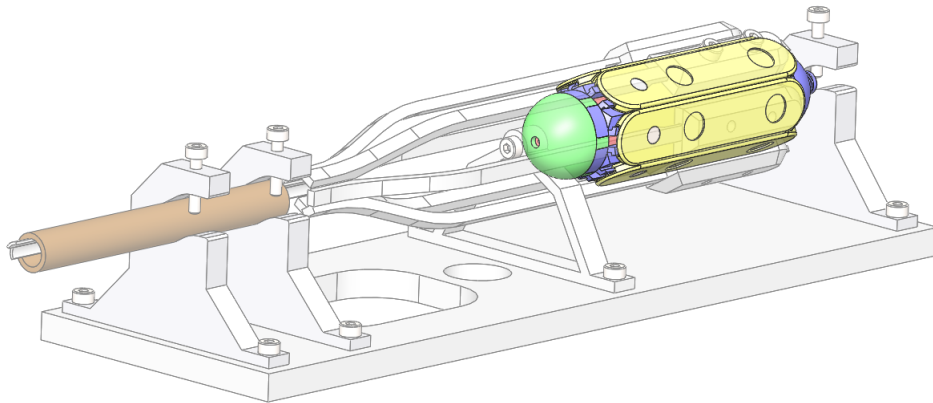


**Figure 42:** Rendered illustration of the location of the endoluminal robot designed by P. Posthoorn [13]. All transparent parts in this figure were added to the mechanism in order to convert its function to a tissue transporting device.

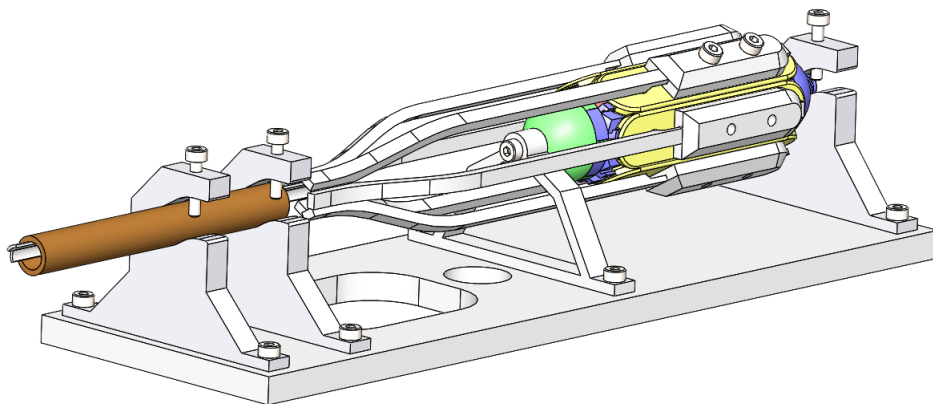


**Figure 43:** Rendered illustration of the assembled prototype.

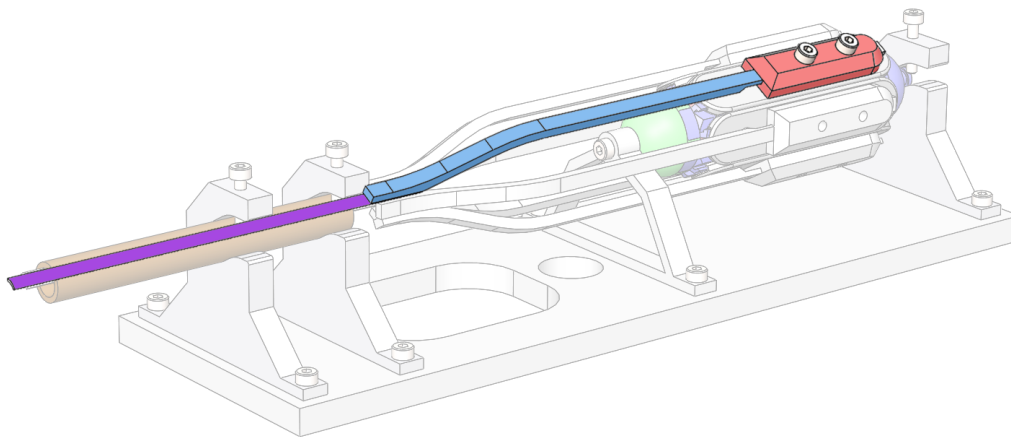


**Figure 44:** Rendered illustration of the assembled prototype with highlighted blade adapters and clamping structures. The structures (red) which are added to the sliding elements of the endoluminal robot allow slender blade adapters (blue) to be clamped by means of two screws. The blade adapters are in turn connected to blades (purple) at the front end of the prototype by means of glue adhesion.

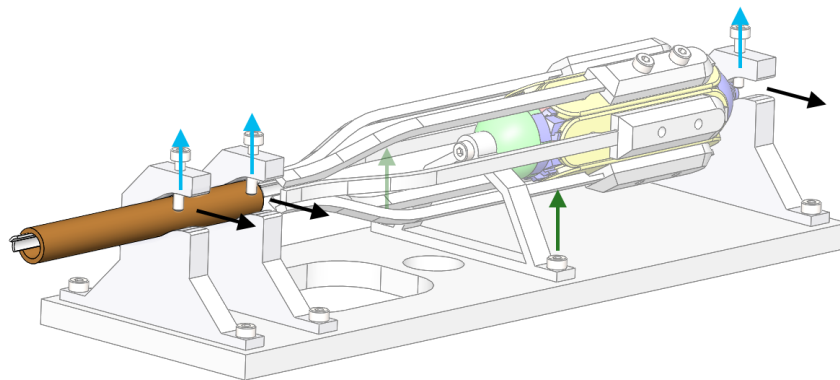


**Figure 45:** Rendered illustration of the assembled prototype. The brown cylinder represents a brass tube through which the blades move back and forth. The green arrows indicate the direction in which the screws need to be removed while the blue arrows indicate which direction the fixing screws needs loosening. These two steps are necessary in order to slide the prototype and the brass tube out of the frame, direction indicated by the black arrows.



## 4 Prototype Development

### 4.1 Prototype Manufacturing

The slightly curved blade adapters such as the one shown in Figure 46 were produced in metal in order to maintain a balance between a thin design and a sufficiently stiff construction. In addition, the 3D-printing of metal allows for the production of complex and curved shapes that do not have to be milled or cast and do not require many fabrication steps. The curved blade adapters were attached to the six sliders on the actuation device by means of six small clamping attachments, Figure 46. The sliders follow the cam path as is shown in Figure 48. In Figure 48 the small ball bearings can be seen protruding through the frame into the cam path. These clamping attachments will contain a slot into which the curved blade adapters can be inserted. Because of the desire to keep the design limited in size and because of the limited mechanical requirements of these structures they were manufactured in plastic using 3D-printing. By means of a pair of setting screws, perpendicularly aligned with the slot, the blade adapter can be clamped down. Thread inserts, called helicoils, were attached within the clamping attachment in order to allow the setting screws to be removed and inserted several times without damaging the plastic. Two sets of six blades were manufactured and these blades were attached to the two sets of blade adapters by means of glue adhesion. The blades were cut from a capillary stainless steel tube with an outer diameter of 5 mm and a wall thickness of 0.5 mm, by means of electrical discharge machining (EDM). A photograph of the circular configuration of the blades within the milled brass tube is shown in Figure 46. The frame base and the four legs of the suspending frame which support the prototype and the tube in which the blades move back and forth were cut (Gweike CO2 130 Watt Lasercutter) from 5 mm thick transparent acrylic. Like the adapter clamps, these parts were provided with metal inserts, called helicoils, which allow screws to be inserted and removed without damaging the acrylic. The setting screws allow for adjustment within the frame so that there is no necessity for high accuracy manufacturing. The base plate and supporting frame are joined to each other with screws. In addition, the base plate was provided with several holes so that the base of the frame can be attached to an experiment rig. The positioning tube shown in Figure 47

in which the blades move back and forth is a commercially available brass tube with an external diameter of 7 mm and a wall thickness of 1 mm. This brass tube was cut to a length of 60 mm and the end was milled off to provide a short tapered cutting edge. The barrel cams which provide the different reciprocating motions were all milled from solid pieces of aluminum, see Figure 49. In Table 4 an overview is presented in which the information concerning the production of the components as described in the preceding Subsections is summarized. In addition, Table 4 also specifies the amount of parts produced and how each part is connected to other parts. Technical drawings of all these parts are given in Appendix D.

### 4.2 Prototype Assembly

The six 3D-printed plastic adapter clamping structures were glued onto the six sliders of the prototype. In addition, the six blades were glued to the blade adapters themselves in the configuration shown in Figure 44. Subsequently, the blade adapters and the attached blades were inserted into the slots within the adapter clamps and clamped down by inserting the settings screws. The blades were then gently inserted into the brass positioning tube in which the blades move back and forth relative to each other. The frame was subsequently assembled by screwing the frame base to the four frame parts which suspend the prototype. This enables the prototype to slide into the grooves which have been cut into the suspending frame parts as shown in Figure 45. After sliding the prototype into the grooves, the three fixing screws were tightened carefully in order to lock the positioning tube in place. A photograph of the assembled prototype is shown in Figure 50.



**Figure 46:** Photograph of two 3D-printed plastic blade adapter clamps glued to sliders (left). One of the sliders is turned upside down in order to display the ball bearing which follows the path on the barrel cams. In addition, a the configuration of the blades within the milled brass tube is shown (right).



**Figure 47:** Photograph of the suspending frame and frame base parts.



**Figure 48:** Photograph of the the sliders which move within the path that is milled into the barrel cam.

#### 4. PROTOTYPE DEVELOPMENT

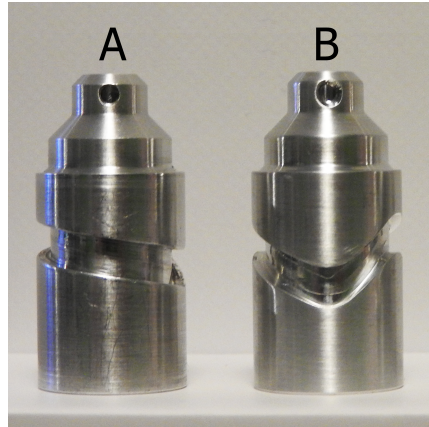


**Figure 49:** Photograph of two barrel cams. (A) Barrel cam that provides the hexasected reciprocating motion. (B) barrel cam that provides the trisected reciprocating motion.

**Table 4:** Overview of the component list. The amount, the production method and the parts to which it is connected are listed for each component. Technical drawings of all these parts are given in Appendix D.

Component	Amount	Production method	Connected to [part] (method)
1. Blade adapter	2 x 6	3D-printing (metal)	Parts [2] (glue); [3] (glue)
2. Adapter clamp	6	3D-printing (plastic)	Parts [1] (screws); [9] (glue)
3. Blades	2 x 6	Wire EDM	Part [1] (glue)
4. Suspending frame	4	Lasercutting	Parts [5] (screws); [9] (screws)
5. Frame base	1	Lasercutting	Part [4] (screws);
6. Positioning tube	1	Milling and turning	Part [4] (screws);
7. Alternative barrel cam	1	Milling and turning	Part [9] (screws);
8. P. Posthoorn prototype	1	Already produced	Parts [2] (glue); [4] (screws)



**Figure 50:** Photograph of the assembled prototype.



## 5 Proof-of-Principle Experiment

### 5.1 Goal of the Experiment

The goal of the experiment is to evaluate the functioning of the assembled prototype in terms of the requirements of Section 3.2 and the possible factors which may influence the transport rate (TR).

### 5.2 Experiment Variables

In this experiment the ability of the prototype to transport tissue and the extent to which the independent variables: gelatin density, particle presence and type of motion sequence contribute to the speed with which transport occurs was assessed with respect to the variable transport rate (TR). This dependent variable is defined as the amount of time (s) it requires to transport 1 milligram of artificial tissue (mg), see Equation 23. In addition, the more easily interpretable inverted transport rate (ITR) is also reported in order to allow the collected transport rates to be compared to the transport rates of current transport systems, see Equation 24.

Independent Variables:

1. Gelatin density: Three different densities of gelatin: D1 (6.25 wt%), D2 (9.10 wt%) and D3 (11.8 wt%)
2. Presence of particles: Gelatin samples with 13 grams of mustard seeds per pouring tray.
3. Type of motion sequence: Hexasected and trisected motion sequence.

Dependent Variables:

1. Transport rate: Amount of time (s) required to transport 1 (mg) of artificial tissue. From this variable the inverted transport rate was also obtained.

The stroke speeds with which the blades move in the hexasected motion sequence and the trisected motion sequence are  $SSH = 4 \left(\frac{mm}{s}\right)$  and  $SST = 8.77 \left(\frac{mm}{s}\right)$ , respectively. The approximate benchmark mass fraction of gelatin to water ratio for determining the other two mass fractions was obtained from a paper which details certain ratios of gelatin to water [16]. Since the aim of the instrument discussed within this document is the transport of organ tissues

this liver mass fraction guideline was selected. In order to differentiate between slightly less- and more dense organ structures, the choice was made to vary the amount of gelatin slightly around this benchmark value. Gelatin samples are a suitable material for representing differing biological material tissue characteristics such as the density and Young's Modulus [17, 18]. The third Sub-experiment will be conducted with minced meat to imitate the transport situation as it is encountered within a medical setting as accurately as possible. The minced meat is pushed manually into the cuboid containers and inserted in the same manner as the gelatin filled cuboid containers. An overview of the mixture ratio's and their designation is displayed in Table 5.

$$TR = \frac{\text{transport time}}{\text{transported weight}} \left[ \frac{s}{mg} \right] \quad (23)$$

$$ITR = \frac{\text{transported weight}}{\text{transport time}} \left[ \frac{mg}{s} \right] \quad (24)$$

### 5.3 Experiment Facility

During the experiment the prototype was placed horizontally. The prototype was then inserted into artificial tissue samples made of a gelatin and water mixture which were prepared beforehand, see Figure 52. These artificial tissue samples were contained within tapered 50 ml cuboid containers (35 x 38 x 52 mm), see Figure 55, and were horizontally aligned with the prototype using a testing jig, see Figure 56. The prototype and the cuboid containers were suspended from the surface of the breadboard by the testing jigs to allow the transported material to fall within a cuboid container placed beneath the prototype. All tests were conducted with the planetary gearhead with a 256:1 gear ratio (218418 [15], 256:1 gear ratio). This rotary motor [14] was powered by a 12 volt (V) battery of which the voltage was manually regulated. Before each experiment the manual button was set to maximum voltage. All experiments were recorded with a camera (Nikon COOLPIX P610). This camera was placed at the back right corner behind the prototype, see Figure 51.

#### 5.3.1 Preparation of Artificial Tissue

A certain amount of gelatin powder (Gelatin Powder 1 Kg, Dr. August Oetker KG, Bielefeld, Germany) was mixed with a fixed amount of water at approximately 90 °C and stirred with

## 5. PROOF-OF-PRINCIPLE EXPERIMENT

**Table 5:** Overview of the different gelatin/water mixtures which are utilized in the experiment. The 13 grams of particles that are introduced into the mixtures numbered G1 to G3 are mustard seeds with an average approximate diameter of 2 mm. (Mustard seeds, Organic Flavour Company B.V., Veenendaal, The Netherlands).

Pure gelatin mixtures		
Mixture no.	Gelatin/water ratio ( <i>wt%</i> )	No. of samples
D1	$\frac{20g}{320g} \cdot 100\% \approx 6.25$ ( <i>wt%</i> )	6
D2	$\frac{30g}{330g} \cdot 100\% \approx 9.10$ ( <i>wt%</i> )	6
D3	$\frac{40g}{340g} \cdot 100\% \approx 11.8$ ( <i>wt%</i> )	6
Grainy gelatin mixtures (particles $\approx$ 13 grams each)		
Mixture no.	Gelatin/water ratio ( <i>wt%</i> )	No. of samples
G1	$\frac{20g}{320g} \cdot 100\% \approx 6.25$ ( <i>wt%</i> )	6
G2	$\frac{30g}{330g} \cdot 100\% \approx 9.10$ ( <i>wt%</i> )	6
G3	$\frac{40g}{340g} \cdot 100\% \approx 11.8$ ( <i>wt%</i> )	6

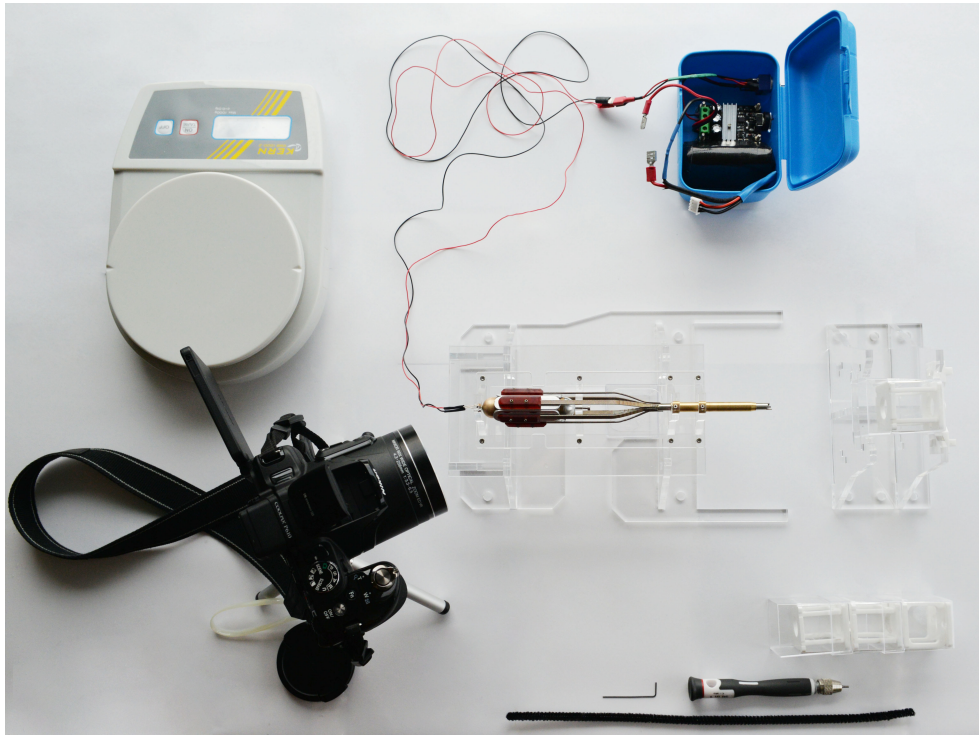


**Figure 51:** Photograph of the experimental setup.

a handheld electrical whisk for approximately 2 minutes. Directly thereafter, the artificial tissue mixture was poured into the pouring trays. The pouring tray was cut (Gweike CO2 130 Watt Lasercutter) from 5 mm thick white acrylic. On each tray a maximum of nine identical cups were placed upside down in the liquid state gelatin. Subsequently, the cuboid containers

were placed upside down within these trays. Due to overflow slots cut within the walls of the gelatin pouring tray at a height of 20 mm, the cuboid containers all contained a 20 mm thick layer of tissue mimicking material leaving an unfilled cavity behind. Afterwards, the trays containing the cuboid containers were cooled within a refrigerator for 14 hours. In addition

## 5. PROOF-OF-PRINCIPLE EXPERIMENT

to pure gelatin mixtures, mustard seeds were introduced to some of the mixtures. These mustard seeds (Mustard seeds, Organic Flavour Company B.V., Veenendaal, The Netherlands) are approximately 2 mm in diameter. The weight of the components of each mixture was determined with a laboratory grade weighing plate (EMB 1000-2, Kern & Sohn GmbH, Balingen, Germany). The cuboid containers which were filled with minced meat were made by pushing the cuboid container on a slab of approximately 20 mm compacted minced meat.

### 5.4 Experiment Protocol

To assess if the prototype was able to transport any material at all, a demonstration of functionality was conducted (see Appendix G). The experimental procedure is graphically represented in Figure 54. The general experiment is subdivided into three sub-experiments. The procedure starts with Sub-experiment I in which three different types of gelatin to water ratios with and without particles are tested. In the second Sub-experiment both the hexasected- and the trisected reciprocating motion sequences were tested on a gelatin/water mixture. In Sub-experiment III the most effective motion sequence will be tested on minced meat. Between all experiments and between each repetition, the tube was mechanically cleared of any remaining tissue mimicking debris on the inside by pushing a 5 mm diameter pipe cleaner several times through the entirety of the transport tube. In Figure 53, the procedure for each experimental repetition is displayed in the column titled 'repetition sequence'. This sequence indicates when, and how, the data necessary to determine the variables as presented in Section 5.2 will be collected. An amount of three repetitions was determined to be the minimum amount of repetitions to be able to perform a statistical analysis on. The data of all sub-experiments are subject to the data collection protocol as prescribed in Figure 53.

#### 5.4.1 Sub-experiment I: Effect of Mixture Density and Particle Presence

The goal of Sub-experiment I was to determine which artificial tissue mixture (of three different densities) allowed for the highest ITR ( $\frac{mg}{s}$ ).

In addition, the prototype was also tested on the same mixtures with added particles. An overview of the different mixture ratios and particles is given in Table 5. This test was conducted with the hexasected reciprocating motion sequence.

#### 5.4.2 Sub-experiment II: Effect of Motion Sequence

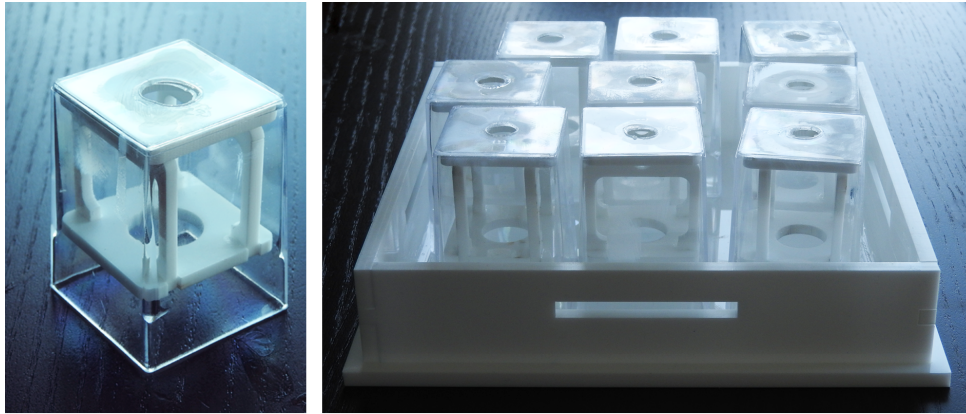
The goal of Sub-experiment II was the determination of the influence of the type of motion sequence. This test was conducted with the hexasected- and the trisected reciprocating motion sequences. The gelatin mixture that was used for this Sub-experiment is mixture D2.

#### 5.4.3 Sub-experiment III: Transport of Minced Meat

The goal of Sub-experiment III was to analyze the function of the prototype when it is introduced into a material which accurately resembles morcellated tissue. The most successful motion sequence from Sub-experiment II, i.e.: the hexasected reciprocating motion sequence, was tested on six cuboid containers which were filled with minced meat.

### 5.5 Data Analysis

The time required to move 1 mg of tissue will be assessed by means of visual inspection. The most successful experimental condition of each Sub-experiment was evaluated by determining the highest transport rate ITR ( $\frac{mg}{s}$ ) within all data sets of each Sub-experiment. Each experiment condition was repeated six times with a minimum of three successful repetitions. The mean ITR and the standard deviation of each experimental condition were presented in textual form for each Sub-experiment and the collected data will be statistically analyzed. This statistical analysis was conducted by performing multiple ANOVA analyses and t-tests on the data for Sub-experiment I and a t-test on the data for Sub-experiment II. The results were also graphically represented in boxplots for each Sub-experiment. All data analysis will be performed with MATLAB R2015b (The Mathworks, Inc., Natick, MA, USA). The Matlab scripts for the t-tests and ANOVA analyses that were used to perform this data analysis can be found in Appendix F.



A.

B.

**Figure 52:** Photograph of cuboid containers and pouring tray. (A) Cuboid container with a hole drilled in the bottom. (B) Gelatin pouring tray.

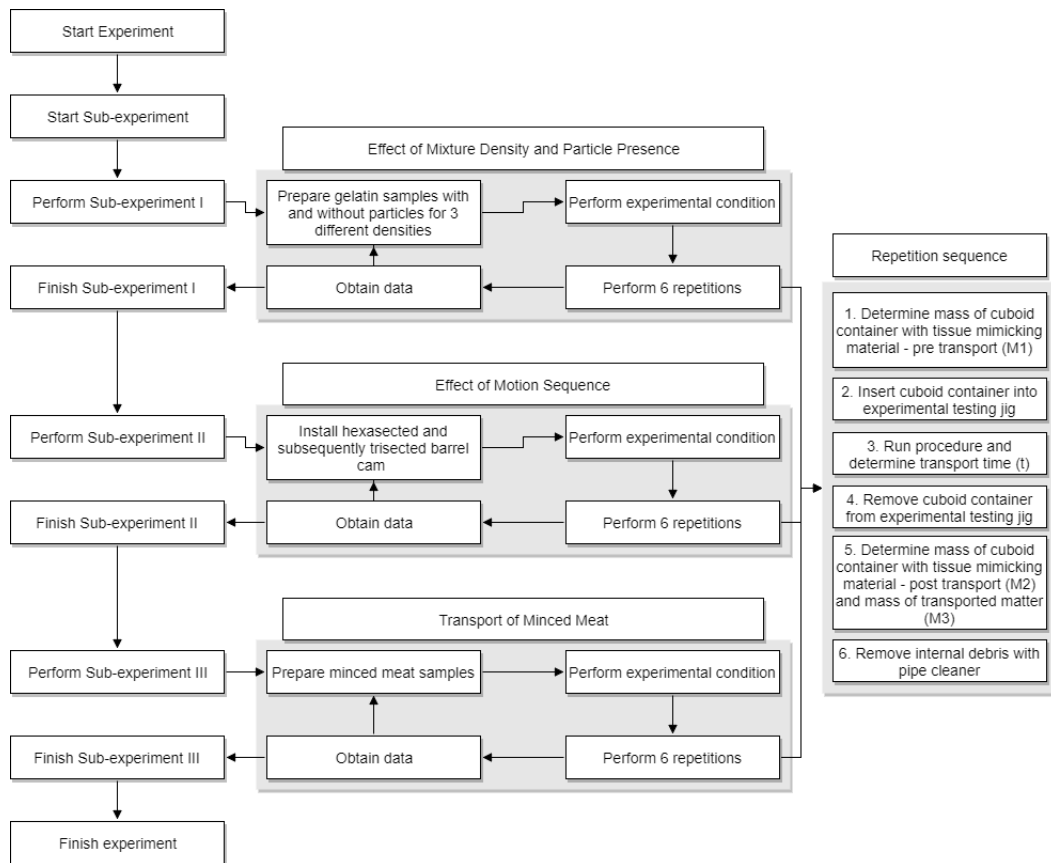


**Figure 53:** Schematic overview of the data collection protocol. The data collection protocol is a systematic method by which data is obtained from each experimental repetition.

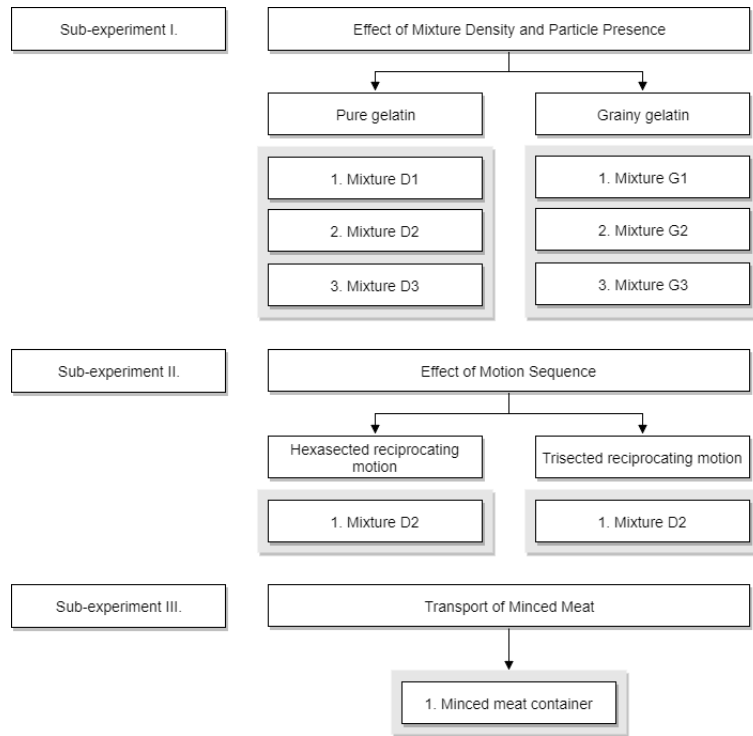


**Figure 54:** Graphic representation of the setup of the experiment.

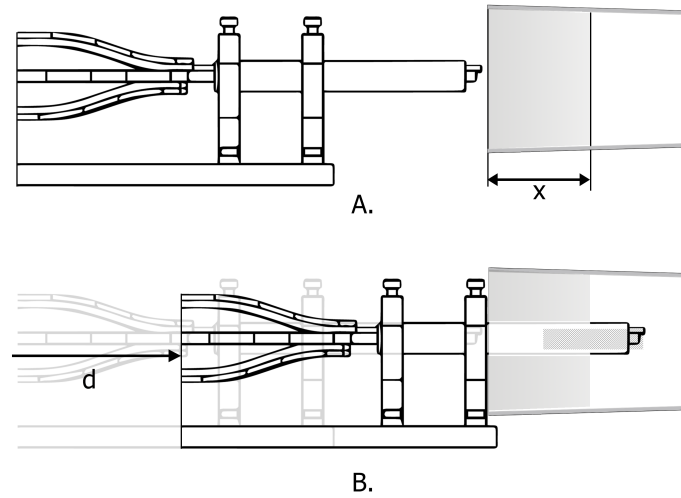


**Figure 55:** Schematic representation of the insertion of the frontal end of the device within the cuboid container. The situation before (A) and after (B) insertion are shown. The frontal end of the device is fully inserted after travelling a distance of  $d = 44$  in mm. The penetrated instrument protrudes approximately 24 mm. The tissue cylinder is indicated in (B) as a dashed rectangle. In order to fully puncture the artificial tissue material (yellow) each cuboid container was filled with 20 mm of material (indicated with  $x$ ) leaving an unfilled pocket. Due to the transparency of the cuboid containers it can be visually assessed if the prototype has fully punctured the artificial tissue.

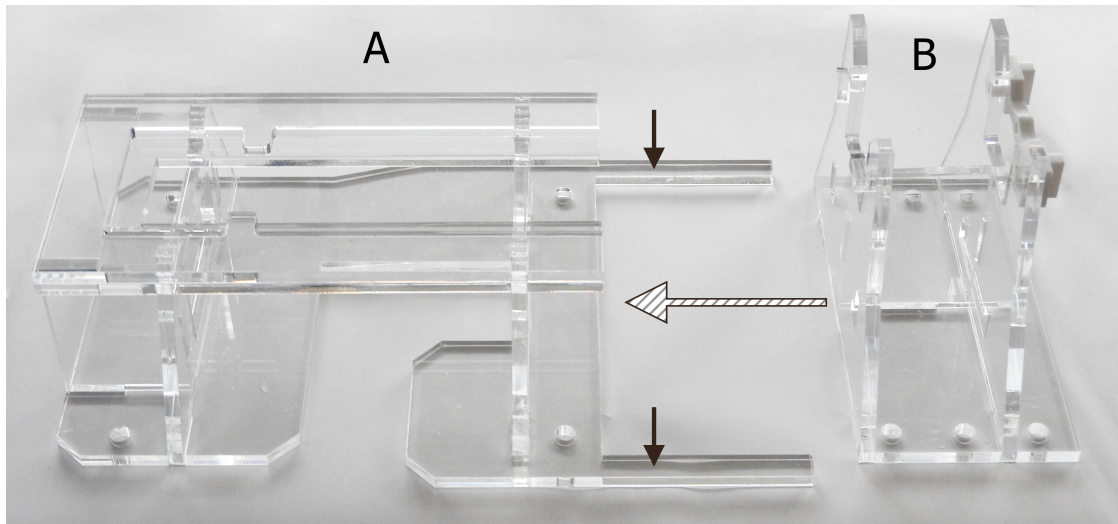


**Figure 56:** Photograph of the experimental jigs. (A) Experimental jig which holds the prototype in place during testing. (B) Experimental jig which holds the cuboid containers in place during the experiment. The insertion takes place by moving (B) in the direction of the dashed arrow along the pronged extruding parts, indicated by the small black arrows, on (A) until the surfaces of both bases touch. The prototype and the cuboid containers are suspended from the surface of the table by the testing jigs to allow transport material to fall within a container placed beneath the prototype.

## 6 Experiment Results

### 6.1 Sub-experiment I: Effect of Mixture Density and Particle Presence

#### 6.1.1 Mixture Density

In Figure 57 the inverted transport rate for the pure gelatin samples is graphically displayed. In addition, the numerical values from the analysis of this experiment are given in Table 6. In Appendix H, Figure 71, the transport rate (TR) as collected from the pure gelatin samples within Sub-experiment I is also graphically displayed. From the results of this experiment it can be concluded that there was a statistically significant difference in inverted transport rate between the different batches of pure gelatin artificial tissue mimicking material as determined by the ANOVA analysis performed in Matlab ( $F(2,13) = 16.25$ ,  $p = 0.0003$ ). The average inverted transport rates for the batches D1, D2 and D3 are respectively  $ITR = 2.4984 \pm 0.5428 \frac{mg}{s}$ ,  $ITR = 4.2068 \pm 0.7379 \frac{mg}{s}$  and  $ITR = 2.5087 \pm 0.3360 \frac{mg}{s}$ .

#### 6.1.2 Particle Presence

In Figure 58 the inverted transport rate for the grainy gelatin samples is graphically displayed. In addition, the numerical values from the analysis of this experiment are given in Table 7. In Appendix H, Figure 72, the transport rate (TR) as collected from the grainy gelatin samples within Sub-experiment I is also graphically displayed. From the results of this experiment it can be concluded that there was no statistically significant difference in inverted transport rate between the different batches of grainy gelatin artificial tissue mimicking material as determined by the ANOVA analysis performed in Matlab ( $F(2,10) = 0.25$ ,  $p = 0.7834$ ). The average inverted transport rates for the batches G1, G2 and G3 are respectively  $ITR = 4.3392 \pm 1.9478 \frac{mg}{s}$ ,  $ITR = 3.5579 \pm 1.7543 \frac{mg}{s}$  and  $ITR = 3.7950 \pm 1.2725 \frac{mg}{s}$ .

Further statistical analysis between the samples without added particles, i.e.: D1, D2 and D3, and those containing particles, i.e.: G1, G2 and G3, show that there was no significant difference in inverted transport rates ITR between sample batches D1 ( $ITR = 2.4984 \pm 0.5428 \frac{mg}{s}$ ) and G1 ( $ITR = 4.3392 \pm 1.9478 \frac{mg}{s}$ ) ( $h=0$ ,  $p = 0.0762$ ), D2 ( $ITR = 4.2068 \pm 0.7379 \frac{mg}{s}$ ), G2 ( $ITR = 3.5579 \pm 1.7543 \frac{mg}{s}$ ) ( $h=0$ ,  $p = 0.4347$ ) and D3 ( $ITR = 2.5087 \pm 0.3360 \frac{mg}{s}$ ) and G3

( $ITR = 3.7950 \pm 1.2725 \frac{mg}{s}$ ) ( $h=0$ ,  $p = 0.0636$ ).

### 6.2 Sub-experiment II: Effect of Motion Sequence

As the highest inverted transport rate (ITR) from Sub-experiment I was determined to be associated with mixture D2, the second Sub-experiment is conducted with samples of mixture D2. The data from this experiment is illustrated in Table 8. In Figure 59 the inverted transport rate is graphically displayed for both motion sequences. Statistical analysis between the D2 mixture samples which were transported with the hexasected motion sequence (DH2) and the samples which were transported with the trisected motion sequence (DT2) show that there was no significant difference in inverted transport rates ITR between sample batches DS2 ( $ITR = 2.5375 \pm 0.8870 \frac{mg}{s}$ ) and DT2 ( $ITR = 3.6754 \pm 2.1387 \frac{mg}{s}$ ) ( $h=0$ ,  $p = 0.3182$ ). It should be noted that only 3 out of 7 samples were successfully transported with the trisected motion sequence. Considering the relatively small amount of successfully transported tissue samples from the trisected motion sequence and considering the fact that there was no statistically significant difference between the inverted transport rate of the hexasected and trisected motion sequence the choice was made to perform Sub-experiment III with the hexasected motion sequence.

### 6.3 Sub-experiment III: Transport of Minced Meat

The prototype was able to transport compacted minced meat. The average inverted transport rate of the batch of minced meat, called O1, is  $2.1917 \pm 1.1367 \frac{mg}{s}$ . The numerical values from the analysis of this experiment are given in Table 9.

## 6. EXPERIMENT RESULTS

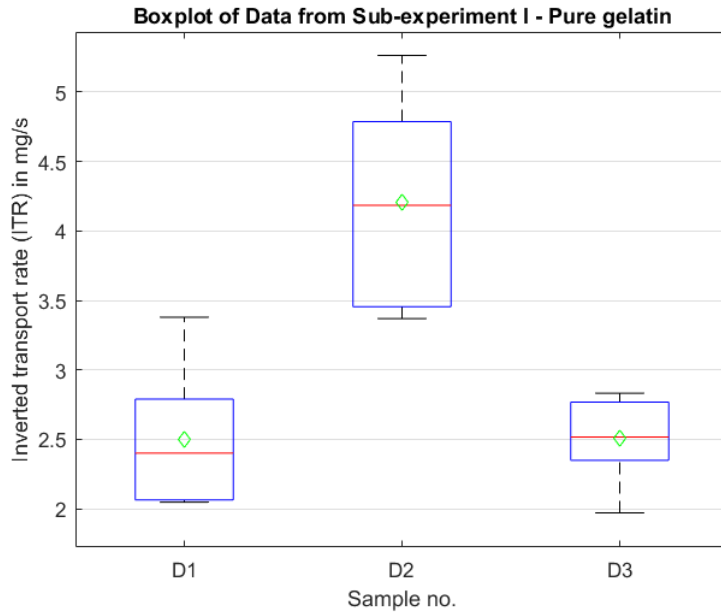


**Figure 57:** Boxplot graph displaying the distribution of data as collected from the pure gelatin samples of Sub-experiment I. The sample batch titles are shown on the x-axis and the inverted transport rate (ITR) in ( $\frac{mg}{s}$ ) is indicated on the y-axis. The maximal values and minimum values are indicated by the outermost horizontal solid lines on each box plot. The median of each dataset is indicated by the horizontal red line in each boxplot, while the mean of each sample batch is indicated by the green diamond.

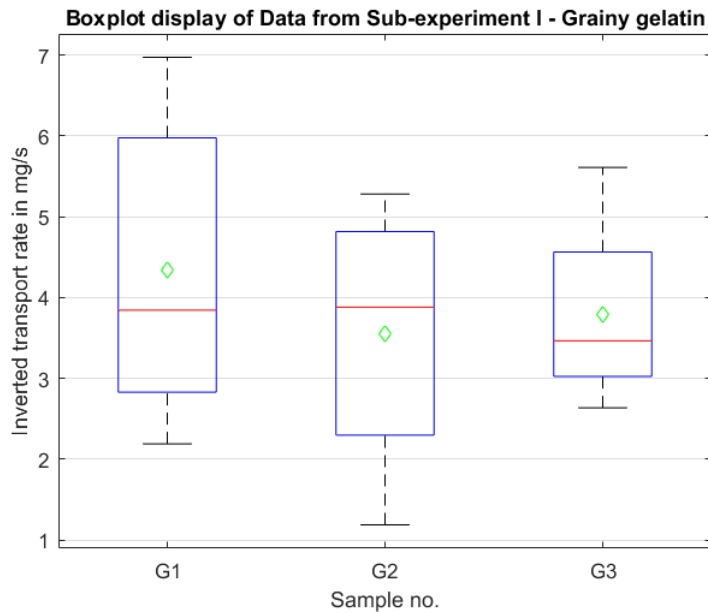


**Figure 58:** Boxplot graph displaying the distribution of data as collected from the grainy gelatin samples of Sub-experiment I. The sample batch titles are shown on the x-axis and the inverted transport rate (ITR) in ( $\frac{mg}{s}$ ) is indicated on the y-axis. The maximal values and minimum values are indicated by the outermost horizontal solid lines on each box plot. The median of each dataset is indicated by the horizontal red line in each boxplot, while the mean of each sample batch is indicated by the green diamond.

**Table 6:** Overview of the different transport rates (TR) of the pure gelatin transport rates that were collected from Sub-experiment I.

<b>Pure Gelatin</b>						
Transport rates						
Batch No.	No.	M1 (g)	M2 (g)	M3 (g)	t (s)	TR $\frac{s}{mg}$
D1	1	35.93	35.76	0.14	58.29	0.4164
	2	40.17	39.95	0.16	47.36	0.2960
	3	35.86	35.67	0.14	53.99	0.3856
	4	40.42	40.28	0.12	57.96	0.4830
	5	39.76	39.61	0.11	53.70	0.4882
D2	1	39.41	39.22	0.16	37.96	0.2373
	2	39.49	39.29	0.16	47.49	0.2968
	3	40.14	39.92	0.17	40.93	0.2408
	4	40.18	39.98	0.19	36.10	0.1900
	5	38.68	38.44	0.19	39.70	0.2089
	6	39.97	39.77	0.16	46.32	0.2895
D3	1	37.62	37.46	0.16	64.62	0.4039
	2	39.16	38.98	0.14	49.43	0.3531
	3	38.51	38.31	0.15	76.10	0.5073
	4	35.95	35.77	0.15	59.59	0.3973
	5	38.03	37.78	0.17	61.89	0.3641
Significance						
Vectors	<i>p</i> value		Significant			
D1,D2,D3	<i>p</i> = 0.0003		Y			

**Table 7:** Overview of the different transport rates (TR) of the grainy gelatin transport rates that were collected from Sub-experiment I.

Grainy Gelatin						
Transport rates						
Batch No.	No.	M1 (g)	M2 (g)	M3 (g)	t (s)	TR $\frac{s}{mg}$
G1	1	40.11	39.95	0.16	41.61	0.2601
	2	43.56	43.38	0.13	42.73	0.3287
	3	37.61	37.50	0.08	36.50	0.4562
	4	40.69	40.48	0.17	30.12	0.1772
	5	39.53	39.28	0.24	34.42	0.1434
G2	1	40.04	39.83	0.16	30.30	0.1894
	2	39.20	39.01	0.17	39.06	0.2298
	3	35.04	34.94	0.05	42.06	0.8412
	4	35.35	35.19	0.12	35.19	0.2932
G3	1	35.81	35.67	0.14	41.00	0.2929
	2	38.74	38.55	0.14	53.08	0.3791
	3	40.22	40.01	0.21	37.43	0.1782
	4	36.77	36.59	0.16	45.49	0.2843
Significance						
Vectors	$p$ value			Significant		
G1,G2,G3	$p = 0.7834$			N		

## 6. EXPERIMENT RESULTS

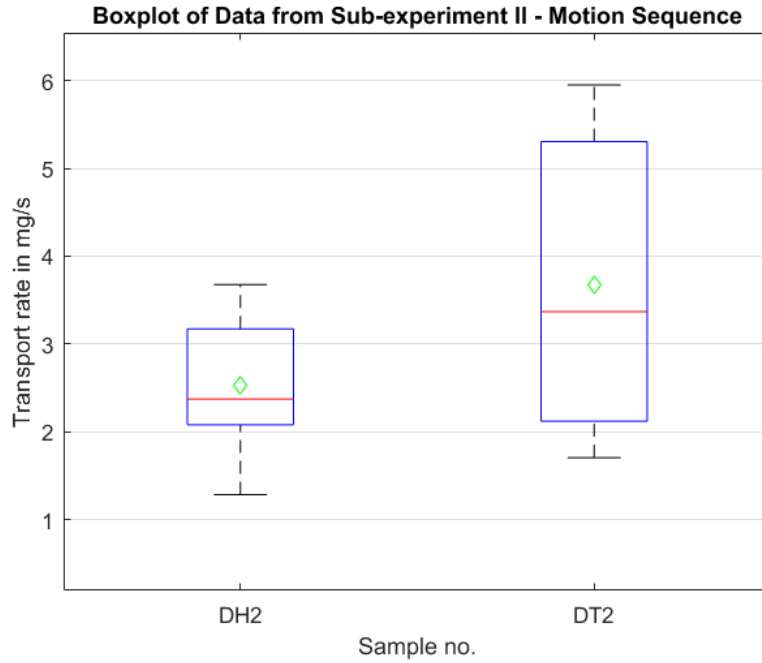


**Figure 59:** Boxplot graph displaying the distribution of data as collected from the gelatin samples of Sub-experiment II. The sample batch titles are shown on the x-axis and the inverted transport rate (ITR) in ( $\frac{mg}{s}$ ) is indicated on the y-axis. The maximal values and minimum values are indicated by the outermost horizontal solid lines on each box plot. The median of each dataset is indicated by the horizontal red line in each boxplot, while the mean of each sample batch is indicated by the green diamond.

**Table 8:** Overview of the different transport rates (TR) of the pure gelatin transport rates that were collected from Sub-experiment II.

Pure Gelatin						
Transport rates						
Batch No.	No.	M1 (g)	M2 (g)	M3 (g)	t (s)	TR $\frac{s}{mg}$
DH2	1	36.54	36.37	0.12	39.92	0.3327
	2	39.96	39.77	0.15	40.80	0.2720
	3	39.95	39.81	0.13	101.09	0.7776
	4	40.38	40.21	0.14	59.70	0.4264
	5	36.77	36.61	0.14	58.97	0.4212
DT2	1	37.95	37.77	0.15	44.52	0.2968
	2	40.55	40.35	0.18	105.49	0.5861
	3	37.35	37.16	0.21	35.29	0.1680
Significance						
Vectors	<i>p</i> value			Significant		
DH2, DT2	<i>p</i> = 0.3182			N		

**Table 9:** Overview of the different transport rates (TR) of the minced meat transport rates that were collected from Sub-experiment III.

<b>Minced meat</b>						
Transport rates						
Batch No.	No.	M1 (g)	M2 (g)	M3 (g)	t (s)	TR $\frac{s}{mg}$
O1	1	35.06	34.87	0.15	40.43	0.2695
	2	38.19	38.06	0.07	35.29	0.5041
	3	36.85	36.78	0.07	51.26	0.7323
	4	38.18	38.09	0.05	48.79	0.9758
	5	38.86	38.61	0.15	42.97	0.2865
	6	38.32	38.23	0.06	38.09	0.6348

## 7 Discussion

### 7.1 Summary of Main Findings

A methodical and theoretical design approach which originated in a problem-based project description was used to design and test a prototype. This biologically inspired mechanism of transport described within this report was designed in order to evade varying types of sub-optimal transport behaviour that occur within laparoscopic devices. The principle at work in this prototype shows that a friction-based alternative to suction can be utilized within laparoscopic equipment in order to reliably and successfully transport tissue along the inside of a tube. Two types of barrel cams, representative of two different motion sequences, were attached to a single rotary motor in order to provide a curve-driven movement that actuated a set of six curved blade adapter structures. These blade adapter structures were connected to a set of reciprocating blades that, as a result of the different barrel cams, ‘pulled’ the cylinder of material along its side within the tube according to different motions. This set of blades was inserted into a tube through which the transport took place. The sub-experiments have shown that the prototype was able to transport different gelatin samples with varying densities successfully. In addition, the prototype was able to transport gelatin samples with added particles and compacted minced meat. Though there was only a statistically significant difference in inverted transport rate for the comparison between pure gelatin mixture densities, the prototype was able to transport all types of tissue successfully. This method of transport has the potential of working within tubes that are limited in diameter. A main advantage of this method is the fact that all the material within the entire length of the tube is pulled along, since the pulling occurs at the sides of the tissue. The proposed method of transport is also independent of the temperature. In addition, the proposed method of transport has the advantage that it is not subject to the length dependent effects such as pressure loss, head loss and boundary layer growth that are associated with suction. Moreover, it is believed that the method of transport is independent of the transport diameter as well. Table 10 contains the titles of each requirement as described in Section 3 and states if this requirement has been met according to the specified standards. In

addition, a short explanation is added.

### 7.2 Limitations, Implications and Recommendations for Future Research

#### 7.2.1 Procedural Limitations

The tests described within this document were not conducted with biological material. The similarity between the experimental conditions and a future instrument can be increased by using tissue which is biological in nature. However, it has been decided that these tests will not be conducted using biological organ tissue due to a lack of availability of biological organ tissue and the consideration that organic tissues cannot be reproduced as easily as artificial tissue samples.

The length of time necessary to fully transport the tissue cylinder within the transport tube was visually assessed on the basis of video images acquired by recording the transport of the mixture with a video camera (Nikon COOLPIX P610). Though care was taken to ensure that no measurement errors occurred, by assessing the transport time multiple times; by repeating each test procedure six times; and by subjecting the data to a statistical analysis, it cannot be ruled out completely that human limitations accounted for some errors in measurement.

The amount of samples that were used to determine the transport rate and transport speed was determined by repeating all experimental conditions six times and taking the average. However, a larger sample size will allow for a better determination of the average value of the data due to the decreased influence of a relatively small number of possibly atypical values within the dataset. For example, the trisected motion sequence was able to transport 3 of the 7 prepared mixtures and the average inverted transport rate was therefore only dependent on 3 measurements. This motion sequence is therefore also somewhat limited in its capacity to transport tissue.

#### 7.2.2 Prototype Limitations

During movement the blades within the brass tube of the prototype appear to touch slightly which generates friction. While it was expected that some friction would occur as the sides of the blades come into contact

## 7. DISCUSSION

**Table 10:** List of the design requirements as described in Section 3. A short clarification to each verdict is added.

No.	Requirement Type	Achieved (Y/N)	Explanation
Geometric			
1	Transport Mechanism Length	Y	The designed principle is independent of length, therefore this requirement is satisfied.
2	Transported Tissue Length	Y	The length of the tissue which is transported is believed to be independent of the transport rate.
3	Transport Mechanism Diameter	Y	The diameter of the transport tube of the prototype is in accordance with the requirements.
Functional			
4	Only Transport	Y	The prototype is able to transport tissue and does not provide a cutting function.
5	Continuous Transport	Y	The prototype should be capable of transporting tissue continuously.
6	Semi-solid Matter Transport	Y	The prototype is able to transport a variety of tissues with varying densities.
Medical			
7	Laparoscopic Instrument Cleaning	Y	The principle used within the part consists of functioning parts which come into contact with tissue. In a functional prototype which functions within a clinical environment, these parts can be made out of material that is either disposable or material which can be cleaned and/or sterilized.
8	Bio-compatible Materials	Y	The principle used is not material dependent and the materials used for the prototype can be changed.
9	Isolated Transport	Y	The outer tube limits the ability of tissue to escape during transport.

with each other, it appears that one of the manufacturing procedures or manual handling during the assembly of the prototype has resulted in a slight bending of the blades. This was noted before assembly and effort was dedicated towards bending the blades back into their original shape. However, it can also be assessed by visual inspection that some slight deformation could not be eliminated. Therefore the efficacy of the prototype, as assessed by the measured transport rate and transport speed values, can be assumed to be negatively influenced by this inaccuracy in manufacturing/assembly.

Since the testing of multiple and varying mechanical settings was desired, the choice was made to make (re)assembly and dis-assembly of the prototype relatively easy. Therefore a relatively large amount of screwing and clamping fastening methods were included in the design of the final prototype. Repeated (re)assembly may account for a slight variation in functioning since the precise identical (re)alignment of components to a previous mechanical setting is hard to achieve manually. In addition, some manufacturing aspects could have contributed to less than expected prototype functioning. The printing quality of several 3D printed parts is somewhat grainy

and brittle.

### 7.2.3 Improved Tissue Mimicking

In order to incorporate the proposed prototype into a future medical device there are several key improvements which warrant further investigation. From the conducted tests it can be concluded that the device is able to transport gelatin with varying densities and minced meat within small tubes effectively. However, in order to assess its functioning with the transport of biological material, tests should be conducted with either material from deceased specimens or a material which more closely resembles all mechanical characteristics of organ tissue. It is also worthwhile to test the prototype with a rotary cutting morcellator in combination with the transport function to more accurately mimic the condition within a medical environment. The mimicking of the cutting step, by which the tissue is detached from the surrounding material, prior to the actual transport process may allow for the testing of more shear resistant materials which more accurately mimic the mechanical characteristics of other organ tissues, such as Polyvinyl alcohol (PVA) [19, 20, 21]. While gelatin and other mixable tissue mimicking materials are valid for testing a proof of principle prototype, the specificity of the statements made in this report can be increased if the underlying material characteristics of the transportable tissue can be regulated and identified. Gelatin has been shown to mimic mechanical characteristics of organ tissues [17, 18]. While the assessing of the material characteristics of several different gelatin mixtures is a time consuming process, it can aid in identifying the responsible material characteristics for improved or decreased functioning of the transport prototype and can therefore substantiate the more general conclusions reached within this document. Since the Young's Modulus represents a materials behaviour as it is subjected to stress and compression it was hypothesized that the transport rate or speed of the device increases when the Young's Modulus of the transportable tissue increases. While the blades move forward and backward, the friction that is applied to the sides of the tissue can either transport or deform the tissue. Therefore it is assumed that artificial mixture which is more easily deformed is not as easily transported since the applied shear deforms rather than transports the tissue.

### 7.2.4 Medical Environment Imitation

Further mimicking of realistic conditions can be achieved by converting the current prototype into a handheld device with a hard plastic casing. The device can then be used to transport tissues within a context that more closely resembles the medical environment for which it is designed. While uniformly constructed mimicking tissues will increase the repeatability of the experiment and will provide a more substantiated comprehension into the underlying causes of the transport behaviour as it is observed, the testing of structures with less coherent material characteristics on the other hand can offer more information about the transport versatility of the transport mechanism. By subjecting the prototype to transport experiments which include more grainy material or by adding lumps of harder material to the gel mixtures the observed transport rate can offer interesting insight about the functioning of the prototype in less accurately predicted transport situations. The testing of the transport mechanism at different angles may also provide valuable information about the effects of gravity on the transport process. In addition, while the author acknowledges the generality of this recommendation, the experimental phase of the evaluation process benefits from a larger amount of samples. Evidently, the adding of the morcellation step, the encasing of the prototype in a hard plastic cover and the selection of appropriate bio-compatible materials will be necessary in order to make this prototype into a fully functioning product which can convincingly cope with the demanding medical environment.

### 7.2.5 Addition of Microstructures and Alternative Motion Sequence

If microstructures are added to the inside of the tube of the prototype, the transport rate may be increased. The inspiration for this is the ovipositor sheath of *Apocrypta westwoodi*. The ovipositor is covered on the inside with a microstructure which prevents the egg from moving in any other direction than the desired transport direction [12]. Small structures which increase friction with the tissue can also prevent retrograde movement of the tissue within the tube of our design. Therefore, another cam may be introduced, see Figure 60. The configuration of the blades for this new motion sequence is graphically displayed in Figure 61. The sequence for this new barrel cam is shown

## 7. DISCUSSION



**Figure 60:** Photograph of the barrel cam that provides the bisected reciprocating motion.

in Figure 62. Two types of microstructures can be applied to the inner blade surface of the tube. In Figure 63 both types of inner blade surface structure are shown. Figure 63-A shows a schematic representation of an inner blade surface structure consisting of dendrites (orange) which are attached to the blades (grey) at a  $90^\circ$  angle. This type of inner blade surface lining is referred to as the *direction independent* structure since it is angled perpendicularly to the transport direction indicated by the black arrow. In Figure 63-B the inner blade surface structure is directed within the transport direction and is attached to the blades at an angle of  $60^\circ$ . This type of microstructure is referred to as the *direction dependent* structure. The inner blade surfaces of the blades can be covered with several types of microstructures. In addition, both motion sequences can also be tested without any added microstructures to the inner blade surface.

### 7.2.6 Increase Motor Speed and Simplify Components

To increase the transport speed the stroke length with which the blades move up and down can be increased. In addition, the current motor can be replaced by a rotary motor with a higher maximum speed. Several gearboxes with the same dimensions as the one used here are available which are able to provide a higher rotary speed [22, 23]. However, in order to reliably increase the speed of the reciprocating motion of the blades more design effort should be dedicated to ensuring that the blades move parallel to each other. This can be done by redesigning the method of motion transfer from

the rotary motion to the reciprocating motion by eliminating the blade adapter structures, of which the curved surfaces complicate the correct parallel alignment of the blades to some extent. If the reciprocating blades can be directly attached to the bearings which slot into the barrel cam path, the alignment- and the blade movement precision can be increased.

### 7.2.7 Radial Locking

Another improvement involves limiting the ability of the blades to move radially inward. The current design of the prototype did not include a radial locking mechanism such as the one that is found within the ovipositor of the wasp, i.e., the olistheter mechanism (see Appendix E). The repeatability and uniformity of the parallel motion of the blades for extended periods of time will be increased if a method of radial locking can be added to the touching surfaces of the blades. A short explanation of the thought process leading up to this conclusion is given in Appendix E. Besides incorporating a radial locking mechanism the redesign of the touching blade surfaces may be used to implement a smart method of locking which in turn has the effect of decreasing the amount of surface contact.

### 7.2.8 Combination with Suction

By combining this friction based transport mechanism with suction the prototype will also be able to transport liquids. This is probably due to the fact that several modes of sub-optimal behaviour, in which the stationary inner wall contributes considerably to the sub-optimal

## 7. DISCUSSION

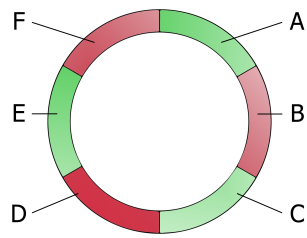


**Figure 61:** Schematic representation of the bisected reciprocating blade configuration.

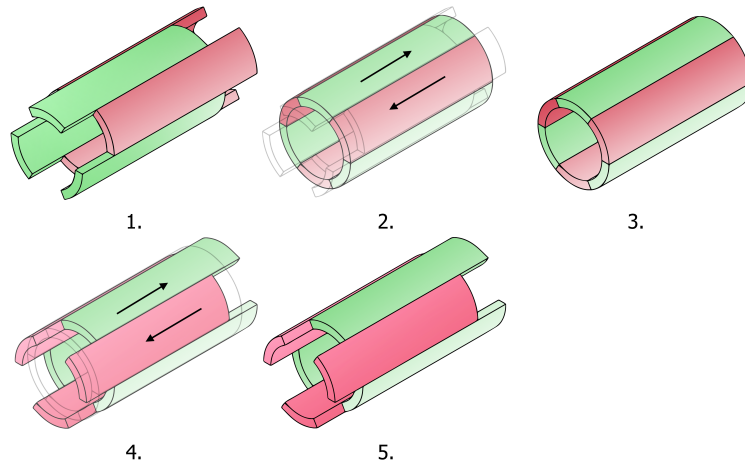


**Figure 62:** Graphic representation of the bisected reciprocating motion sequence. The colour coding corresponds to the code shown in Figure 61. Step 1 shows the green blade triple at the maximum stroke location while the red blade triple is at the minimum stroke location. Step 2 shows the green blade triple retreating to 0 stroke location while the red blade triple advances to 0 stroke location. In Step 3 the green blade triple is at the 0 stroke location while the red blade triple is also positioned at the 0 stroke location. In Step 4 the green blade triple moves further backward to the minimum stroke location while the red blade triple moves further forward to the maximum stroke location. Step 5 shows the green blade triple at the minimum stroke location while the red blade triple is at the maximum stroke location.

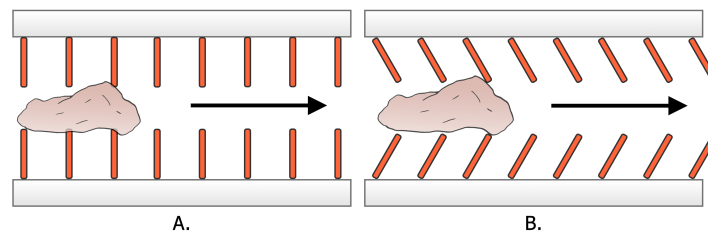


**Figure 63:** Schematic representation of direction independent inner blade surface structure (A) and direction dependent inner blade surface structure (B) from a side view. The desired transport direction is indicated by the arrow. The wall structures are shown in black, the grey rectangles represent the blades and the pink shape represents the tissue to be transported.

function of the transport process, are now less applicable since the inner structures are constantly moving back- and forwards.

### 7.2.9 Generalization of Application

Finally, the prospect of applying this mechanism of transport to fields other than the medical may greatly improve transport of semi-solid

## 7. DISCUSSION

material within tubes in general. Other fields, such as sewer cleaning or the transport of raw produce, may also benefit from a mechanism which does not obstruct as easily as other forms of endo-tubular transport. This would definitely require scaling the prototype to fit the needs of other fields. This scaling effect may in turn also prove to provide interesting information which allows for an assessment of a possible dimension element to the functioning of the instrument. Therefore it may be rewarding to generalize this transport principle and to apply it to other fields in order to assess the general applicability of this mechanism and to utilize the advantages offered by this mechanism to the largest extent.

manoeuvre through the body necessitates an increase in length, the amount of suction needs to increase in order to provide the same transport functionality. Due to the increased suction, however, close proximity to the rotating morcellator head will also be more likely to suck in healthy tissue. It is a strain on the imagination to envision a steerable instrument with an outer diameter of 1 mm that is able to transport tissue effectively using suction. Since several problems attributed to suction increase as the diameter decreases, it is unlikely that future instruments will rely as much on suction as is currently the case.

### 7.3 Future Vision

Minimally invasive surgery is an appealing alternative to open surgery and is increasingly replacing traditional surgical procedures [1]. The main goal of minimally invasive surgery is the limiting of the minimum amount of tissue damage that is necessary to successfully perform a surgical procedure. As the field of minimally invasive surgery is developed, the diameter of the instrument sheaths that are inserted will inevitably decrease. The post-operative cosmetic demands of the patient will also include minimizing the incision length of the entries into the body of the patient and therefore necessitates the further miniaturization of the instruments used within these types of procedures. In addition, the development of steerable instruments will allow the surgeon to evade organs which impede the desired access route towards the operation site. The use of miniature steerable instruments will furthermore allow for endovascular access. Miniature steerable instruments will be able to perform delicate endovascular surgeries which are currently still performed using the traditional approach of open surgery. In order for the transport method as outlined in this report to be future proof, it will have to be developed into a steerable method of transport. Ideally, it should also be miniaturized even further. The potential of this instrument lies in its miniaturizability and its independence of transport length. Suction transport falls short as the trends of miniaturized- and steerable instruments gain ground. In addition, the pulling effect of suction transport does not discriminate between tissue which should be extracted and tissue which should not be extracted. As the ability of instruments to

## 8 Conclusion

In this report the methodical design, prototype development and subsequent experimental verification of a continuously operating, biologically inspired endo-tubular transport mechanism is presented. This transport mechanism, inspired by the egg-laying tube (ovipositor) of a wasp, was subjected to a repeatable and reproducible test procedure which showed that the prototype was able to successfully transport gelatin tissue mimics which varied in density but also in particle presence. A second experiment showed that the influence of an alternative curve-driven motion sequence was also able to transport tissue, though there was no statistically significant difference in inverted transport rate (ITR) between these two motion sequences. In addition, the prototype was able to transport compacted minced meat which, due to the prior morcellation step, accurately resembles several types of morcellated biological material. Further research should be directed towards development into a fully functional laparoscopic prototype, a better mimicking of tissue material or testing on biological material and the increasing of the speed and reliability with which transport occurs. This instrument has the potential to change the way tissue is transported and may improve transport within medical instruments in particular.



## References

- [1] Jenny Dankelman, Cornelis A. Grimbergen, and Henk G. Stassen. *Engineering for Patient Safety*. Lawrence Erlbaum Associates, Publishers Inc., Mahwah, New Jersey, 2005.
- [2] Thomas L. Foster and Frederick D. Roemer. Flexible cannula, March 18 2004. Pub. No.: US 2004/0054377 A1.
- [3] Shailendra K. Parihar, Patrick J. Minnelli, Gregory W. Johnson, Mark J. Bookbinder, Nabeel M. Jadeed, and Frederick E. Shelton. Tissue retrieval device with resilient member, July 18 2011. Pub. No.: US 2011/0184311 A1.
- [4] Eduard Altman and Nina Altman. Device and method for evacuating refuse from tissue of the body, November 18 1999. Pub. No.: WO 99/58066.
- [5] Gregory P. Schmitz, Juan D. Perea, Ming-Ting Wu, T. Chen, Richard, and Arun. Veeramani. Minimally invasive micro tissue debriders having targeted rotor positions, May 1 2014. Pub. No.: WO 2014/066542 A1.
- [6] Schlueter & Smith Childers. Update: New johnson and johnson/ethicon mdl created for morcellator cancer cases, 2016. URL: <http://www.cssfirm.com/>, last visited on Apr. 18, 2017.
- [7] GRC Surgical. Lina xcise morcellator, 2017. URL: <http://grcsurgical.com/lina-xcise/>.
- [8] S.R. Driessen, E.A. Arkenbout, A.L. Thurkow, and Jansen F. Electromechanical morcellators in minimally invasive gynecologic surgery: An update. *The Journal of Minimally Invasive Gynecology*, 21(3):377–383, 2014.
- [9] LLC themedicalbiochemistrypage.org. Introduction to blood coagulation, 2017. URL: <https://themedicalbiochemistrypage.org/blood-coagulation.php>.
- [10] Isaac Newton. *Newton's Principia : The Mathematical Principles of Natural Philosophy*. Daniel Adee, New-York, 1846.
- [11] Natural History Museum. Wasp id required, 2012. URL: <http://www.nhm.ac.uk/natureplus/message/22734>, last visited on Jan. 30, 2018.
- [12] M.H. Rahman, M.G. Fitton, and D.L.J. Quicke. Ovipositor internal microsculpture in the braconidae (insecta, hymenoptera). *Zoologica Scripta*, 27(4):319–331, 1998.
- [13] Posthoorn P. The design of a self-propelling mechanism for an endoluminal robot. *TU Delft repository*: <http://repository.tudelft.nl/>, pages 1–43, 2017.
- [14] Maxon motor. Maxon motor re 10mm 1.5w, partnumber: 118400, 2017. URL: <https://www.maxonmotor.nl/maxon/view/product/motor/dcmotor/re/re10/118400>.
- [15] Maxon motor. Maxon planetary gearhead gp 10mm, partnumber: 218418, 2017. URL: <https://www.maxonmotor.nl/maxon/view/product/gear/planetary/gp10/218418>.
- [16] R. Bude and R. Adler. An easily made, low-cost, tissue-like ultrasound phantom material. *Journal of Clinical Ultrasound*, 23:271–273, 1995.
- [17] A. Farrer, H. Odéen, J. de Bever, B. Coats, D. Parker, A. Payne, and D. Christensen. Characterization and evaluation of tissue-mimicking gelatin phantoms for use with mrgfus. *Journal of Therapeutic Ultrasound*, 3:1–11, 2015.
- [18] S. Cournane, A. Fagan, and J. Browne. Review of ultrasound elastography quality control and training test phantoms. *Ultrasound*, 20(1-2):1–13, 2012.
- [19] T.L. de Jong, L.H. Pluymen, D.J. van Gerwen, G. Kleinrensink, J. Dankelman, and J. van den Dobbelen. Pva matches human liver in needle-tissue interaction. *Journal of the Mechanical Behavior of Biomedical Materials*, 69:223–228, 2017.

## REFERENCES

- [20] S. Jiang, S. Liu, and W. Feng. Pva hydrogel properties for biomedical application. *Journal Of The Mechanical Behaviour Of Biomedical Materials*, 4:1228–1233, 2011.
- [21] C. Hassan and N. Peppas. Structure and morphology of freeze/thawed pva hydrogels. *Macromolecules*, 33:2472–2479, 2000.
- [22] Maxon motor. Maxon planetary gearhead gp 10mm, partnumber: 218416, 2017. URL: <https://www.maxonmotor.nl/maxon/view/product/gear/planetary/gp10/218416>.
- [23] Maxon motor. Maxon planetary gearhead gp 10mm, partnumber: 218417, 2017. URL: <https://www.maxonmotor.nl/maxon/view/product/gear/planetary/gp10/218417>.
- [24] T. Ahmed, T. Zhang, K. He, S. Bai, and Z Wang. Sense organs on the ovipositor of macrocentrus cingulum brischke (hymenoptera: Braconidae): their probable role in stinging, oviposition and host selection process. *Journal of Asia-Pacific Entomology*, 16:343–348, 2013.
- [25] K. Nakajima and O. Schwarz. How to use the ovipositor drilling mechanism of hymenoptera for developing a surgical instrument in biomimetic design. *Int. J. of Design & Nature and Ecodynamics*, 9(2):177–189, 2014.
- [26] J.F.V. Vincent and M.J. King. The mechanism of drilling by wood wasp ovipositors. *Biomimetics*, 3(4):187–201, 1995.
- [27] M. Scali, T.P. Pusch, P. Breedveld, and D. Dodou. Ovipositor-inspired steerable needle: design and preliminary experimental evaluation. *Bioinspiration & Biomimetics*, *accepted*, pages 1–21, 2017.
- [28] L. Frasson, S.Y. Ko, A. Turner, T. Parittotokkaporn, J.F. Vincent, and F.R. Baena. Sting: a soft-tissue intervention and neurosurgical guide to access deep brain lesions through curved trajectories. *Proceedings of the Institution of Mechanical Engineers, Part H*, 224:775–788, 2009.

## A Database Search Queries

### A.1 Explanatory Note

The advanced search queries shown here contain both verbs and nouns relating to the subject to accurately describe what *type* of object should fulfill which *function*. The query is made up of bracketed segments which contain synonyms of either verbs or nouns. The syntax between these bracketed segments indicates if combinations (AND-statements) or variations (OR-statements) should be made. The asterisk in these search queries is a symbol that is commonly used to find words that start with the same selection of letters and therefore helps with broadening the amount of findings by searching for variations of a word without adding more search terms. For example, *morcellat\** will retrieve documents containing both the word *morcellation* or *morcellating*.

AND laparos\*) OR TTL/((transport\* OR retriev\* OR extract\* OR retract\* OR evacuat\*) AND (instrument\* OR device\* OR tool\* OR morcellat\*) AND tissue\* AND laparos\*)

### A.2 Espacenet Search Query

A selection of keywords regarding the topic of transport in medical instrumentation was established in order to conduct an advanced search in the Espacenet patent database. Shown here is the search query entered into the title query according to the syntax appropriate for the Espacenet patent database. In addition the relevant cooperative patent classification (CPC A61: Medical or veterinary science; hygiene) was included in the search criteria. This search query is shorter than the search entered in the FPO patent database for the reason that the advanced search option in Espacenet does not allow for a search query exceeding 10 search terms, excluding syntax statements.

(transport\* OR evacuat\* OR extract\* OR retriev\*) AND (instrument\* OR device\* OR tool\*) AND tissue\*

### A.3 FPO Search Query

A selection of keywords regarding the topic of transport in medical instrumentation was established in order to conduct an advanced search in the Freepatentsonline patent database. Shown here is the search query according to the syntax appropriate for the Freepatentsonline patent database.

ABST/((transport\* OR retriev\* OR extract\* OR retract\* OR evacuat\*) AND (instrument\* OR device\* OR tool\* OR morcellat\*) AND tissue\*



## B Preliminary Knowledge of Fluid Mechanics

The principle of transport by aspiration has been introduced in the report. However, it is of importance to highlight a few fundamental basics of fluid transport in order to more accurately understand the sub-optimal behaviour as described within this report. While the theory discussed here applies to fluids in general, only non-Newtonian liquids will be considered in this document.

### B.1 Liquid Flow in Narrowing and Expanding Ducts

In the situation shown in Figure 64 a duct is shown which narrows in diameter and subsequently increases again. It is assumed that this duct is filled with a liquid, with a density  $\rho$  in  $[\frac{Kg}{m^3}]$ , which flows in laminar fashion in the direction indicated by the red arrows. When the diameter of such a pipe is decreased (see Figure 64-B), the velocity is increased and the pressure drops. The expression at Equation 25 is called the Bernoulli equation and shows the relation between the energy in [J] at one location in the pipe (A) relative to another location in the pipe (B). From the knowledge regarding the preservation of energy it is known that the amount of energy [J] expressed on the left side of the equation should be equal to the amount in [J] on the right side of the equation. Therefore, energy at location A should remain equal to the energy at location B. When the radius  $r$  mm increases again (see Figure 64.C), the pressure  $P_x$  in pascal [Pa] begins to rise and the velocity  $v_x$   $[\frac{m}{s}]$  decreases again.

$$P_A + \frac{1}{2} \cdot \rho \cdot v_A^2 + \rho \cdot g \cdot h_A = P_B + \frac{1}{2} \cdot \rho \cdot v_B^2 + \rho \cdot g \cdot h_B \quad [J] \quad (25)$$

In short, the Bernoulli Equation can be used to simulate the effects of a constriction which is introduced into a pipe. Such constrictions can be deliberate, such is the case in narrowing pipe ducts, but can also be incidental, such as pieces of debris which obstruct the liquid flow. From Equation 25 the effect of an obstruction or constriction in the diameter can be deduced. Let us look with a little more detail what happens when this example is considered parametrically. The expression shows us the energy contribution in terms of height difference at both sides of the expression. This is represented by the height expression  $h_x$  in [m]. Since the tube is oriented

horizontally in our example, these components can be neglected and the expression can be rewritten so that it becomes Equation 26 and it is now an expression of a measure of difference in velocity.

$$v_B^2 - v_A^2 = \frac{2 \cdot (P_A - P_B)}{\rho} \quad [J] \quad (26)$$

$$v_B^2 - v_A^2 = \frac{2 \cdot \Delta P}{\rho} \quad [J] \quad (27)$$

From the rewritten expression shown in Equation 26 it can be gathered that the velocity  $v_x$  in  $[\frac{m}{s}]$  is coupled to the pressure difference  $\Delta p$  in [Pa] and the density of the liquid flow in  $\rho$   $[\frac{Kg}{m^3}]$ . From this expression it can be observed that the decrease in pressure is a result of an increase in velocity. If a pressure value of  $P_B$  [Pa] such that  $P_B > P_A$  is assumed, the value on the right side of Equation 26 will be negative. Consequently, the change in velocity will be positive as can be seen from the left side of Equation 26. This is the numerical representation of the converse effect between altering velocities and pressures. A biologically occurring example of narrowing in ducts is the medical condition known as *stenosis*, in which the passage of blood can be severely inhibited due to an unintended narrowing of the blood vessel.

### B.2 Newtonian Versus Non-Newtonian Liquid Behaviour

A liquid is considered to represent Newtonian behaviour when the viscosity is independent of the amount of shear applied to it. However, perfect Newtonian liquids are nonexistent and Newtonian behaviour can only be emulated. The liquid behaviour best known for its accurate resemblance to Newtonian behaviour is that of water.

However, when a liquid does not comply to the aforementioned behaviour it is said to portray non-Newtonian behaviour. Different kinds of non-Newtonian behaviour exist. For example, when the viscosity of a fluid is increased as a result of an increase in applied shear stress the behaviour is referred to as *shear thickening*. These fluids are called *dilatant* fluids of which a well known example is the aforementioned combination of cornflour and water. When the viscosity decreases as a result of increased shear stress this behaviour is described by

## B. PRELIMINARY KNOWLEDGE OF FLUID MECHANICS

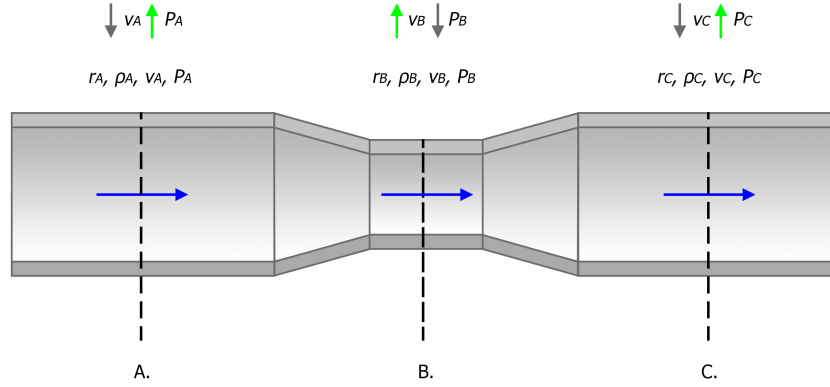


**Figure 64:** Schematic representation of duct with narrowing- and subsequent expanding inner diameters. The duct is filled with a liquid which flows in the direction of the blue arrows. The parameters which represent the flow at different locations are defined as such:  $r_x$  is the radius at  $x$ ,  $\rho_x$  [ $\frac{Kg}{m^3}$ ] is the density of the liquid at location  $x$ ,  $v_x$  is the flow velocity in [ $\frac{m}{s}$ ] at  $x$  and  $P_x$  [ $Pa$ ] is the pressure at  $x$ . The situation at (A) can be considered to be the initial condition of the liquid flow within the duct, which is altered when the duct narrows at (B) and expands again at (C). The effects on the pressure and the velocity are represented at each location. The green arrows indicate an increase of the associated property while the gray arrows indicate a decrease of the associated property.

the term *shear thinning* and the fluids in this situation are known as *pseudoplastic* fluids. A good example of a pseudoplastic liquid is ketchup which becomes less viscous when shear is applied to it.

Furthermore, it is interesting to note that viscosity can be considered to be a kind of friction in that both friction and viscosity represent forces which are counteractive to the direction of motion. However, the term viscosity is uniquely used to describe resisting forces in fluid layers. Using this explanation of both friction and viscosity as forces counteracting the motion of matter the decrease of friction can be understood to be a type of lubrication. In a similar way it can subsequently be accepted that this same definition is valid for resisting forces within fluid layers. Consequently it can be stated that a layer of reduced friction (or reduced viscosity) between two layers with relatively higher friction or viscosity can be considered a type of lubrication. This definition will prove to be valuable in defining the effects of sub-optimal behaviour modes in following sections.

### B.3 Flow Loss in Ducts and Boundary Layers

Flow loss can be the result of friction between the interface of the flowing fluid and the surface of the inner diameter of the duct. This friction

does not only occur in one plane between the fluid and the inner diameter's surface but can rather be represented as a layer in which the friction gradually increases as the flow develops and becomes constant as it progresses. This layer is called a boundary layer and is graphically represented in Figure 65. The thickness  $\delta$  in mm of a boundary layer, indicated by the red arrow in Figure 65 adjacent to the  $\delta$ , can be determined by using the boundary layer equations for laminar flow, which is shown in Equation 28. Boundary layers are also present in turbulent flowing fluids and the boundary layer thickness for these fluids is given by Equation 29. In Equation 28 the thickness  $\delta_L$  is determined by the free flow velocity  $v_0$  in [ $\frac{m}{s}$ ] and the kinematic viscosity  $\nu$  in [ $\frac{m^2}{s}$ ]. The turbulent flow boundary layer thickness  $\delta_T$  is determined by the distance from the start of the boundary layer which is denoted with  $x$  mm, the density of the liquid flow  $\rho$  in [ $\frac{Kg}{m^3}$ ], the free-stream velocity  $v_0$  in [ $\frac{m}{s}$ ] and the viscosity  $\mu$  in [ $Pa \cdot s$ ] as shown in Equation 29. Please note that the velocities in Equations 28 and 29 are in boldface in order to distinguish between the velocity  $v_0$  and the kinematic viscosity  $\nu$ .

$$\delta_L \approx 5 \cdot \sqrt{\frac{\nu_x}{\mathbf{v}_0}} \quad [\text{mm}] \quad (28)$$

$$\delta_T \approx \frac{5 \cdot x}{\sqrt{\frac{\rho \cdot \mathbf{v}_0 \cdot x}{\mu}}} \quad [\text{mm}] \quad (29)$$

Flow loss can also occur as a result of pressure

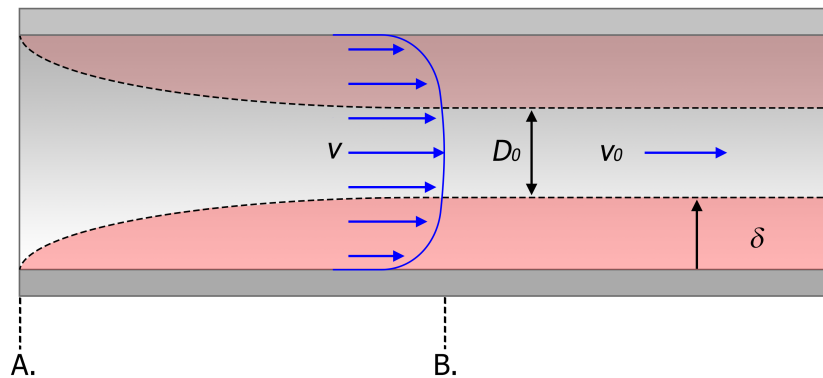


**Figure 65:** Schematic representation of a duct with a boundary layer representation on both sides of the inner surface of the duct. The boundary layer, shown in red, is representative of the amount of fluid friction within the tube and can be seen to gradually develop from zero at (A) into a maximum value at (B). The free-stream velocity  $v_0$  in  $[\frac{m}{s}]$  for which the value is constant only occurs in the region between the opposite sides of the boundary layer, as indicated in the schematic representation with the diameter  $D_0$ . The thickness of the boundary layer,  $\delta$  [m] is indicated with the black arrow. The velocity profile shown in blue and denoted with  $v$  shows the development of the velocity within the internal diameter of the duct.

loss due to a difference in height. The result of a height difference ensues that the contribution to the total amount of energy as a result of potential energy cannot be neglected. In these situations, the pressure is decreased at a relatively higher position due to the fact that the pressure has to counteract the effects of gravity. Since it was assumed in a preceding section that the pipe in our example was horizontally oriented and was filled with a parallel flowing liquid, the potential energy components in Equation 25 were ignored.



## C Biological Inspiration

The biological inspiration for this design is the ovipositor sheath and the associated process of oviposition, as is found in females of the insect order Hymenoptera. The purpose of oviposition is the deposition of eggs in a suitable substratum such as a host creature, a piece of fruit or the bark of a tree in order to provide the wasp's progeny with nutrition during the early stages of development [24, 25, 12, 26, 27, 28]. A cross sectional oblique view of the ovipositor is shown in Figure 66. The ovipositor is made up out of three segments called valves. The top segment, which is the largest segment, is called the dorsal valve and is connected by means of the olistheter to the other two valves, called the ventral valves. The olistheter is a sliding connection which consists of a tongue (rachis) on the dorsal valve and a groove (aulax) on the ventral valve. All valves are parallel to each other and the olistheter connection allows the valves to slide relative to each other while staying parallel.

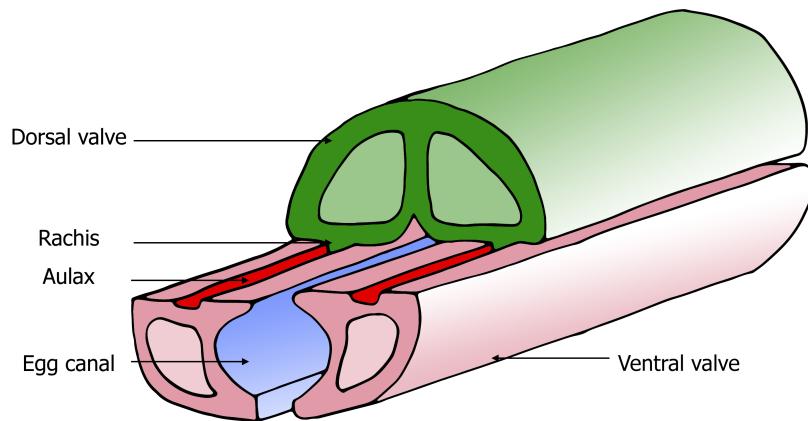


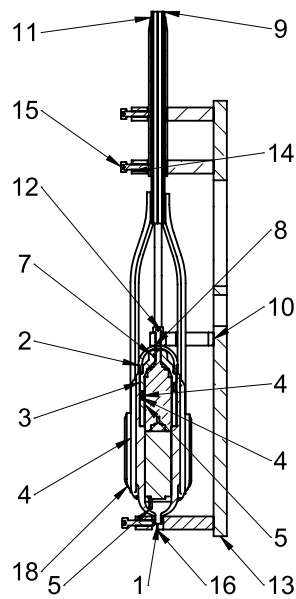
**Figure 66:** Schematic representation of a cross sectional oblique view of the ovipositor mechanism. The ovipositor is made up out of the dorsal valve (green) and is connected by means of the olistheter to the ventral valves (pink). The olistheter is a sliding connection which consists of a tongue, called the rachis, on the dorsal valve and a groove (red), called the aulax, on the ventral valve. Figure adapted by the author from Rahman, Fitton and Quicke [12].



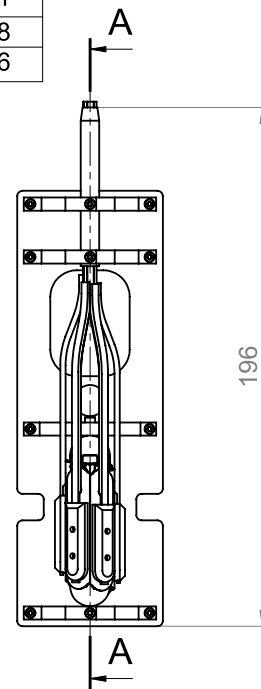
## D Technical Drawings

### D.1 Assembly

NO.	PART NUMBER	QT Y:
1	1 Housing bottom	1
2	2 Housing top	1
3	3 Rotor	1
4	4 Slider with bearing	6
5	5 Motor Gearhead assembly	1
6	ISO 4026 - M2 x 3-N	3
7	ISO 4026 - M2 x 2.5-N	1
8	BA (blade adapter)	6
9	BS (blade - single)	6
10	SF-S3 (suspending frame stand 3)	1
11	OT (outer tube)	1
12	B18.3.1M - 2 x 0.4 x 4 Hex SHCS -- 4NHX	1
13	SF-BP (suspending frame base plate)	1
14	SF-S1 (suspending frame stand 1)	2
15	B18.3.1M - 2 x 0.4 x 10 Hex SHCS -- 10NHX	3
16	SF-S4 (suspending frame stand 4)	1
17	B18.3.1M - 2 x 0.4 x 5 Hex SHCS -- 5NHX	8
18	AC (adapter clamp)	6



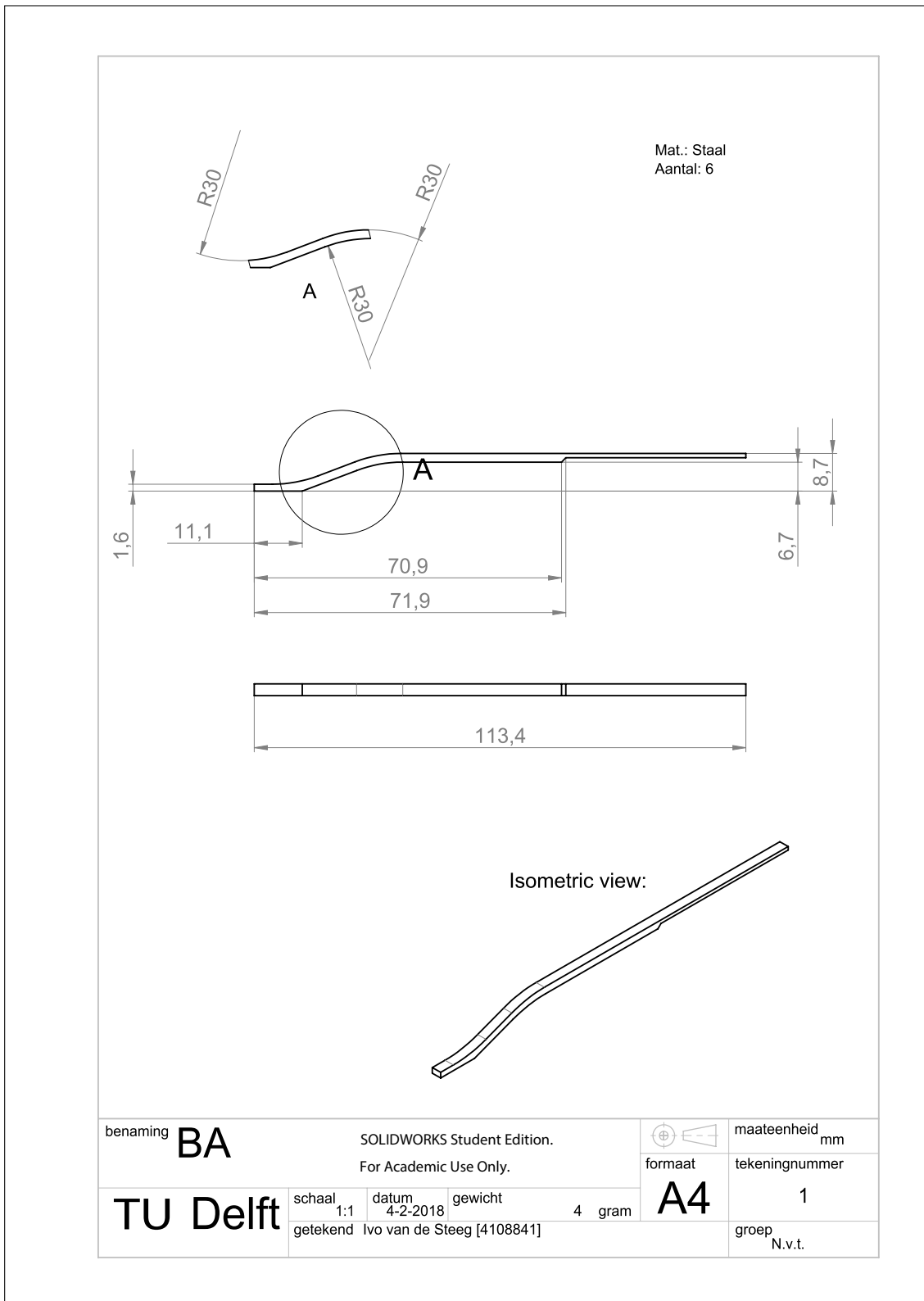
A-A (1 : 2)



benaming		<b>ASSEM</b>		SOLIDWORKS Student Edition. For Academic Use Only.		maateenheid mm	
TU Delft		schaal 1:1	datum 4-2-2018	gewicht	gram	formaat <b>A4</b>	tekeningnummer 1
		getekend Ivo van de Steeg [4108841]				groep N.v.t.	

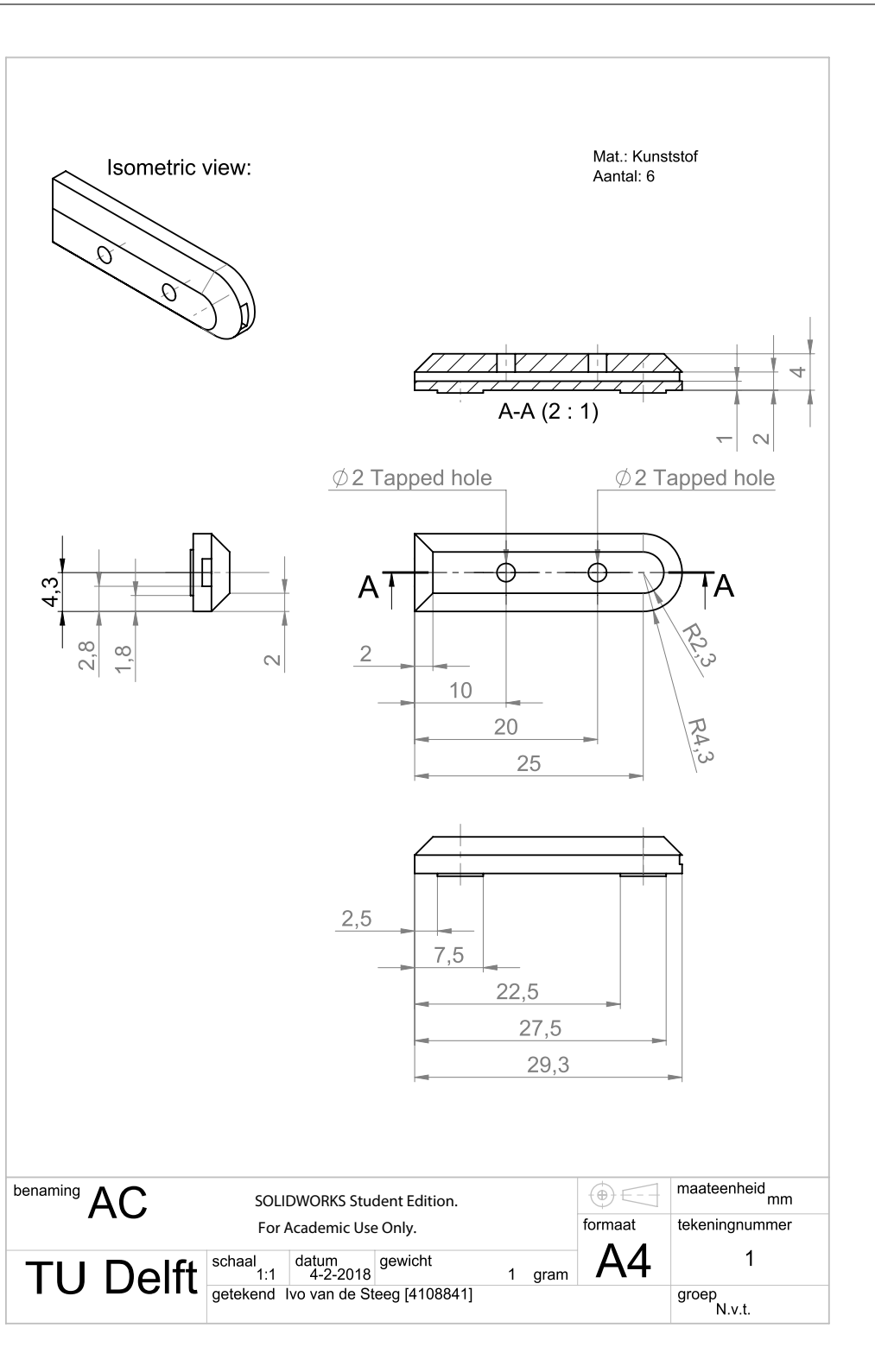
D. TECHNICAL DRAWINGS

D.2 Blade Adapter



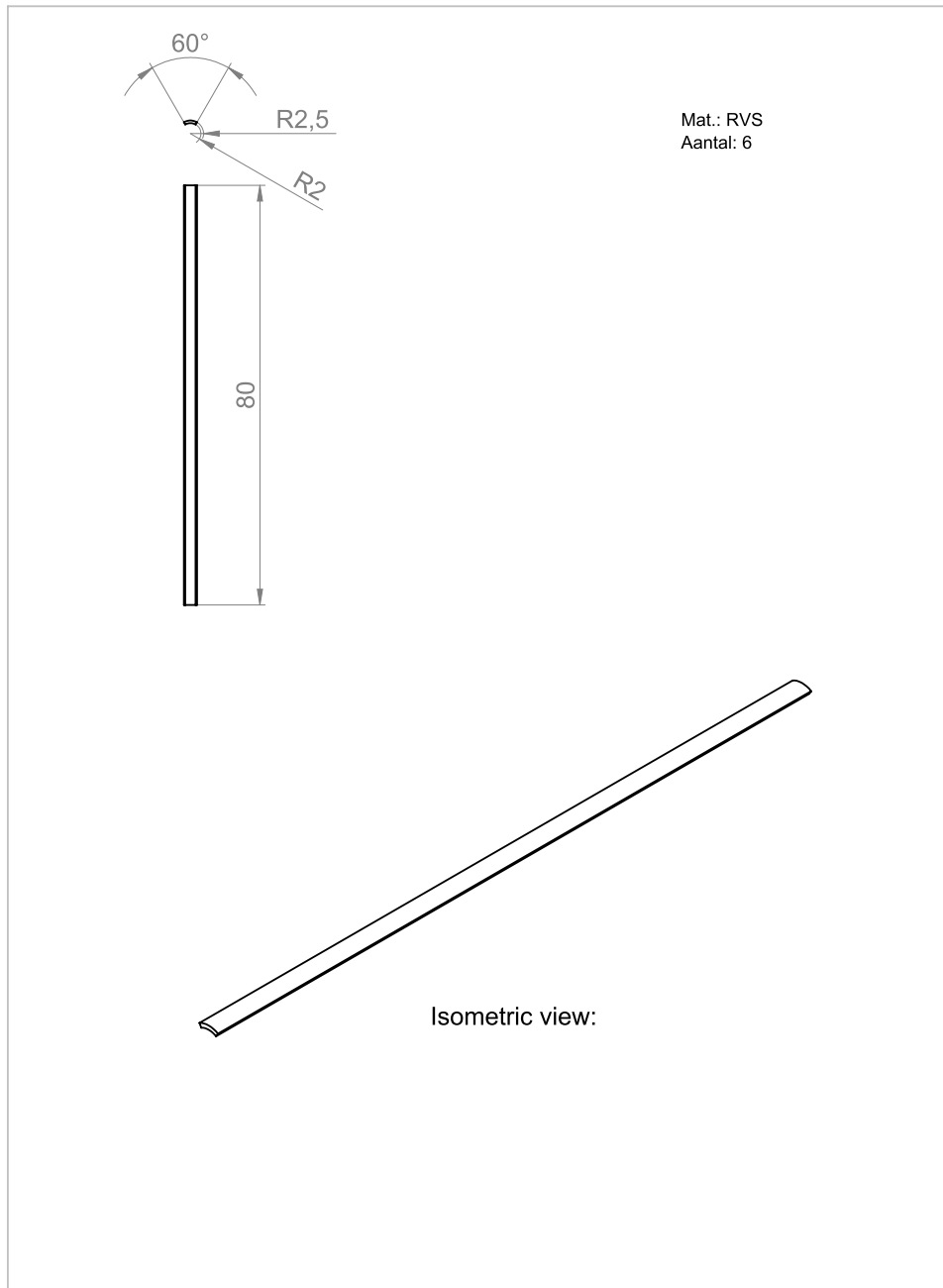
D. TECHNICAL DRAWINGS

D.3 Adapter Clamp



D. TECHNICAL DRAWINGS

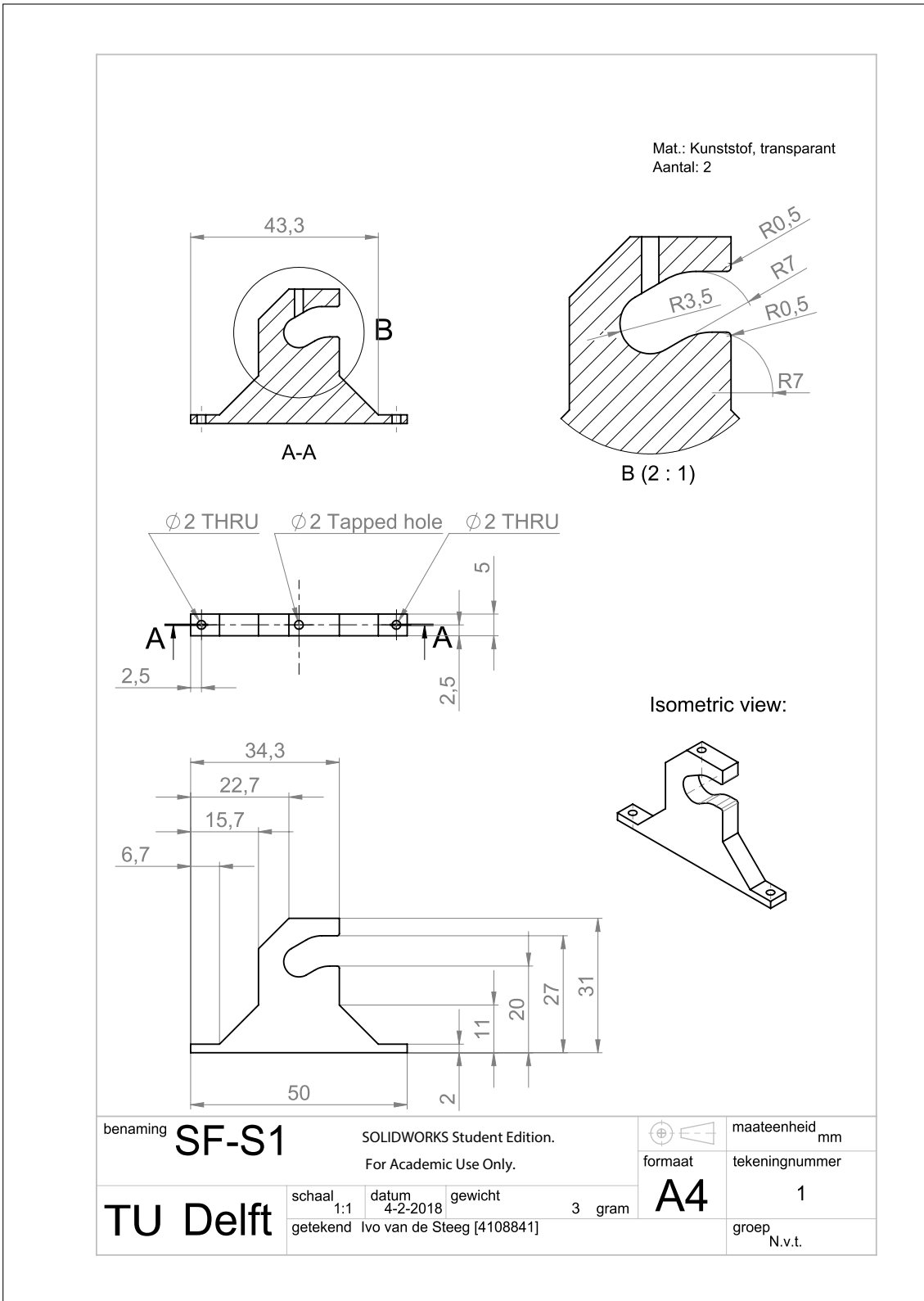
D.4 Blade



benaming <b>BS</b>		SOLIDWORKS Student Edition.		maateenheid mm	
		For Academic Use Only.		tekeningsnummer	
<b>TU Delft</b>	schaal 1:1	datum 4-2-2018	gewicht 1 gram	<b>A4</b>	1
	getekend	Ivo van de Steeg [4108841]			groep N.v.t.

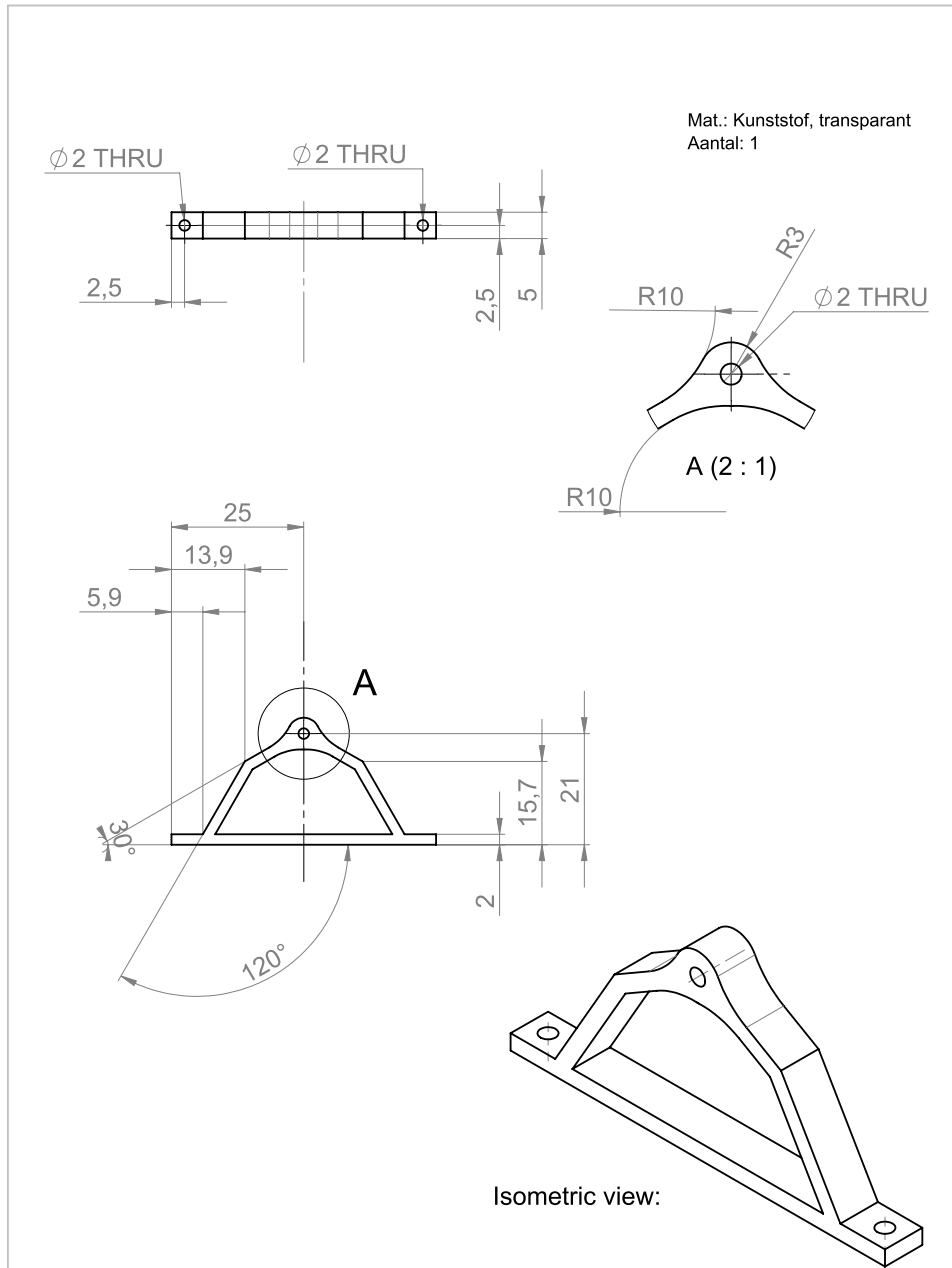
D. TECHNICAL DRAWINGS

D.5 Suspending Frame - Stand 1



D. TECHNICAL DRAWINGS

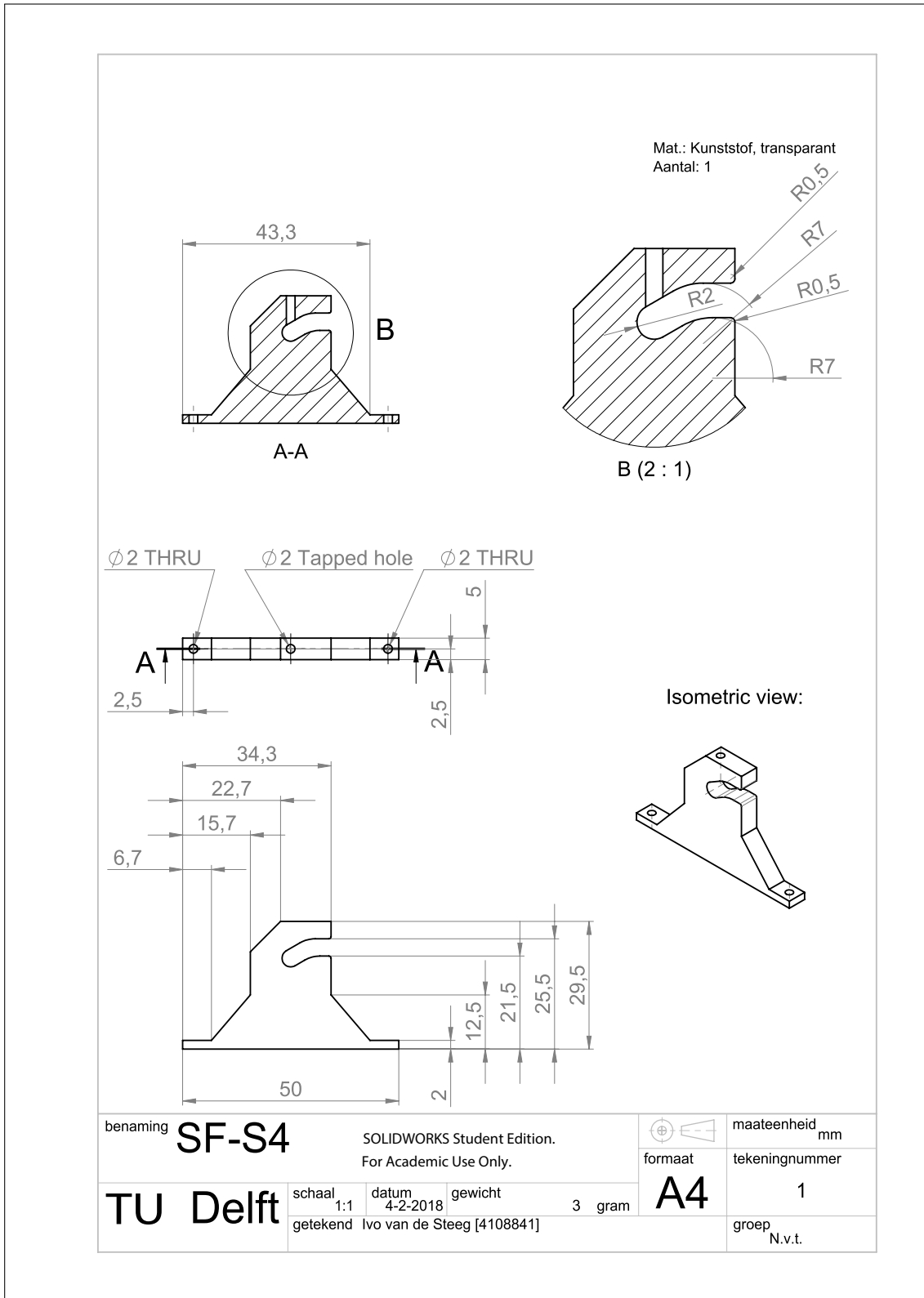
D.6 Suspending Frame - Stand 3



benaming <b>SF-S3</b>		SOLIDWORKS Student Edition. For Academic Use Only.		 maateenheid mm	
TU Delft		schaal 1:1	datum 4-2-2018	gewicht 1 gram	formaat <b>A4</b> tekeningnummer 1
		getekend Ivo van de Steeg [4108841]			groep N.v.t.

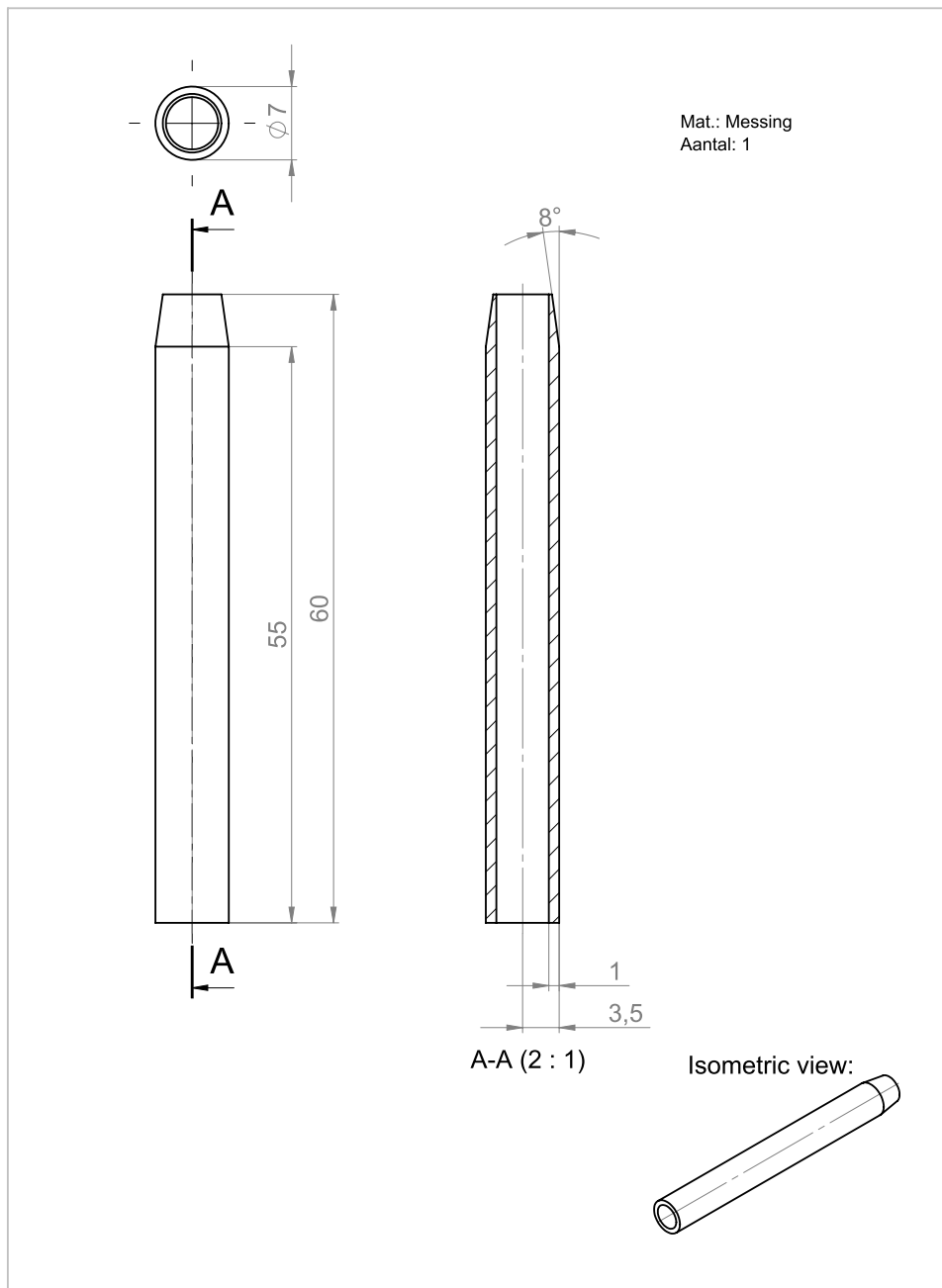
D. TECHNICAL DRAWINGS

D.7 Suspending Frame - Stand 4



D. TECHNICAL DRAWINGS

D.8 Outer Tube



Mat.: Messing  
Aantal: 1

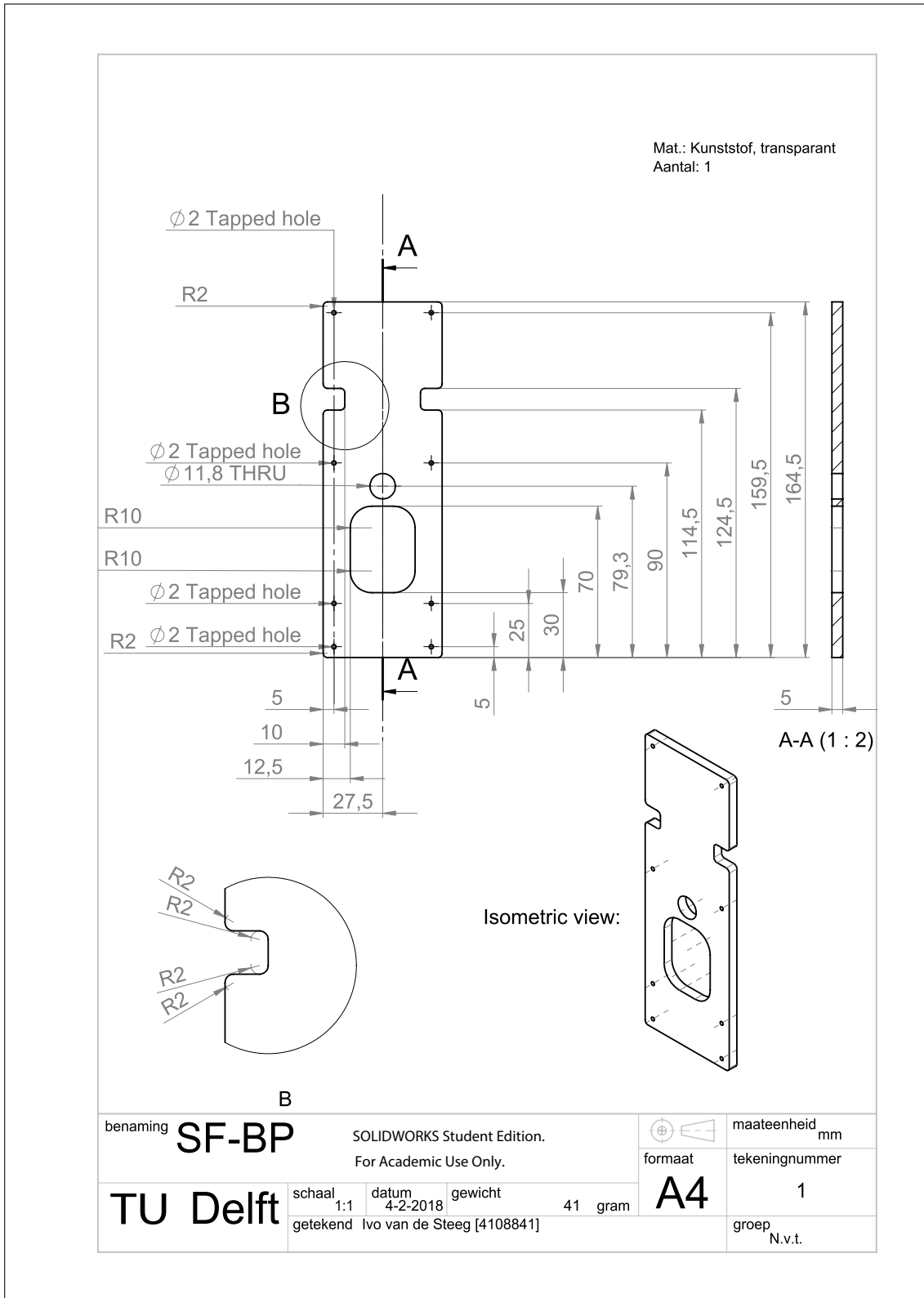
A-A (2 : 1)

Isometric view:

benaming <b>OT</b>		SOLIDWORKS Student Edition. For Academic Use Only.		maateenheid mm	
TU Delft		schaal 1:1	datum 4-2-2018	gewicht 9 gram	formaat <b>A4</b>
		getekend Ivo van de Steeg [4108841]		tekeningnummer 1	
				groep N.v.t.	

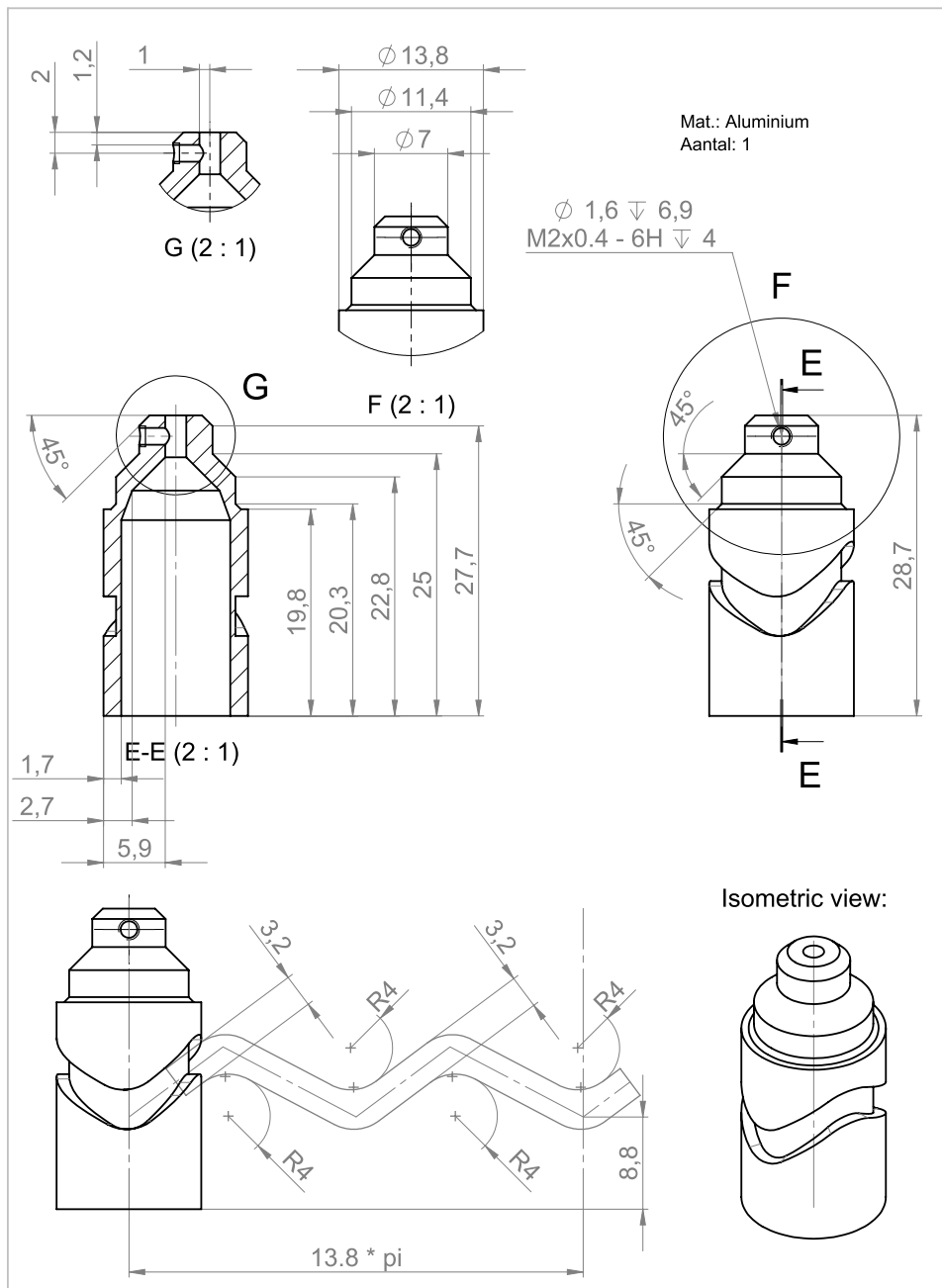
D. TECHNICAL DRAWINGS

D.9 Suspending Frame - Base Plate



D. TECHNICAL DRAWINGS

D.10 Rotor



benaming <b>R2</b>		SOLIDWORKS Student Edition.		maateenheid mm	
		For Academic Use Only.		formaat <b>A4</b>	
<b>TU Delft</b>		schaal 1:1	datum 3-2-2018	gewicht	gram
		getekend Ivo van de Steeg [4108841]		tekeningnummer <b>1</b>	
				groep N.v.t.	

## E Radial Locking Method

The ovipositor sheath's valves which move relative to each other in a parallel manner are connected by means of a tongue and groove joint known as the olistheter (shown in Figure 66). Similarly, the mechanism described within this report may profit from such a locking principle. In the current design, the blades are meant to be held together by their shape alone. In architecture, this principle is found in arches, see Figure 67. The shape of the stones comprising the arch limit the ability of each stone to move inward, similarly to the blades of the instrument reported within this document. However, the thickness of the blades affects the ability to lock them in place relative to each other to a large extent. In order to block thin blades from moving inwards or outwards during movement, i.e., limiting the movement in the radial direction, a shape lock can be added at the surfaces at which the blades touch. The direction is defined as going radially outwards from the centerline of the cylinder in Figure 68. This shape locking mechanism is intended to keep the blades in a cylindrical configuration during movement and to keep the blades moving parallel to each other. Radial movement freedom can be limited by adding a shape grip at either the out- or inside of the blades or by incorporating the shape lock within the blades. However, the addition of a shape lock on the outside of the blades will require extra material to extend radially outwards and will therefore increase the diameter of the instrument. Adding material to the inside of the blades will limit the diameter through which tissue is intended to be transported. The option of integrating a shape locking mechanism within the thickness of the blades therefore seems to be the least volume demanding option. Now that the ideal location at which the shape lock can be achieved is identified, it is important that the amount of friction which occurs between the touching surfaces is minimized. In general, there are three options when trying to reduce the amount of friction.

1. The introduction of intermediate material layers which have a low coefficient of friction to the touching surface. Sliding bearings are a good example of this principle.
2. The sliding friction can also be replaced by rolling friction. Rolling element bearings are commonly found between parts which have a large velocity difference between

them.

3. The mechanical interfaces can also be lubricated, which requires the introduction of a liquid. Lubricating gears or hinges and other moving parts is very common and examples where lubrication is very common include mechanical watches, combustion engines and bike chains.

Ideally, the smooth functioning of the prototype does not require the introduction of another substance, i.e., lubrication. In addition, the scale at which the parts will have to be manufactured limits the possibility of incorporating small elements such as ball bearings. Therefore, the addition of a low friction intermediate layer as a barrier between components of the same materials is the most viable option. The intermediate layer can also incorporate the shape locking function. Shape locks can be achieved within layers by providing a groove to one of the touching surfaces, while adding a tongue to the other. As a result of manufacturing processes the edges of such grooves and tongues will, in reality, be filleted. This small fillet radius is considered to be an advantage for our purpose, since the stress distribution will occur over a larger area and the risk of breaking of the narrow edges will be decreased while the ability to form a shape lock is maintained.

## E. RADIAL LOCKING METHOD

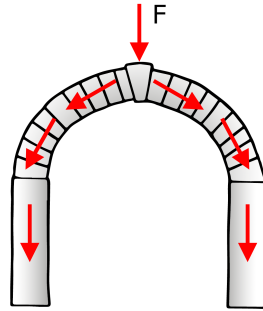


**Figure 67:** Schematic representation of an arch. The stones of such an arch are shaped in order to limit each stone from moving inward and to transfer the forces from the material above towards the ground on which the arch is built. The red arrows represent the fashion in which that force, represented by  $F$ , is transferred from stone to stone by means of the keystone and subsequently further downwards in the direction of gravity. This force transfer is due to the semi-circular configuration which is also seen in the design discussed within this document.

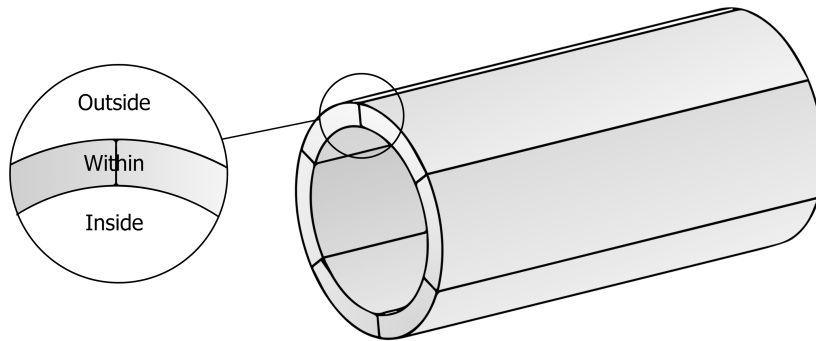


**Figure 68:** Schematic representation of the blades in a cylindrical configuration. The detail balloon shows the mechanical interface location of two blades. Radial movement freedom can be limited by adding a shape grip at either the out- or inside of the blades or by integrating the shape lock within the thickness of the blades.

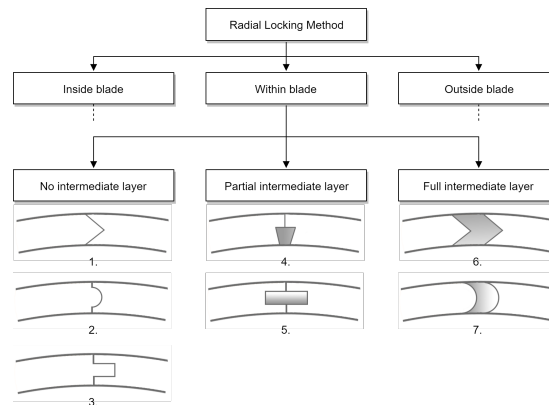


**Figure 69:** Schematic diagram of the categorization of the different radial shape locking methods. The first subdivision step is based on the location at which the locking method is applied. Limiting the radial movement freedom can be achieved at three locations: on the inside walls of the blades, within the thickness of the blades or at the outside of the blades, graphically represented in Figure 68. The second step is based on the extent to which an intermediate layer separates the two touching surfaces in order to minimize friction. These categories can be further subdivided into categories containing shape locking methods without intermediate layer, with a partial intermediate layer and with a full intermediate layer.

## F Matlab Scripts for Data Analysis

### F.1 ANOVA Test Sub-experiment I - Pure Gelatin

The script shown in Listing 1 was written in order to perform an ANOVA statistical analysis on the dataset that was acquired during Sub-experiment I.

```

% This script analyses the data obtained during this Experiment and
% generates plots for the different experimental conditions.

% Author: Ivo van de Steeg
% Created: 2018 january 12

%% 1.0 Initialize Script
% Close all non-associated files and clear the memory.
clear; close all; clc;

%% 1.1 Load Data
% Reported transport times in seconds (s):
TimeD1 = [58.29 47.36 53.99 57.96 53.70];
TimeD2 = [37.96 47.49 40.93 36.10 39.70 46.32];
TimeD3 = [64.62 49.43 76.10 59.59 61.89];
% Combine into one vector:
Time = [TimeD1 TimeD2 TimeD3];

% Reported weights of the transported material in mg:
% Pure gelatin:
WeightD1 = [140 160 140 120 110];
WeightD2 = [160 160 170 190 190 160];
WeightD3 = [160 140 150 150 170];
% Combine into one vector:
Weight = [WeightD1 WeightD2 WeightD3];

% Load the dataset of transport rates in ( '.' s/mg) in this vector
% written as: trans_rate = [D1_1, D1_2, ..., D2_x]:
Trans_rate = rdivide(Time,Weight);

% Designation of sample batch:
Sample_no = {'D1', 'D1', 'D1', 'D1', 'D1', 'D2', 'D2', 'D2', 'D2', 'D2', 'D2', 'D2', 'D3', ...
            'D3', 'D3', 'D3', 'D3'};

%% 1.2 Perform Analysis
% Run ANOVA analysis on the dataset:
[p,tbl] = anova(Trans_rate,Sample_no,'boxstyle','off');

%% 1.3 Control Output of Data
% Generate boxplot
bxplot = boxplot(Trans_rate,Sample_no);

% Only display y-axis in the Figure display:
ax = gca;
ax.XGrid = 'off';
ax.YGrid = 'on';

% Title of the boxplot
title('Boxplot of Data from Sub-experiment I - pure gelatin','FontSize',10)
% Label x-axis as the Sample number:
xlabel('Sample no.')
% Label y-axis as the Transport rate in (s/mg):
ylabel('Transport rate in s/mg')

% Calculate means of batches:
Mean_D1 = mean(Trans_rate([1 2 3 4 5 ]));
Mean_D2 = mean(Trans_rate([6 7 8 9 10 11 ]));
Mean_D3 = mean(Trans_rate([12 13 14 15 16]));
% Combine into one vector:
Mean_D1_D2_D3 = [Mean_D1 Mean_D2 Mean_D3];

% Overlay the means as green diamonds within the boxplot display:

```

## F. MATLAB SCRIPTS FOR DATA ANALYSIS

```
hold on
plot(Mean_D1_D2_D3, 'dg')
hold off

% Calculate standard deviations:
sd1=std(Trans_rate([1 2 3 4 5 ]));
sd2=std(Trans_rate([ 6 7 8 9 10 11 ]));
sd3=std(Trans_rate([ 12 13 14 15 16 ]));
% Combine into one vector:
Std = [sd1 sd2 sd3];
```

Listing 1: Experiment Data Analysis Matlab Script

### F.2 ANOVA Test Sub-experiment I - Grain Gelatin

The script shown in Listing 2 was written in order to perform an ANOVA statistical analysis on the data that was acquired during Sub-experiment I.

```
% This script analyses the data obtained during this Experiment and
% generates plots for the different experimental conditions.

% Author: Ivo van de Steeg
% Created: 2018 january 12

%% 1.0 Initialize Script
% Close all non-associated files and clear the memory.
clear; close all; clc;

%% 1.1 Load Data
% Reported transport times in seconds (s):
% Grain gelatin:
TimeG1 = [41.61 42.73 36.50 30.12 34.42];
TimeG2 = [30.30 39.06 42.06 35.19 ];
TimeG3 = [41.00 53.08 37.43 45.49];
% Combine into one vector:
Time = [TimeG1 TimeG2 TimeG3];

% Reported weights of the transported material in mg:
% Grain gelatin:
WeightG1 = [160 130 80 170 240];
WeightG2 = [160 170 50 120];
WeightG3 = [140 140 210 160]
% Combine into one vector:
Weight = [WeightG1 WeightG2 WeightG3];

% Load the dataset of transport rates in ( '.' s/mg) in this vector
% written as: trans_rate = [G1_1, G1_2, ..., G2_x]:
Trans_rate = rdivide(Time,Weight);

% Designation of sample batch:
Sample_no = {'G1','G1','G1','G1','G1','G2','G2','G2','G2','G3','G3','G3','G3'};

%% 1.2 Perform Analysis
% Run ANOVA analysis on the dataset:
[p,tbl] = anova(Trans_rate,Sample_no,'boxstyle','off');

%% 1.3 Control Output of Data
% Generate boxplot
bxplot = boxplot(Trans_rate,Sample_no);

% Only display y-axis in the Figure display:
ax = gca;
ax.XGrid = 'off';
ax.YGrid = 'on';

% Title of the boxplot
title('Boxplot display of Data from Sub-experiment I - grainy gelatin','FontSize',10)
% Label x-axis as the Sample number:
```

## F. MATLAB SCRIPTS FOR DATA ANALYSIS

```
xlabel('Sample no.')
% Label y-axis as the Transport rate in (s/mg):
ylabel('Transport rate in s/mg')

% Calculate means of batches:
Mean_D1 = mean(Trans_rate([1 2 3 4 5]));
Mean_D2 = mean(Trans_rate([ 6 7 8 9]));
Mean_D3 = mean(Trans_rate([10 11 12 13 ]));
% Combine into one vector:
Mean_D1_D2_D3 = [Mean_D1 Mean_D2 Mean_D3];

% Overlay the means as green diamonds within the boxplot display:
hold on
plot(Mean_D1_D2_D3, 'dg')
hold off

% Calculate standard deviations:
sd1=std(Trans_rate([1 2 3 4 5]));
sd2=std(Trans_rate([ 6 7 8 9]));
sd3=std(Trans_rate([10 11 12 13]));
% Combine into one vector:
Std = [sd1 sd2 sd3];
```

Listing 2: Experiment Data Analysis Matlab Script

### F.3 T-Test Sub-experiment I

The script shown in Listing 3 was written in order to perform a t-test statistical analysis on the dataset that was acquired during Sub-experiment I.

```
% This script analyses the data obtained during this Experiment and
% generates plots for the different experimental conditions.

% Author: Ivo van de Steeg
% Created: 2018 january 12

%% 1.0 Initialize Script
% Close all non-associated files and clear the memory.
clear; close all; clc;

%% 1.1 Load Data
% Reported transport times in seconds (s):
% Pure gelatin:
%TimeD1 = [58.29 47.36 53.99 57.96 53.70];
%TimeD2 = [37.96 47.49 40.93 36.10 39.70 46.32];
TimeD3 = [64.62 49.43 76.10 59.59 61.89];
% Grain gelatin:
%TimeG1 = [41.61 42.73 36.50 30.12 34.42];
%TimeG2 = [30.30 39.06 42.06 35.19 ];
TimeG3 = [41.00 53.08 37.43 45.49];
% Combine into one vector:
Time = [TimeD3 TimeG3];

% Reported weights of the transported material in mg:
% Pure gelatin:
%WeightD1 = [140 160 140 120 110];
%WeightD2 = [160 160 170 190 190 160];
WeightD3 = [160 140 150 150 170];
% Grain gelatin:
%WeightG1 = [160 130 80 170 240];
%WeightG2 = [160 170 50 120];
WeightG3 = [140 140 210 160];
% Combine into one vector:
Weight = [WeightD3 WeightG3];

% Load the dataset of transport rates in ( '..' s/mg) in this vector
% written as: trans_rate = [D1_1, D1_2, ..., D2_x]:
Trans_rate = rdivide(Time,Weight);
```

## F. MATLAB SCRIPTS FOR DATA ANALYSIS

```
x = Trans_rate([1 2 3 4 5]);
y = Trans_rate([6 7 8 9]);
% Designation of sample batch:
Sample_no = {'D3', 'D3', 'D3', 'D3', 'D3', 'G3', 'G3', 'G3', 'G3'};

%% 1.2 Perform Analysis
% Run t-test analysis on the dataset:
[h,p] = ttest2(x,y)

%% 1.3 Control Output of Data
% Generate boxplot
bxplot = boxplot(Trans_rate,Sample_no);

% Only display y-axis in the Figure display:
ax = gca;
ax.XGrid = 'off';
ax.YGrid = 'on';

% Title of the boxplot
title('Boxplot of Data from Sub-experiment I - Pure VS. Grainy','FontSize',10)
% Label x-axis as the Sample number:
xlabel('Sample no.')
% Label y-axis as the Transport rate in (s/mg):
ylabel('Transport rate in s/mg')

% Calculate means of batches:
Mean_D1 = mean(x);
Mean_G1 = mean(y);
% Combine into one vector:
Mean_D1_G1 = [Mean_D1 Mean_G1];

% Overlay the means as green diamonds within the boxplot display:
hold on
plot(Mean_D1_G1, 'dg')
hold off

% Calculate standard deviations:
sd1=std(x);
sd2=std(y);
% Combine into one vector:
Std = [sd1 sd2];
```

Listing 3: Experiment Data Analysis Matlab Script

### F.4 T-Test Sub-experiment II

The script shown in Listing 4 was written in order to perform a t-test statistical analysis on the dataset that was acquired during Sub-experiment II.

```
% This script analyses the data obtained during this Experiment and
% generates plots for the different experimental conditions.

% Author: Ivo van de Steeg
% Created: 2018 january 12

%% 1.0 Initialize Script
% Close all non-associated files and clear the memory.
clear; close all; clc;

%% 1.1 Load Data
% Reported transport times in seconds (s):
% Pure gelatin:
TimeDH2 = [39.92 40.80 101.09 59.70 58.97];
% Pure gelatin:
TimeDT2 = [44.52 105.49 35.29];
% Combine into one vector:
Time = [TimeDH2 TimeDT2];
```

## F. MATLAB SCRIPTS FOR DATA ANALYSIS

```
% Reported weights of the transported material in mg:
% Pure gelatin:
WeightDH2 = [120 150 130 140 140];
% Grain gelatin:
WeightDT2 = [150 180 210];
% Combine into one vector:
Weight = [WeightDH2 WeightDT2];

% Load the dataset of transport rates in ( '..' s/mg) in this vector
% written as: trans_rate = [D1_1, D1_2, ..., D2_x]:
Trans_rate2 = rdivide(Time,Weight);
Trans_rate = 1./Trans_rate2;

x = Trans_rate([1 2 3 4 5]);
y = Trans_rate([6 7 8 ]);
% Designation of sample batch:
Sample_no = {'DH2', 'DH2', 'DH2', 'DH2', 'DH2', 'DT2', 'DT2', 'DT2'};

%% 1.2 Perform Analysis
% Run t-test analysis on the dataset:
[h,p] = ttest2(x,y)

%% 1.3 Control Output of Data
% Generate boxplot
bxplot = boxplot(Trans_rate,Sample_no);

% Only display y-axis in the Figure display:
ax = gca;
ax.XGrid = 'off';
ax.YGrid = 'on';

% Title of the boxplot
title('Boxplot of Data from Sub-experiment II - Motion Sequence','FontSize',10)
% Label x-axis as the Sample number:
xlabel('Sample no.')
% Label y-axis as the Transport rate in (mg/s):
ylabel('Transport rate in mg/s')

% Calculate means of batches:
Mean_DH2 = mean(x);
Mean_DT2 = mean(y);
% Combine into one vector:
Mean_Motion = [Mean_DH2 Mean_DT2];

% Overlay the means as green diamonds within the boxplot display:
hold on
plot(Mean_Motion, 'dg')
hold off

% Calculate standard deviations:
sd1=std(x);
sd2=std(y);
% Combine into one vector:
Std = [sd1 sd2];
```

Listing 4: Experiment Data Analysis Matlab Script

### F.5 Script for Sub-experiment III

The script shown in Listing 5 was written in order to analyze the dataset that was acquired during Sub-experiment III.

```
% This script analyses the data obtained during this Experiment and
% generates plots for the different experimental conditions.

% Author: Ivo van de Steeg
% Created: 2018 january 12
```

## F. MATLAB SCRIPTS FOR DATA ANALYSIS

```
%% 1.0 Initialize Script
% Close all non-associated files and clear the memory.
clear; close all; clc;

%% 1.1 Load Data
% Reported transport times in seconds (s):
TimeO1 = [40.43 35.29 51.26 48.79 42.97 38.09];
% Combine into one vector:
Time = [TimeO1];

% Reported weights of the transported material in mg:
% Pure gelatin:
WeightO1 = [150 70 70 50 150 60];
% Combine into one vector:
Weight = [WeightO1];

% Load the dataset of transport rates in ( '..' s/mg) in this vector
% written as: trans_rate = [D1_1, D1_2, ..., D2_x]:
Trans_rate = rdivide(Time,Weight);
Trans_rate2 = 1./(Trans_rate);
% Designation of sample batch:
Sample_no = {'D1', 'D1', 'D1', 'D1', 'D1', 'D1'};

% Calculate means of batches:
Mean_O1 = mean(Trans_rate2([1 2 3 4 5 6]));

% Calculate standard deviations:
sdl=std(Trans_rate2([1 2 3 4 5 6]));
```

**Listing 5:** Experiment Data Analysis Matlab Script

## G Preparatory Experiment - Demonstration of Functionality

In order to assess if the prototype is able to complete a transport procedure, a short experiment was conducted. A rectangular piece of melamine cleaning sponge (approximate dimensions: width = 4 mm, height = 4 mm and length = 20 mm) was soaked in liquid hand soap and was subsequently manually inserted into the proximal end of the transport tube. In order to capture the transport procedure from the side of the device the polarity of power supply was switched. As the images within Figure 70 show, the device is able to transport the rectangular piece of melamine within approximately 11 seconds along the whole length of the device. The data from this preparatory experiment will not be included in the data analysis and are therefore also not subject to the data collection protocol as outlined in Figure 53.

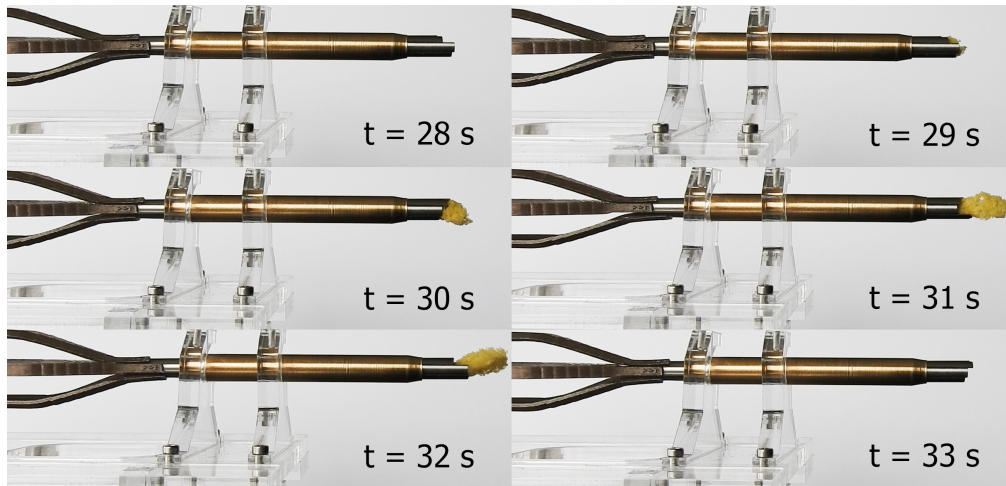


**Figure 70:** A series of screen captures (arranged from left to right, top to bottom) with a camera (Nikon COOLPIX P610) of the demonstration with a rectangular piece of melamine cleaning sponge (yellow). The recorded images show the instances right before the melamine sponge appears at the distal end of the instrument to right after the appearance. Time stamps are included in each screen capture.



## H Transport Rates of Sub-experiment I

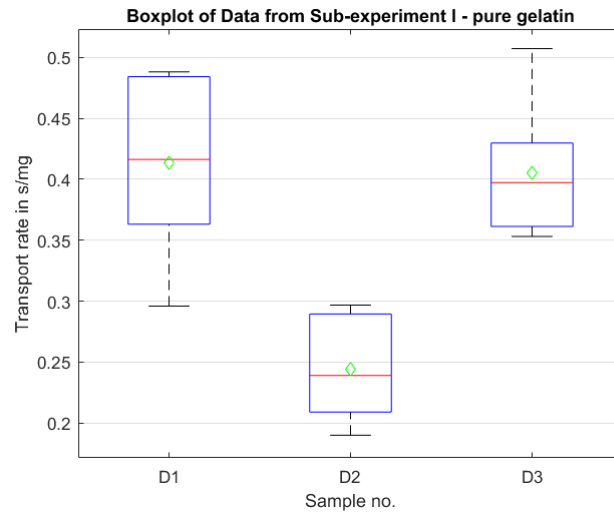


**Figure 71:** Boxplot graph displaying the distribution of data as collected from the pure gelatin samples of Sub-experiment I. The sample batch titles are shown on the x-axis and the transport rate in  $(\frac{s}{mg})$  is indicated on the y-axis. The maximum- and minimum values are indicated by the outermost horizontal solid lines on each box plot. The median of each dataset is indicated by the horizontal red line in each boxplot, while the mean of each sample batch is indicated by the green diamond.

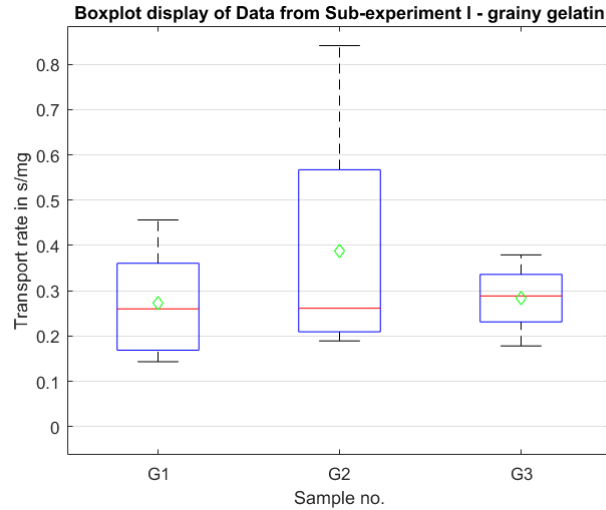


**Figure 72:** Boxplot graph displaying the distribution of data as collected from the grainy gelatin samples of Sub-experiment I. The sample batch titles are shown on the x-axis and the transport rate in  $(\frac{s}{mg})$  is indicated on the y-axis. The maximal values and minimum values are indicated by the outermost horizontal solid lines on each box plot. The median of each dataset is indicated by the horizontal red line in each boxplot, while the mean of each sample batch is indicated by the green diamond.

